POLITECNICO DI TORINO

Master of Science in Aerospace Engineering
Master Thesis

Variable wings configuration assessment for hypersonic transportation system

Supervisors:
Prof.ssa Nicole Viola
Prof.ssa Roberta Fusaro

Candidate:
Oscar Gori

March 2019

Abstract

A preliminary study investigating the possible variable wing options for the reusable booster of SpaceLiner is described here. This investigation is motivated by a critical condition that arises during the first part of the booster descent, which must be avoided. Based on the previous SpaceLiner 7-3 configuration some modifications on the wing geometry are performed, with the main objective of reducing the wing span. Three wing types are studied here: a fixed wing, a variable sweep wing and a foldable wing.

In the study's first step the geometry of the wing is designed for each of the wing type considered. Mass, centre of gravity and aerodynamic data sets are evaluated with the main purpose of maximizing the aerodynamic performances and keeping the mass as low as possible. Particular attention is paid on the subsonic part of the descent, when the booster is supposed to be in-air captured by a towing aircraft. Some simplified and preliminary calculations are done to estimate the flight performances during this part of the mission. Moreover, an analysis on the existence of a trimmed condition for the entire Mach range is carried on. The most promising configuration among those studied is selected for further investigations.

The second part of the study includes the simulation of the ascent and the descent trajectory. The TSTO mission is taken as a reference for this study. Once the descent trajectory is computed, the Thermal Protection System is designed. Two different set of materials are considered for the TPS: one is composed by non-metallic materials only, while the other is made of both metallic and non-metallic materials. The optimization of the ascent trajectory is then performed and the mission payload mass is evaluated.

The whole analysis is performed using tools developed at DLR. Then, the aerodynamic coefficients of the new booster configuration are also analysed with Missile Datcom and the results are compared to the aerodynamic data that have been calculated previously. A preliminary design of the vertical fins is also carried out.

Table of Contents

List Of Figures

List Of Tables

Nomenclature

α	Angle of attack	°
γ	Flight path angle	°
δ_{flap}	Flap deflection angle	°
ρ	Density	kg/m^3
σ	Bank angle	°
b	Span	m
C_D	Drag coefficient	-
C_L	Lift coefficient	-
C_M	Pitching moment coefficient	-
C_Y	Yaw moment coefficient	-
D	Drag	s
g_0	Standard gravity acceleration	N
I_{sp}	Specific impulse	m/s^2
L	Lift	N
M	Mach number	-
m	Mass	kg
m_p	Propellant mass	kg
n_z	Acceleration along z-axis/ g_0	-
R	Range	km
T	Thrust	N
m_p	Propellant mass	kg
W	Weight	N

Abbreviations

AETB	Alumina Enhanced Thermal Barrier
AFRSI	Advanced Flexible Reusable Surface Insulation
CAC	Calculation of Aerodynamic Coefficients
CMC	Ceramic matrix Composite
COG	Centre of Gravity
FRSI	Felt Reusable Surface Insulation
LH2	Liquid Hydrogen
RLV	Reusable Launch Vehicle
SL	Space Liner
STSM	Space Transportation System Mass
TABI	Tailorable Advanced Blanket Insulation
TOP	Thermal Optimization Program
TOSCA	Trajectory Optimization and Simulation of Conventional and Advanced Space Transportation Systems
TPS	Thermal Protection System
TSTO	Two Stages To Orbit
TUFI	Toughened Uni-piece Fibrous Insulation

Introduction

The SpaceLiner concept has been originally proposed by the German Aerospace Centre (DLR) and it is under investigation since 2005, with the main purpose of providing sustainable low-cost space transportation to orbit. The SpaceLiner is a rocket propelled, suborbital, hypersonic transport vehicle. The standard configuration is composed by two fully reusable stages, an unmanned booster and a 50 passenger orbiter, while an extended variant is designed to house up to 100 passengers. The reference mission is supposed to cover the distance between Western Europe and Australia in a 90 minutes flight, while an alternative route between Western Europe and the North America West Coast is also under investigation.

This new application for launch vehicle has the potential to revolutionise the space transportation, since it is a valid and promising alternative to the present low-speed subsonic flight. It could enable ultra-long-distance travel between two main agglomerations on Earth, strongly reducing the flight time. However, the number of launches per year should be strongly increased in order to allow manufacturing and operating costs to be dramatically reduced. The SpaceLiner could play an important role in the intercontinental travel market and production rates of RLVs could be strongly raised in a way that is not possible for other earth-orbit space transportation applications [1].

However, this is not the only possible application for the SpaceLiner, since a different type of mission could be achieved with a similar configuration: during the last few years, a mission providing low-cost space cargo transportation to orbit has been taken into account for the SpaceLiner.

At lift-off the two stages are arranged in parallel, with the passenger stage that is attached on top of the booster. The two stages separates at the end of the ascent, when the main engine is cut-off. The upper stage continues the mission with a high-speed gliding flight towards its destination. The booster, instead, starts an unpowered descent back to Earth.

Some configurations have been developed at DLR in recent years and the most recent one is represented by the SpaceLiner 7-3. However, this configuration presents an important limitation. A recent calculation on the hypersonic descent of the booster, made with Euler CFD, has highlighted a shock wave interaction with the wing outboard leading edge [2].

The main objective of this study is to avoid any shock interaction at the booster wing leading edge in hypersonic regime. For that reason, some modifications on the booster wing geometry are required. Since a wing with a high span is not needed for the hypersonic re-entry, the wing dimension can be reduced. However, this solution is in conflict with the

L/D ratio and in-air-capturing requirements that are present in the subsonic regime. At low speed, a wing with a high aspect ratio can be the best solution to improve aerodynamic performance. For that reason, particular attention is paid on the possible use of a variable wing: with this concept the wing span can be varied during the flight and can be adapted to satisfy the constraints at each Mach number. The aerodynamic characteristics of different configurations are investigated. A preliminary analysis on longitudinal stability and trimmed condition for the whole flight is done. Some preliminary and simplified calculations are also performed for the tow-back flight, in order to verify the feasibility of the flight in that conditions. Once the most promising configuration is chosen, its ascent and descent trajectories are simulated. The main objective is to minimize the structural and thermal loads that the booster experiences during the descent. Different set of materials are considered for the TPS and their influence on the overall booster mass is evaluated.

SpaceLiner configuration during the ascent

Chapter 1 SpaceLiner

The original SpaceLiner passenger configuration is considered as the baseline for any other derivative. The overall configuration involves a reusable booster and a passenger stage, the latter one being attached on top and parallel to the booster during lift-off and ascent. The launch configuration is shown in Figure 1.1. Stage attachments are following a tripod design. The axial thrust of the booster is introduced through the forward attachment from booster intertank into the nose gear connection of the orbiter [3].
The TSTO configuration is directly derived from the passengers configuration and the overall shape of the SpaceLiner remains quite similar. The booster is the same that is considered for the original mission, while the second stage is adapted to store the cargo inside.

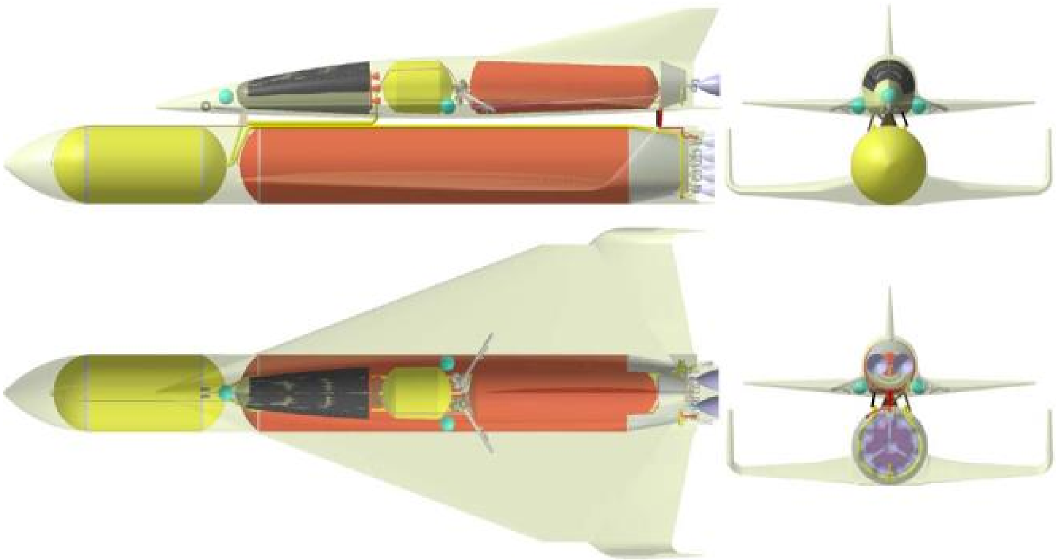

Figure 1.1 - SpaceLiner 7-3 launch configuration with passenger stage on top and booster stage at bottom position

1.1 SpaceLiner mission

The route connecting Europe to Australia has been used as the reference mission since the very beginning of the SpaceLiner design. This distance is supposed to be served for 50 passengers on a daily basis in both directions. However, this is not the only possible mission and some shorter cases, which can potentially generate a larger market demand, are taken into account. For that purpose, an alternative 100 passenger configuration has been also studied.
Ascent noise and sonic boom constraints, that are present while operating near populated areas, must be taken into account in the definition of the operational scenarios. Those

constraints play a fundamental role in the selection of launch and landing sites as well as for the ground tracks determination.
For that reason, the launching site must be located far from densely populated areas. Three potential solutions exist for the launching site:

- On-shore closed to sea or ocean;
- Artificial islands;
- Off-shore launch site and on-shore landing site;

These three options have already been considered in the past and they appear feasible for future missions. The choice for the best site depends on many factors, such as climate and geographical location.
For what concerns the reference Europe-Australia mission, two on-shore sites are preliminary selected: one launching site is located in Queensland, Eastern Australia and the other one is in the German North-Sea-coastal region. Both locations have the advantage of the complete launch ascent and supersonic gliding approach capable of being performed over the sea while still being relatively close to each continent's major business centres [4].
The SpaceLiner mission can be divided into three phases: ascent, booster descent and orbiter descent.

1.1.1 Ascent phase

The launch site characteristics have been briefly described previously for what concerns the passenger case and they vary according to the route that is selected for the SpaceLiner passengers mission. Something different can be asserted for what concerns the TSTO case: the launch site is considered to be Kourou, French Guyana.
The launch configuration is the one illustrated before. The orbiter remains attached on top of the booster for the entire duration of the ascent flight. When the MECO conditions are reached, the orbiter separates from the booster and continues the flight toward its destination. The separation phase is shown in Figure 1.2.

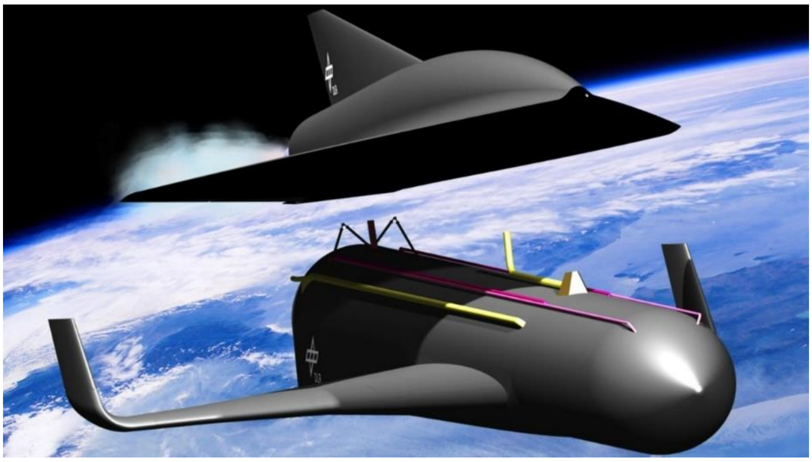

Figure 1.2 - SpaceLiner concept at stage separation with passenger stage on top

1.1.2 Booster descent

The SpaceLiner booster is equipped with wings and it is able to fly back to the landing site in a controllable way. It is not possible to consider a powered fly-back because the Mach number at separation is very high (approximately 13) and the requested amount fuel would be too much. For that reason, the descent is performed without any engine being used. However, when the booster decelerates to subsonic velocities, an in-air-capturing method can be used. From that point on, the booster is towed back by an airplane to the landing site without any necessity of an own propulsion system [5]. Then, prior to the landing, the booster is released and it is able to perform an autonomous gliding landing on a runway.

1.2 SpaceLiner 7-3 geometry

SpaceLiner was first proposed in 2005 and it is under investigation at DLR since then. Different configurations have been analysed and a numbering system has been created for all those types investigated in a certain level of detail. The current configuration, the SpaceLiner 7-3, is described in the following sections.

1.2.1 SpaceLiner booster

The SpaceLiner Booster is a high-performance reusable launch vehicle which operates as a first stage for the passenger/orbiter stage. It is equipped with two large integral tanks for LOX and LH2 and with nine liquid rocket engines that provide thrust for the mated ascent flight.

At a certain altitude the booster separates from the second stage and starts the descent with all the engines being not operative. Later during the subsonic part of the descent an in-air capturing method is used and the booster is towed back by an airplane. Then, it is released and it is able to perform an autonomous landing on a runway.

The current booster geometry is presented in Figure 1.3 and its dimensions are reported in Table 1.1.

Length [m]	82.3
Span [m]	36
Fuselage diameter [m]	8.6
Wing leading edge angles [°]	82/61/43
Wing pitch angle [°]	3

Table 1.1 - Geometrical data of SpaceLiner 7-3 booster stage

Each system mass and the total booster mass are reported in Table 1.2. System margins of 14% (12% for propulsion) are added to all mass data. This conservative approach is selected in this preliminary phase in order to guarantee a solid development of this advanced vehicle with ambitious safety and reusability requirements.

Structure [Mg]	124.6
Propulsion [Mg]	37.3
Subsystem [Mg]	20.1
TPS [Mg]	19.0
Total dry [Mg]	201
Total propellant loading [Mg]	1 284
GLOW [Mg]	1 485

Table 1.2 - Mass data of the SpaceLiner 7-3 booster stage

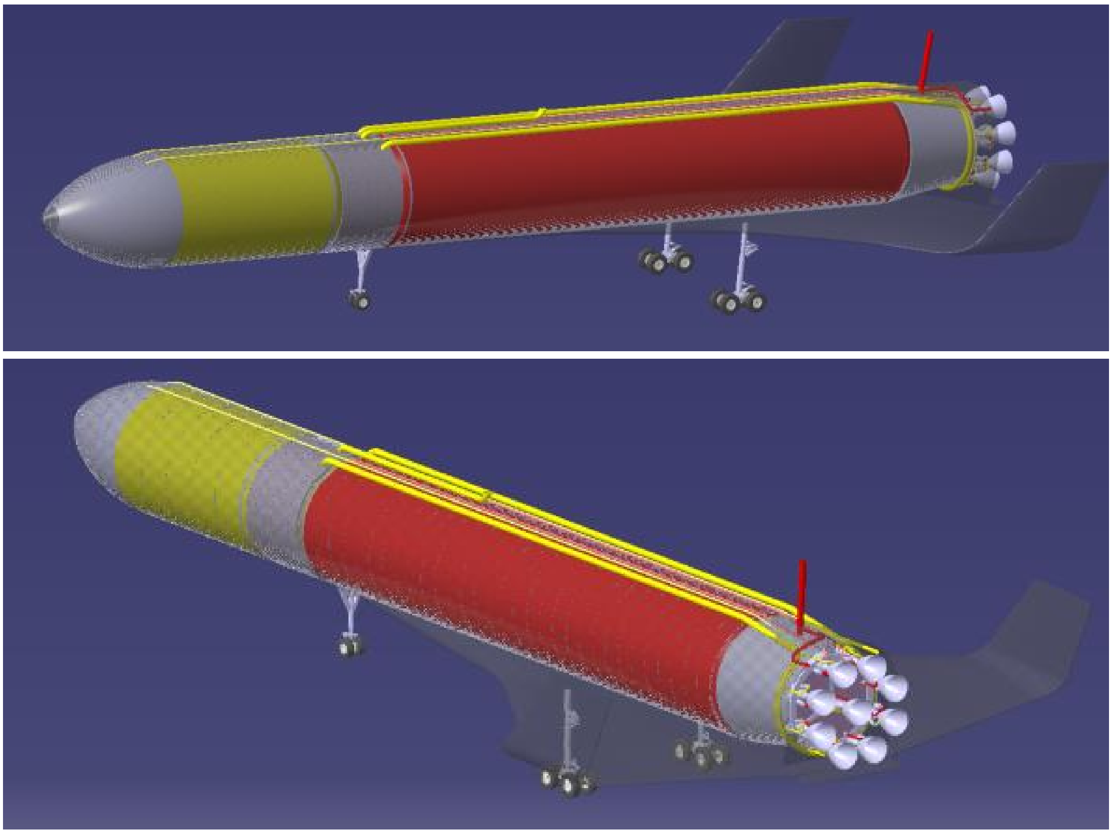

Figure 1.3 - CAD model of SpaceLiner 7-3 booster with semi-transparent outer surface showing internal arrangement of tanks and propellant feedand pressuritarion line

1.2.2 SpaceLiner orbiter

The SpaceLiner orbiter experiences a wide range of flight conditions during the descent, since its Mach number stretches from the hypersonic to the very low subsonic speed at landing. Detailed aerodynamic analysis of the orbiter descent have been conducted yet and the obtained coefficients have been used to establish the aerodynamic data base.

The geometrical data of the orbiter are presented in Table 1.3, while the masses are reported in Table 1.4.

Length [m]	65.6
Span [m]	33.0
Fuselage diameter [m]	6.4
Wing leading edge angles [°]	70
Wing pitch angle [°]	0.4

Table 1.3 - Geometrical data of the SpaceLiner 7-3 orbiter stage

Structure [Mg]	56.3
Propulsion [Mg]	10.6
Subsystem [Mg]	46.5
TPS [Mg]	26.6
Total dry [Mg]	140
Total propellant loading [Mg]	230
GLOW [Mg]	370

Table 1.4 - Mass data of SpaceLiner 7-3 orbiter stage

The take-off mass for the reference mission is now approximately 1855 Mg. This value, even if it is quite large, is still limited if compared for example with the Space Shuttle STS: in this case the mass is more than 2000 Mg. Recent analysis on reference mission trajectories indicated that generous performance margins exists. Some further studies, however, are requested for a precise assessment of a future configuration with a reduced size and mass.

Total dry mass [Mg]	341
Total propellant loading [Mg]	1514
GLOW (incl. passengers & payload) [Mg]	1855

Table 1.5 - Mass data of SpaceLiner launch configuration

Chapter 2 Variable wing

The requirement for a shorter wing span has been briefly mentioned before and it will be discussed in detail later in this thesis, with all the other constraints that are present in the analysis. Here it is important to highlight that the limit imposed on the wingspan is valid only for the hypersonic, so it does not affect the subsonic regime. For that reason, it is possible to think about a configuration with a wing span that can be modified during flight, in order to maximize the performances in subsonic, supersonic and hypersonic regime. If this is done, a shorter wing span is used during hypersonic, while a bigger one is used for subsonic.

A possible solution that allows to accomplish this objective is represented by a variable-sweep wing. This concept has already been used in the past, especially for military aircraft, in order to guarantee a feasible and optimized flight both in subsonic and supersonic regimes. The wing is manipulated to meet diverse flight requirements: good low speed performance, good cruise performance and good transonic or supersonic characteristics can be achieved simultaneously [6]. Usually, the unswept wing is suitable for low speed and at take-of or landing, while a swept wing is more appropriate for higher speed. A trade-off between wing geometry, mechanism complexity and weight is needed to maximize the aircraft performance.

In past decades, three main reasons existed to sweep a wing forward or backward [7]:

1. To improve longitudinal stability by reducing the distance between the aircraft centre of gravity and the wing aerodynamic centre;
2. To provide longitudinal and directional stability for tailles wings;
3. To delay transonic drag rise;

Historically, variable wing have been used mostly for military aircraft. Indeed, new military capabilities and requirements appeared in 1950s that lead to the improvement of variable wings. Some of these needs were the long range subsonic cruise, the high supersonic flight combined with the low altitude transonic strike and the operations on limited length runways. Many experimental designs were carried on from the 1940s into the 1970s.

One of the first example of an aircraft with a variable sweep wing is represented by the Bell X-5, shown in Figure 2.1. NASA developed this experimental vehicle in early 1950s to improve the characteristics of the flight in the transonic speed regime. The sweep angle could be varied from 20° to 60°. With the variation of the sweep angle, the position of the aerodynamic forces relative to the centre of gravity changed. A rail carriage was also present in order to provide a system to translate the wing when modifying the sweep angle. This mechanism was needed to avoid an excessive shift of the neutral point at high sweep angles. The sweeping mechanism was demonstrated to be trouble-free during the whole duration of the program. However, the aircraft showed some problems for what concerns the pitching characteristics in flight. However, the experience of the X-5 program showed that a wing sweep mechanism could be designed and operated in flight [8].

Figure 2.1 - Bell X-5

The second historical example of an aircraft with a variable sweep wing is represented by the Grumman XF10F-1, illustrated in Figure 2.2. The sweep wing rotation is linked to a simultaneous forward translation of the wing pivot, thanks to the presence of a slotted track. This arrangement is adopted in order to avoid an excessive rearward shift of the neutral point at high angles of attack. The feasibility of this variable geometry wing was demonstrated and this solution provided some major performance improvements at both ends of the speed regime. However, this aircraft never entered service since it had extremely poor flying characteristics.

Figure 2.2 - Grumman XF10F-1

The first variable sweep wing aircraft that entered production was the General Dynamics F-111 in early 1960s. It was directly derived from the Grumman F10F and the sweep angle varied from 16° to 72.5°.

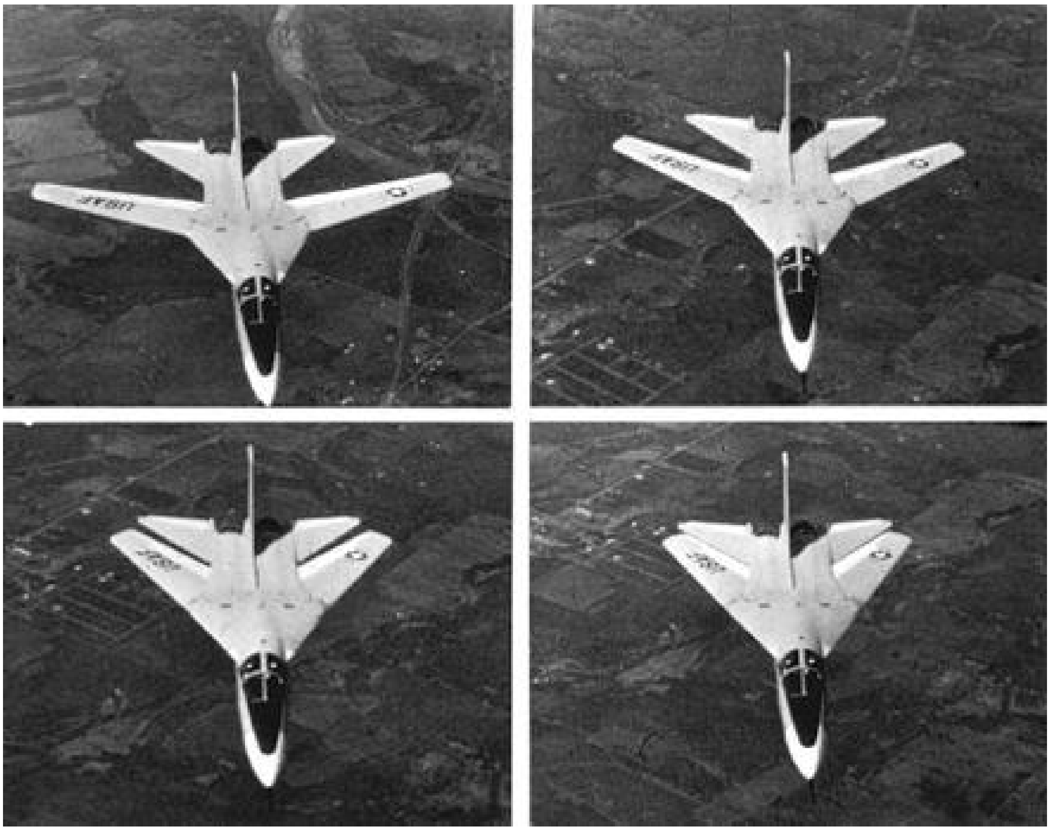

Figure 2.3 - General Dynamics F-111

The Grumman F-14A was the most successful US example of a variable sweep wing fighter aircraft. The sweep angle could be varied from 20° to 68°. When the maximum sweep was selected, the wing trailing edge was aligned with horizontal tails, as can be seen in Figure 2.4. The sweep angle was automatically controlled by the central control system, which was able to set the optimal value as a function of Mach number, during the entire speed regime. The wings were mounted inside a titanium box, that occupied the entire lateral side of the fuselage. The wing rotated upon two pivot points that were placed as a connection between the wing and the fuselage. When the wing retracted, about 25 percent of its trailing edge tucked beneath an over-wing fairing, which left a gap between the aft section of the wing and fuselage. Inflatable canvas bags attached to the fuselage closed the gap. The bags also provided a smooth contour to blend the wings trailing edges and the aft fuselage, allowing a smooth flow of air [9].

Figure 2.4 - Grumman F-14

The development of variable sweep wing was not only limited to United States. Also in the Soviet Union and in Europe some aircrafts with a variable wing were designed. Some examples are the Sukhoi Su-17,Su-18 and Su-24, the Tupolev Tu-22 and Tu-160 in the Soviet Union and the Panavia Tornado in Europe. The latter one had many similarities with the F-111, being smaller than the US fighter, but with more advanced onboard systems and avionics. The wing sweep angle could be varied from 25° to 67° and each angle was linked to a precise speed range.

The variable wing concept has been used especially for military applications, but some investigations have been done also for civil aircrafts. For example, during 1960s Boeing was trying to develop a variable sweep supersonic transport vehicle. In this case, the idea was to maximize the performance in different flight regimes, from take-off to supersonic cruise and low speed landing. This concept was selected in 1966 to be the first US commercial SST, but the variable wing was abandoned later due to increasing difficulties for the wing/tail integration.

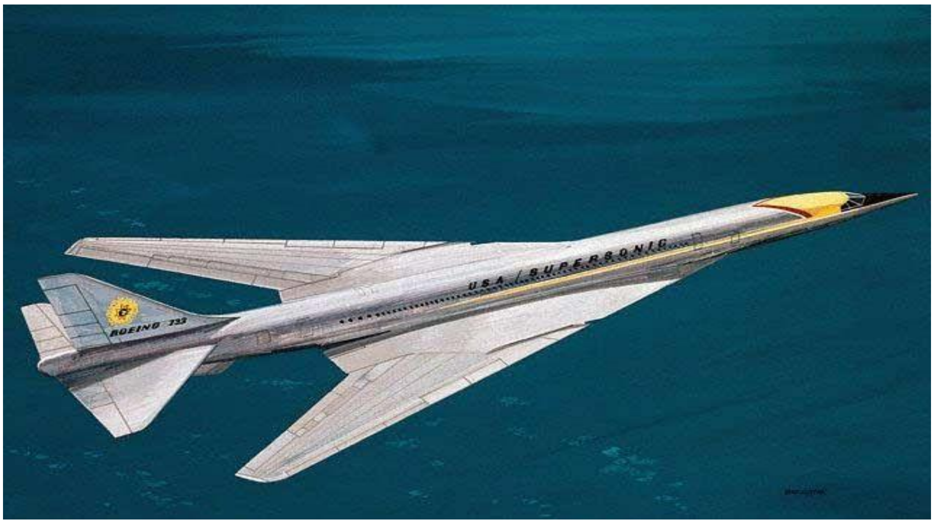

Figure 2.5 - Boeing supersonic transport vehicle

While variable-sweep wing provides many advantages in terms of flight performance during diverse speed regime, it causes a strong increase in mass and complexity. For that reason, with the advent of new technologies in the stability flight control systems many of the disadvantages of a fixed wing were overcome and variable wings were not used anymore.

2.1 Variable wings for the SpaceLiner

The use of a variable sweep wing could be the best solution for what concern the SpaceLiner booster. The reasons behind this possible choice are different from the ones that existed for military aircraft in the past. The limit imposed on the wingspan is valid only for the hypersonic, so it does not affect the subsonic regime. It is possible to think about a configuration with a wing span that can be modified during flight, in order to increase the performance in subsonic, supersonic and hypersonic regime.
During low speed flight, a high aspect ratio is required to improve aerodynamic performance and to maximise the lift to drag ratio. For what concerns the hypersonic regime, instead, a large wing is not needed. Moreover, the shock interaction at wing leading edge can be avoided if the span is reduced. A possible solution is represented by a variable-sweep wing. If this wing type is selected, a lower wing span is used during hypersonic, while a bigger one is used for subsonic.

The configuration that has been considered for the SpaceLiner booster is composed of a two segments wing (an inner and an outer part) and it is provided with a sweeping mechanism. The outer part of the wing can be rotated around a pivot and it can be placed in two different positions:

1. Stored: the outer part is stored inside the inner part;
2. Deployed: the outer part is fully deployed;

During supersonic and hypersonic flight, the outer wing is included inside the inner wing, and the span is reduced, being equal to the wingspan of the inner part alone. For what concerns the subsonic regime instead, the outer part can be fully deployed to increase the wing span.

However, if such a complex configuration (with respect to the fixed wing) is chosen, some further constraints need to be considered. Dimensions of the outer and the inner part of the wing are strictly connected: the outer part must be included in the inner part, which has to be big and thick enough to contain the movable wing. Moreover, it must be considered that, when the wing is not deployed, it can't be placed inside the fuselage of the booster, since this space is already occupied by fuel tank. Another aspect that plays a fundamental role in designing a variable wing is the increase in mass: the addition of the sweeping mechanism must be considered when the overall mass of the configuration is evaluated. A detailed description of those constraint will be presented in section 4.2.

Chapter 3 Study description

3.1 Constraint Analysis

A hypersonic flight analysis on the SpaceLiner 7-3 booster has been made at ESA with Euler CFD. The results of this analysis show that, during descent, the maximum heat load is reached at M=10. In proximity of this condition, a critical interaction between the shock wave and the outer part of the SpaceLiner booster wing has been identified. This shock wave interaction is shown in Figure 3.1 and Figure 3.2 [2]. The portion of wingspan that is affected by this interaction is of about 2.5 m on each side of the wing. To guarantee a feasible flight, this condition needs to be avoided and the total wing span of the original SpaceLiner configuration must be reduced of at least 5 m. Since the current SpaceLiner 7-3 booster wing span is equal to 36 m, the maximum acceptable wing span must be now limited to 31 m. However, this constraint affects only the hypersonic flight and there is no restriction for what concern the wingspan in subsonic or supersonic flight.

A reference limit on the minimum wing span is also present and it is equal to 20 m. This value is chosen from a previous version of the SpaceLiner with a reduced wing span. However, some preliminary analysis performed on this configuration have highlighted that the flight is not feasible for the entire Mach range. For that reason, a shorter span has not been considered during this study. The wing span ranges between 20 m < b < 36 m.

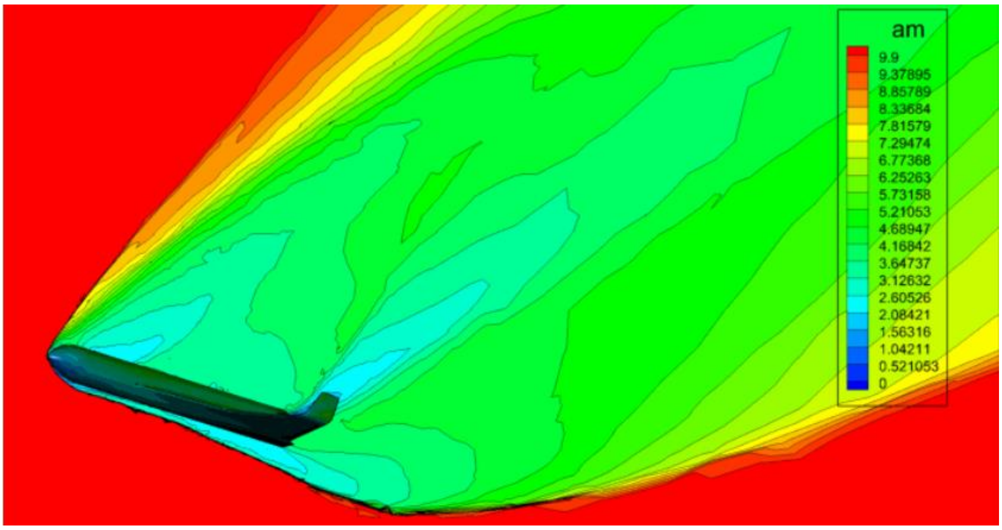

Figure 3.1 - Mach contour of SL7-3 booster at M=10 and α=35°

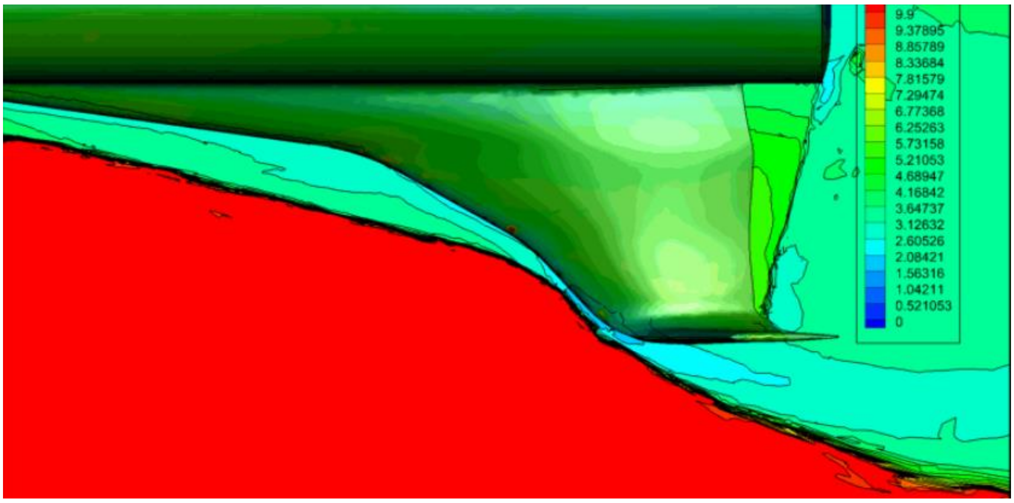

Figure 3.2 - Shock wave interaction with the wing

The previous one is not the only major constraint that has to be considered. Once the wing geometry is modified, the feasibility of the flight with the new configuration must be assured. For that reason, an analysis on the longitudinal stability of the booster needs to be accomplished for each Mach number: the existence of a trimmed condition for different angles of attack must be analysed. The booster is supposed to fly at different α during the descent. The range of angles of attack for each Mach number is presented in Table 3.1. The requirement about the trimmed condition of the booster should be investigated for those angles of attack.
In addition to this, aerodynamic performance is evaluated in terms of lift, drag and L/D ratio. The main purpose is to maximise lift, while keeping drag as low as possible.

Mach number	Angle of attack [°]
M<1	α <15°
1<M<4	α ≈ 20°
5<M<9	20°< α <30°
M>9	40< α <50

Table 3.1 - Angles of attack with different Mach

Flaps are also designed in this phase in order to satisfy this constraint. Two aspects are considered while designing the geometry of the flaps:

1. They should guarantee the existence of a stable and trimmed condition during the whole flight, with a deflection that should not be too high (δ_{flap}<30°);
2. Their chord should not be too large with respect to the wing chord;

For what concerns the subsonic regime, a further investigation is needed. The booster is supposed to be in-air-captured during the descent and to be carried to the landing site by a towing aircraft. The flight performances of the booster in this phase are also preliminary evaluated.

During the tow-back flight the engines of the booster are not operative, so the thrust is provided by the aircraft only. The booster, however, generates some contributions in terms of lift and drag: these forces have to be considered, together with the ones of the towing aircraft, while computing the tow-back flight performances.
Some constraints, concerning the configuration of the SpaceLiner booster and the towing aircraft connected together, emerge:

1. *L/D ≥ 5*
2. *L/W ≥ 1*
3. *T/D ≥ 1*

The lift generated during the tow-back flight has to be greater than the drag produced by booster and towing aircraft together. However, a limited value of glide ratio (e.g. L/D=2 or 3) could be not enough to guarantee an efficient flight. For that reason, a minimum value of L/D=5 is chosen. The lift should also be sufficiently high to balance the overall weight. The same can be said for the thrust to drag ratio, but it must be highlighted again that the thrust is only provided by the engines of the towing aircraft.
Even if this is a very preliminary estimation, it still gives a first description of the subsonic performance. For that reason a maximization of the three ratios presented before is required in this phase.

3.2 Computational tools

During this study on the SpaceLiner booster, each analysis is performed with some tools developed at DLR and SART. The only exception is represented by Missile Datcom, which is used in the final part of the study to compare and validate the aerodynamic results. Here these tools are presented and briefly described.

STSM

STSM (Space Transportation System Mass) is able to estimate the final mass of each subsystem and its position (COG) in the vehicle-fixed coordinate system. It also provides data of the entire vehicle. If the mass of a certain element is already known it can be directly inserted as an input, otherwise it will be estimated by the tool.

CAC

CAC (Calculation of Aerodynamic Coefficients) is able to calculate the aerodynamic coefficients (C_L, C_D, C_M and the centre of pressure) of pre-determined geometries as a function of angle of attach and Mach number. It is used for preliminary estimations of lift and drag coefficients, as well as for stability and trimmability analysis. Although based on simple basic geometry neglecting any interference, it is possible to obtain results in good agreement with wing tunnel measurements or results of much more time consuming CFD-calculations. The entire Mach range can be investigated with CAC, but in this thesis it has been used only for subsonic and supersonic evaluation.

HOTSOSE

HOTSOSE is the tool used for the hypersonic speed regime. It is able to evaluate aerothermodynamic characteristics of pre-determined geometries. It is used both for the calculation of the aerodynamic coefficients and for the estimation of the thermal loads that exists during the hypersonic part of the descent.

TOSCA

TOSCA TS (Trajectory Optimisation and Simulation of Conventional and Advanced space Transportation System) is the main trajectory simulation and optimisation software used in SART.

TOP

TOP (Thermal protection system Optimization Program) is a software for dimension the TPS of Space Vehicles. It calls HOTSOSE and TOSCA to estimate the heat loads. Based on the temperature distribution on the surface of the vehicle several temperature regions are identified and appropriate TPS material are selected for each area. Then, the necessary TPS thickness is determined by solving the 1D heat flux equation.

RTS

RTS is usually run with TOSCA and it is able to compare the masses resulting from TOSCA and STSM. It also provides the payload that is possible to bring to orbit if the cargo mission is considered.

Missile Datcom

Missile Datcom is a tool developed by the United States Air Force. It is used for preliminary missile design: it is able to estimate the aerodynamic coefficients of a wide variety of configuration design. The fundamental purpose of Missile Datcom is to provide an aerodynamic design tool which has the predictive accuracy suitable for preliminary design [10].

3.3 Study logic

Each of the tools that has been described before requires a certain set of inputs. In Table 3.2 a detailed list of inputs and outputs is reported, together with the task that the tool performs.

Tool	*Task*	*Input*	*Obtained from*	*Output*
STSM	*-Stage mass* *-COG analysis*	*-Wing data* *- Geometric arrangement of component* *-COG of each component*	*-User input* *-User input* *-User input*	*-Stage mass* *-Stage COG*
CAC/ HOTSOSE	*-Aerodynamic data* *-Trim analysis*	*-Stage COG* *-Wing geometric data* *-Fuselage geometric data* *-Flap geometric data*	*-STMS* *-User input* *-User input* *-User input*	-$C_D(M,\alpha)$ -$C_L(M,\alpha)$ -$C_M(M,\alpha)$ *-Flap deflections*
TOSCA	*-Trajectories simulation and optimization*	*-Aerodynamic data* *-Stage mass*	*-CAC/HOTSOSE* *-STSM*	*-Descent trajectory* *-Ascent trajectory*
TOP	*-TPS*	*-Descent trajectory data* *-Stage mass* *-Set of materials*	*-TOSCA* *-STSM* *-User input*	*-TPS mass* *-TPS cog*
RTS	*-Payload*	*-Ascent trajectory*	*-TOSCA*	*-Payload*

Table 3.2 - Input and output data for each tool

The flow chart representing the steps of this study is shown in Figure 3.3 and Figure 3.4. The rectangular boxes represents the tool that is used in the step, while the text between the parenthesis indicates the output of each step.

The study's first step is based on the definition of new geometrical arrangements of the wing, taking into account the constraints described before.

Then, STSM is used to calculate the SpaceLiner booster stage mass and the position of the centre of gravity (COG). The inputs required in STSM include the geometric data and the centre of gravity of the wing, which is computed for every wing geometry.

Once the position of the COG is evaluated, it is possible to compute the aerodynamic data of the new configuration for the entire Mach range. In particular, it is possible to obtain the drag, lift and moment coefficient as a function of angle of attack and Mach number. Two different tools are used for that estimation, depending on the speed range:

1. CAC is used for subsonic and supersonic;
2. HOTSOSE is used for hypersonic;

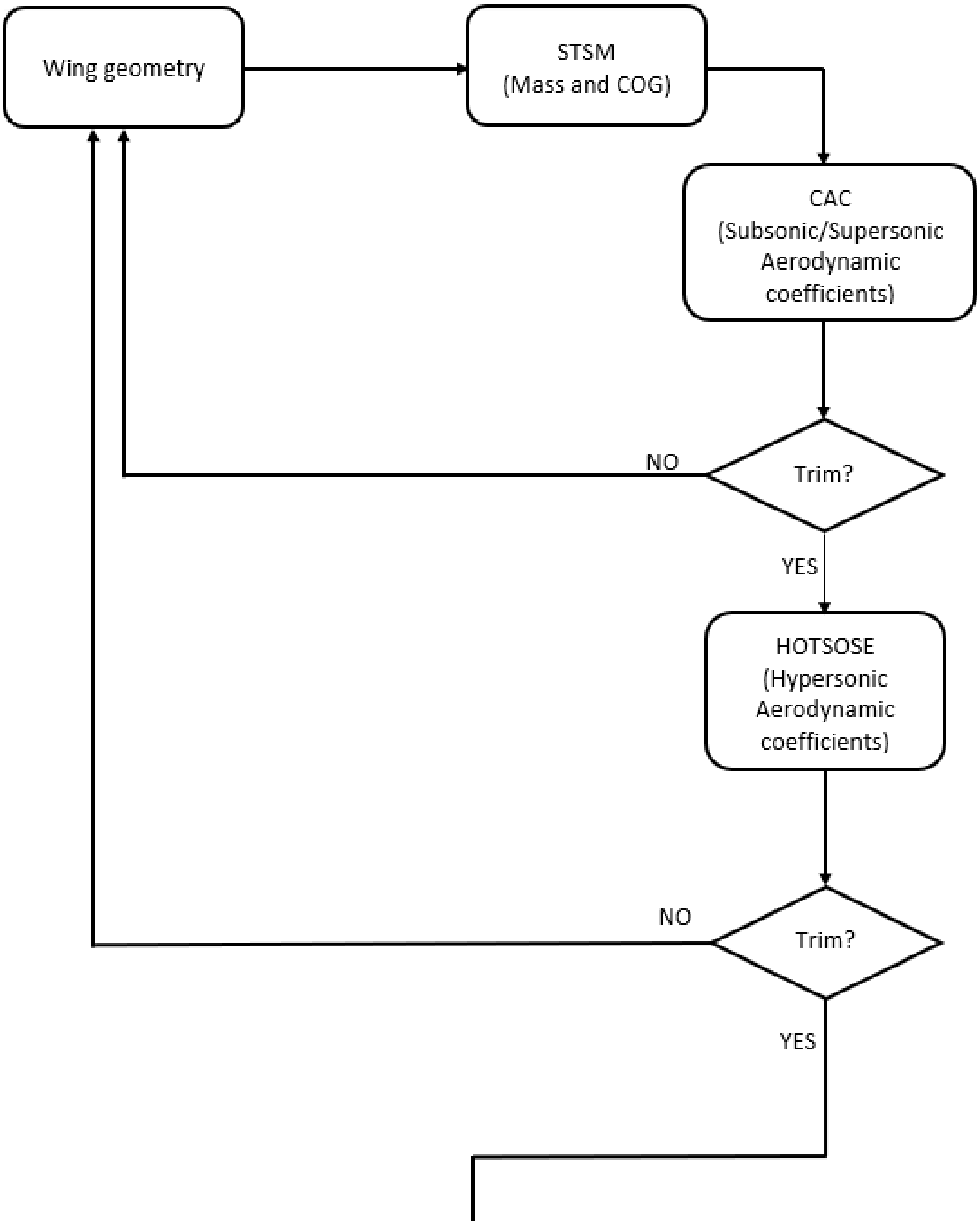

Figure 3.3 - Flow chart of the study logic (part 1)

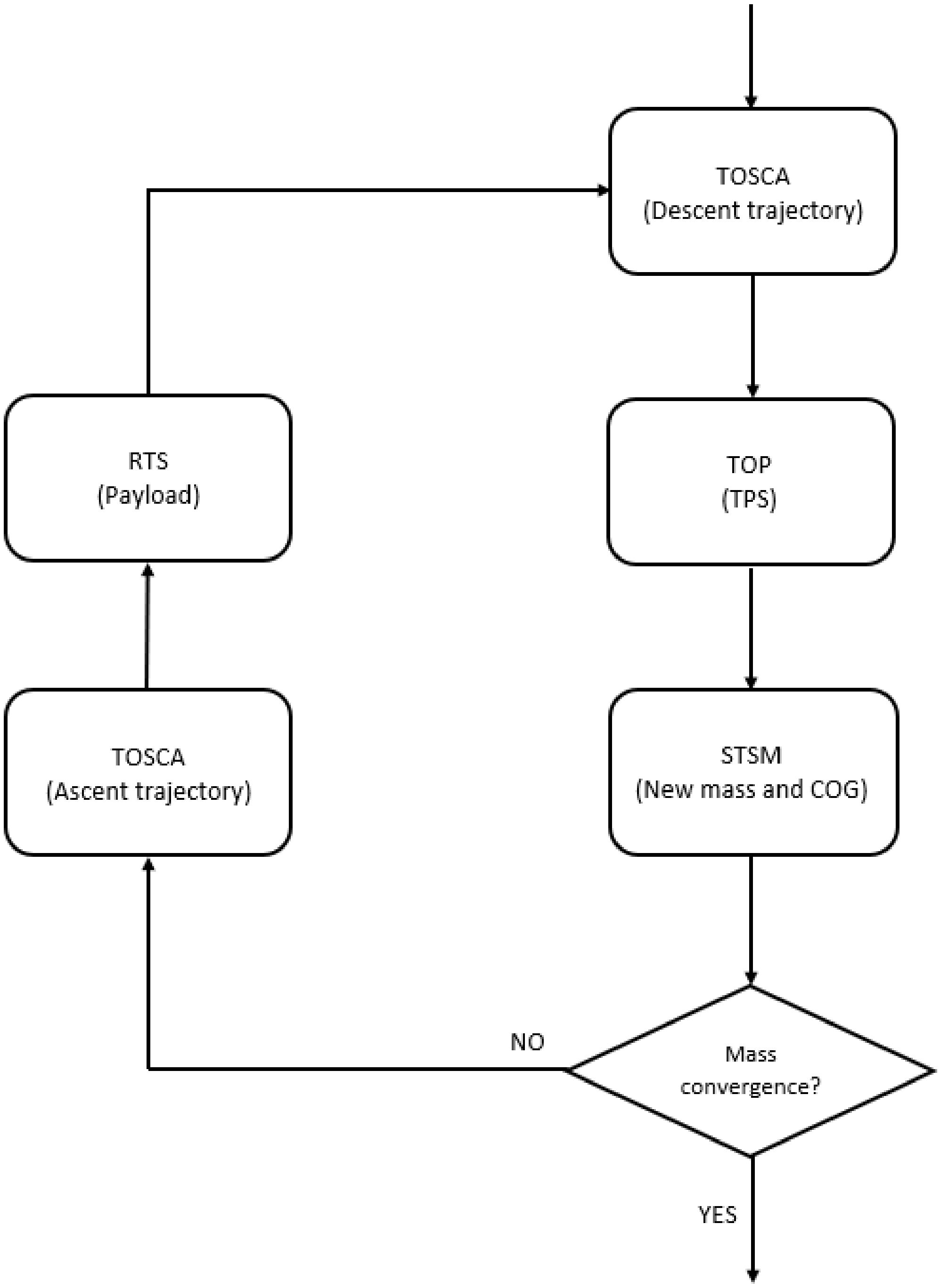

Figure 3.4 - Flow chart of the study logic (part 2)

The Mach number ranges that are used for that calculation are presented in Table 3.3.

	Subsonic	Supersonic	Hypersonic
M range	0<M<1	1<M<5	5<M<13
Tool	CAC	CAC	HOTSOSE

Table 3.3 - Mach range for each tool

An additional computation has been carried on for the subsonic flight. Once the aerodynamic data have been computed with CAC, the configuration involving both the SpaceLiner booster and the towing aircraft has been studied, with the main purpose of maximizing the aerodynamic performances in subsonic. This gives a preliminary and simplified estimation of the feasibility of the tow-back flight. Indeed, even if the SpaceLiner is a hypersonic vehicle, the low speed flight is of great importance for the wing design. It is investigated first, since it dictates the most binding conditions in terms of lift and drag.

Then, the best configurations are chosen among those considered for the next step of the analysis. The main focus is placed on the identification of a trimmed condition for each configuration. During the descent, the booster flies at different angles of attack: α is usually between 20° and 50° for hypersonic flight and approximately 20° for supersonic flight, while it is usually below 15° for subsonic flight. For that reason, it is sufficient that the trimmed condition is found for those ranges of angles of attack. Flap dimension and its deflection angles, that are necessary to satisfy this requirement, are also determined in this phase. If a trimmed condition cannot be found for the entire Mach range, the wing geometry is modified. The check on the existence of a trimmed condition is performed for the subsonic and supersonic regimes first, and in a second step for the hypersonic regime. Lift and drag coefficients are also calculated at different Mach numbers in order to evaluate glide ratio (L/D) and to maximise the aerodynamic performance. Different configurations, involving both variable and fixed wings, can be analysed and compared. Then the most promising one is chosen for further investigation.

The next step is based on the determination of both the descent and the ascent trajectory. Geometry, mass and aerodynamic data that have been calculated with STSM, CAC and HOTSOSE are now used as inputs. First the descent trajectory is evaluated, using as starting conditions the parameters valid for the SpaceLiner Booster 7-3. The actual conditions are obtained from the final parameters of the ascent. Since those parameters are not known at the beginning of the process, the data of the previous configuration are used for a first estimation.

Then the trajectory is manually optimized, varying the angle of attack during descent and considering its effects on the maximum values of dynamic pressure, acceleration and stagnation point heat flux. Once those values are minimized, the thermal protection system mass is calculated using TOP and the total mass of the Booster can be updated with this new value. Considering the TPS mass, it is possible to calculate the ascent trajectory. The new initial conditions for the descent are an output of this computation and can be used to evaluate the descent again. An iterative process is needed for the ascent and the descent trajectories, to reach a convergence in mass. Once the iterative process is finished, the payload mass is obtained from the ascent computation with RTS.

3.4 Tow-back flight performance

The SpaceLiner booster is supposed to be in air-captured during subsonic flight and subsequently towed back by an airplane to the landing site. Performances during the tow-back flight have never been computed and here a first and simplified estimation is done. The reference aircraft that has been selected to accomplish the tow-back is the Boeing 747, since it was used in the past for similar purpose with the Space Shuttle mission. The booster is placed on top of the B747 and parallel to it.

The following assumptions are considered for this evaluation:

1. The aerodynamic forces, generated by the configuration that includes both the booster and the B747, are evaluated as the sum of the forces produced by each component alone. Any interference is not considered as a first estimation.

$$L = L_{Tot} = L_{Booster} + L_{B747}$$
$$D = D_{Tot} = D_{Booster} + D_{B747}$$
$$W = W_{Tot} = W_{Booster} + W_{B747}$$

   Where L is the lift, D is the drag and W is the weight.

2. Thrust is provided by the towing aircraft only, because the booster engines are not operative during this phase.

$$T = T_{B747}$$

   Since only the thrust at the take-off (T_{TO}) is known for the B747 engines, the value of the available thrust for this flight conditions is estimated with the following equation:

$$T = T_{TO} \cdot \frac{q}{q_{TO}} \cdot 0.5$$

   Where q is the dynamic pressure at flight conditions, q_{TO} is the dynamic pressure at take-off and 0.5 is a factor that considers the reduced throttle during cruise with respect to the take-off conditions.

Some other simplifying assumptions are made for this preliminary evaluation of the tow-back flight performances:

1. Speed is constant during the flight;
2. Altitude is constant during the flight;
3. A constant distance is assumed for the flight;

The tow-back flight is supposed to happen at an altitude of about 4 to 5 km, with a Mach number of 0.4 to 0.5. The flight condition chosen for the tow-back flight are presented in Table 3.4.

Range [km] *[11]*	Altitude [m]	M
1 500	4 000	0.5

Table 3.4 - Flight conditions

If these flight conditions are assumed, the aerodynamic performances of the B747 are the ones reported in Table 3.5.

α [°]	C_L	C_D	S [m^2]	Mass [kg]
6.8	0.68	0.0393	473.9	288 483

Table 3.5 - B747 data [12] [13]

Once this data are known, it is possible to evaluate the lift and drag generated by the B747 with the following equations:

1. $L = \frac{1}{2}\rho V^2 C_L S$
2. $D = \frac{1}{2}\rho V^2 C_D S$

Where ρ is the air density, V is the aircraft speed, C_L and C_D are the lift and drag coefficients and S is the wing surface.
Lift and drag generated by the booster are also computed, using the same equations described before. C_L and C_D values for different α are obtained from CAC. The angle of attack is not defined for the booster, so another hypothesis is done: α is supposed to be the same for the booster and the towing aircraft.

The propellant mass that is needed for the tow-back flight is an additional parameter which can be obtained with this simplified evaluation, using the Breguet Range equation.
During the flight the aircraft burns some fuel and loses weight: this loss depends on specific fuel consumption (c_j) and on the thrust (T) that is required. This variation in the airplane weight can be expressed as [14]:

$$dW = -c_j T\, dt$$

If the definition of the velocity V is considered ($V = {ds}/{dt}$), the previous equation can be written as:

$$\frac{ds}{dW} = -\frac{V}{c_j T}$$

During the flight the thrust required is supposed to be equal to drag and can be written as:

$$T = D = \frac{D}{L}W = \frac{C_D}{C_L}W \rightarrow \frac{ds}{dW} = -\frac{V\, {C_L}/{C_D}}{c_j W}$$

Since c_j, C_L/C_D and V are constant during flight, the equation can be integrated to evaluate the range R:

$$R = \int ds = \int -\frac{V \, {C_L}/{C_D}}{c_j} \frac{dW}{W} = \frac{a\,M \, {C_L}/{C_D}}{c_j} \ln\left(\frac{W_0}{W_1}\right)$$

Where $V = Ma$, W_0 is the initial weight and W_1 is the final weight. The propellant mass is equal to the difference between these two weights and the equation can be written as:

$$m_p = m_1 \left[e^{\frac{R}{I_{sp} \, {C_L}/{C_D} \, M\,a}} - 1 \right] = m_1 \left[e^{\frac{R}{I_{sp} \, {L}/{D} \, M\,a}} - 1 \right]$$

Where m_1 is the final mass of the aircraft and I_{sp} is the specific impulse ($I_{sp} = {1}/{c_j}$), while L and D are the sum of the lift and drag generated by the B747 and the booster alone, as described previously.

The propellant mass required is then compared to the maximum value that is possible to store on board the B747, which is equal to 147 132 kg.

Chapter 4 Study of different options for the wings of the SpaceLiner booster

The main objective of this study is to find a new configuration for the SpaceLiner booster wing, considering all the constraints that have been described previously. Different solutions can be adopted to achieve this request. Since the first constraint is the one concerning the shock interaction, the wing span must be decreased. First, a fixed wing is considered, in which the wing span is reduced to a value lower than the maximum one allowed. However, since the constraint about the limited wing span is referred to the hypersonic flight only, some other solutions can be designed. Two types of wing are defined and studied here: a variable sweep wing and a foldable wing. The wing is divided into two parts, a fixed and a movable one. Two positions are considered for the latter, which can be moved to vary the overall wing span. If a variable sweep wing is used, the outer part can be deployed or rotated inside the inner part. If a foldable wing is considered, the outer part can be deployed or moved to a vertical position. In both cases the wing span is not constant and it can be modified during the mission, in order to satisfy the constraints and to improve the performances at different Mach ranges. In the following sections those three configurations are analysed.

4.1 Fixed wing configuration

The wing span of the booster has been modified to satisfy the constraint on the maximum span and to avoid any interaction with the hypersonic shock wave. First, the focus is placed on the subsonic performances during the tow back flight. Different wing configurations are considered here, with the main purpose of maximizing lift and in the same time minimizing drag and weight. Once the performances for that part of the mission are optimized, the new configuration is studied in greater detail.

The aerodynamic coefficients of the different booster configurations are evaluated with CAC. The wing geometry is defined in the input file, where the following geometrical data have to be specified [Figure 4.1]:

- X,Y and Z co-ordinates of the first point of the wing;
- b_i = span of the inboard panel;
- c_{ri} = root chord length (inboard panel);
- g_{mi} = leading edge sweep angle (inboard panel);
- b_o = span of the outboard panel;
- c_{ro} = root chord length (outboard panel);
- g_{mo} = leading edge sweep angle (outboard panel);
- c_{re} = tip chord length (outboard panel);

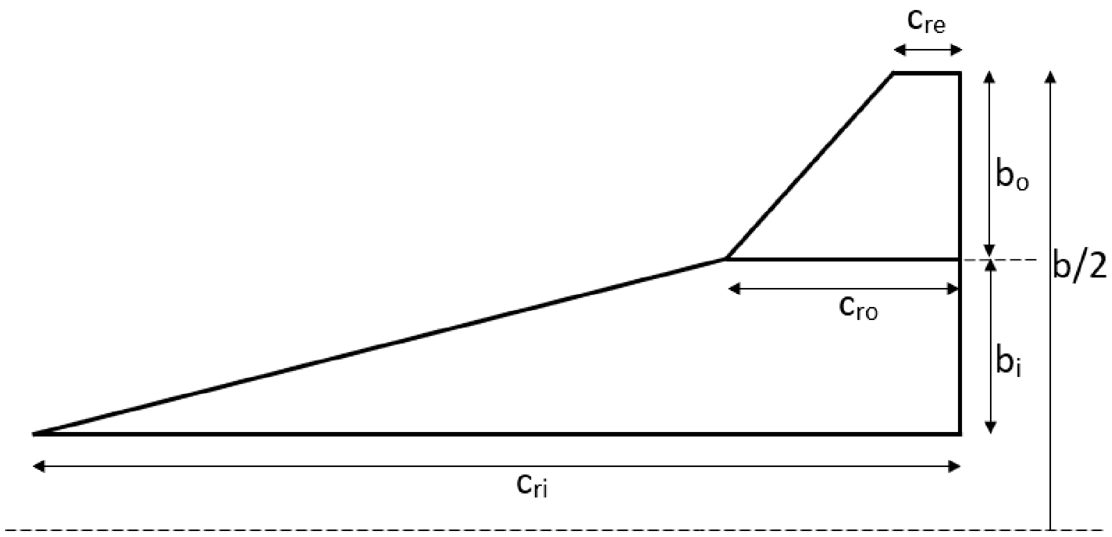

Figure 4.1 - Wing geometry

In Table 4.1 the lift to drag ratio (L/D), the lift to weight ratio (L/W) and the thrust to drag ratio (T/D) of the tow-back configurations, involving both the booster and the towing aircraft, are reported. It is immediately clear that the value of the L/D ratio is not an issue for that configuration, as it presents values near 10. A similar statement can be done for the T/D ratio, since it has values higher than one for each case. Moreover, the propellant mass required is below the limit of 147 132 kg for every configuration. For that reason, the focus is mainly on the L / W ratio, which presents values near unity.

The nomenclature used here for the fixed wing is composed by two parts: the first letter indicates the wing type (Fixed wing→F), while the number refers to the different geometries with the same wing type.

	F-1	F-2	F-3	F-4	F-5
L/D	10.24	10.64	10.00	10.07	9.57
L/W	0.91	0.88	0.93	0.97	1.00
T/D	3.17	3.40	3.00	2.94	2.70
m_p [kg]	119 520	114 514	123 100	121 137	128 490

Table 4.1 - Subsonic performances during tow-back flight

The geometric data of the configuration F-1 are reported in Table 4.2.

Configuration	b_i [m]	b_o [m]	b [m]	c_{ri} [m]	c_{ro} [m]	c_{re} [m]
F-1	4.0	6.0	28.6	40.9	12.44	5.23

Table 4.2 - Geometrical data of the configuration F-1

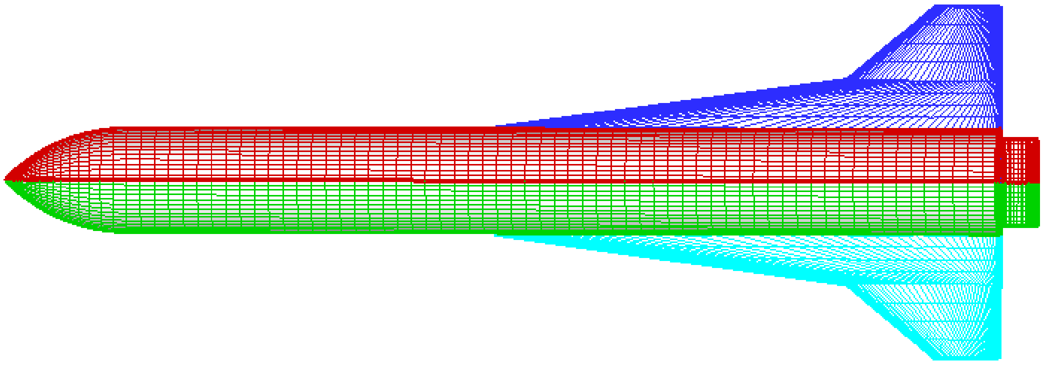

Figure 4.2 - Configuration F-1

In subsonic flight the smallest wingspan of 28.6 m is not sufficient: the lift produced by the first configuration (Figure 4.2) is not enough during the tow-back flight. An increase in wingspan is needed and the maximum allowed value of 31 m is chosen for the next analysis of the Fixed 2 configuration (Figure 4.3).

Configuration	b_i [m]	b_o [m]	b [m]	c_{ri} [m]	c_{ro} [m]	c_{re} [m]
F-2	4.0	7.2	31.0 m	35.26	10.0	3.52

Table 4.3 - Geometrical data of the configuration F-2

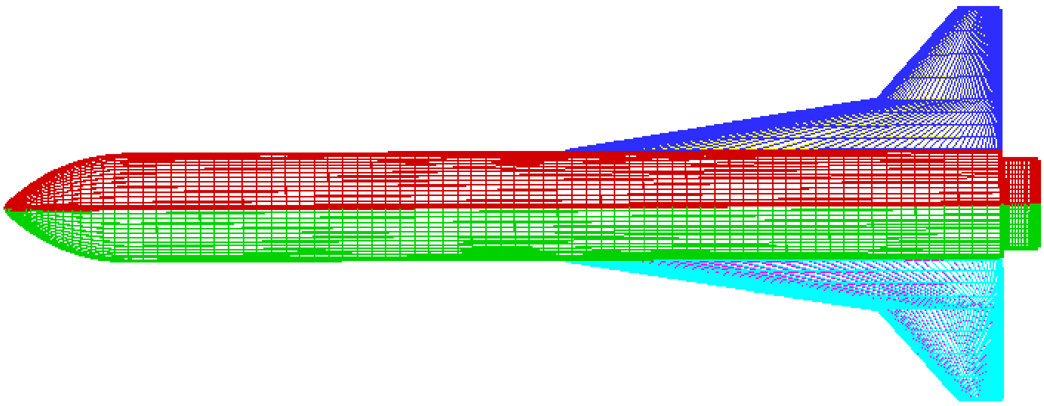

Figure 4.3 - Geometrical data of the configuration F-2

The increment of the span has a positive effect in terms of lift and drag, since the first one is increasing, while the latter is decreasing. However, an increase of the mass is also present, so the overall L/W is lower than before.
For that reason the shape of the wing is changed while the wingspan is kept constant. The wing area is increased as shown in Table 4.4.

	F-2	*F-3*
c_{ri} *[m]*	*35.26*	*41.46*
c_{ro} *[m]*	*10.00*	*13.00*
c_{re} *[m]*	*3.52*	*4.42*

Table 4.4 - Comparison between configuration F-2 and F-3

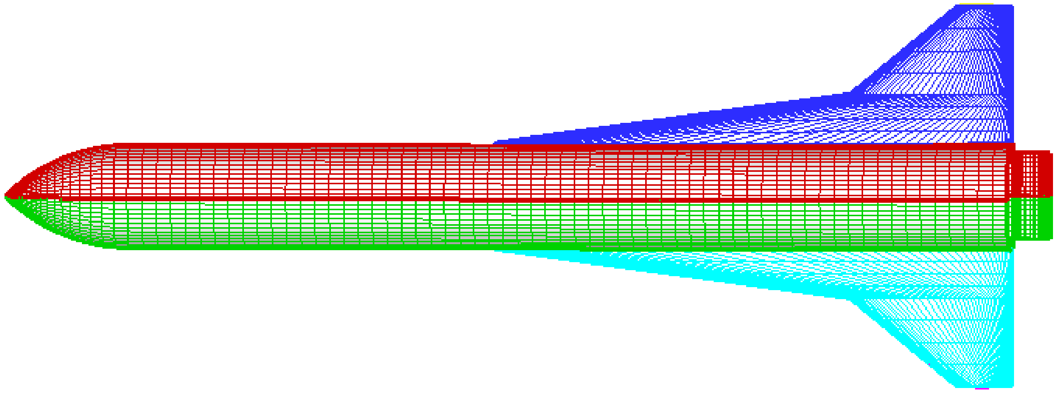

Figure 4.4 - Configuration F-3

The resulting L/W ratio, even if increased, is still below one and, for that reason, further changes in wing geometry are required to improve the lift and avoiding an excessive increase of weight. To reach that result, the span of the inner and the outer part of the wing has been modified, but their sum has been kept constant and equal to the maximum acceptable value of 31 m.

In a first step the span of the inner part has been increased from 4 m to 5 m, while the span of the outer part has been reduced from 7.2 m to 6.2 m [Table 4.5].

Configuration	b_i [m]	b_o [m]	b [m]	c_{ri} [m]	c_{ro} [m]	c_{re} [m]
Fixed 4	5.0	6.2	31.0 m	41.46	11.0	3.61

Table 4.5 - Geometrical data of the configuration F-4

With this configuration the lift to weight ratio is still below one. An additional modification is done, until the Fixed 5 configuration is defined. In this case the L/W is increased and reaches a value equal to one. A higher L/W ratio is difficult to achieve due to the limited wingspan. For that reason the last one has been selected as the final configuration with fixed wing and some analysis on the pitching moment coefficient at different Mach numbers has been executed.

4.1.1 Final fixed wing configuration

The wing geometrical data are reported in Table 4.6 and Table 4.7, while Figure 4.5 and Figure 4.6 show the complete booster configuration.

cri [m]	cro [m]	bi [m]	Leading edge sweep angle [°]
41.46	11.43	6	78.7

Table 4.6 - Geometrical data of the final configuration with fixed wing (inner part)

c_{ro} [m]	c_{re} [m]	b_o [m]	Leading edge sweep angle [°]
11.43	3.42	5.2	57

Table 4.7 - Geometrical data of the final configuration with fixed wing (outer part)

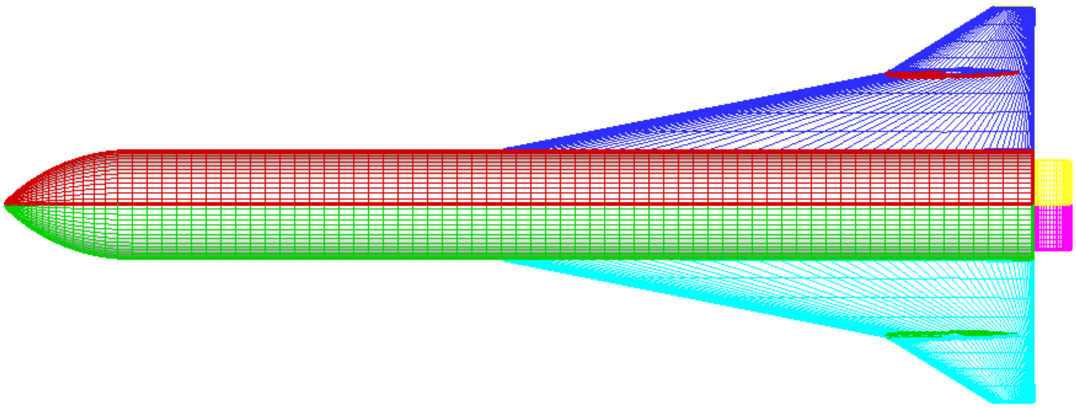

Figure 4.5 - Final configuration with fixed wing (top view)

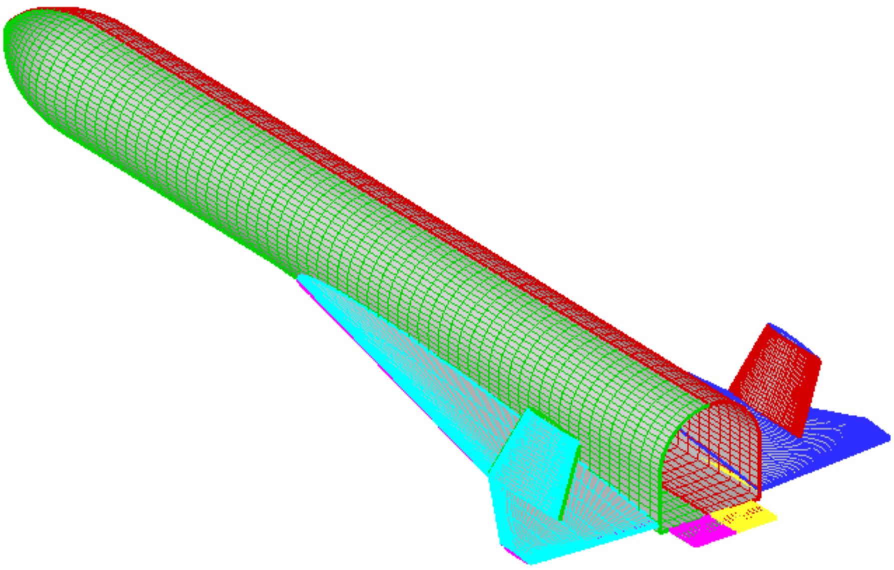

Figure 4.6 - Final configuration with fixed wing (lateral view)

4.1.2 Aerodynamic coefficient analysis

In this section, the existence of a trimmed condition for different angles of attack is investigated. The lift and drag coefficient are also analysed here.

First, it has to be considered that some control surfaces are required for the longitudinal control of the booster during the flight. For what concerns the configuration with a fixed wing, flaps are placed on the wing trailing edge. They occupy the whole wing span, since they stretch from the root to the tip of the wing, as can be seen in Figure 4.7.

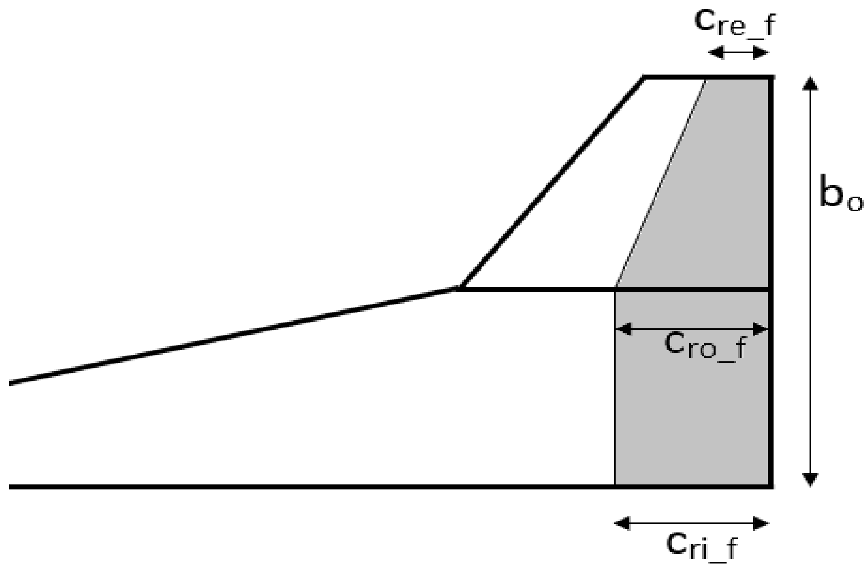

Figure 4.7 - Flap geometry

The flap geometry is adapted to the wing configuration: the first part of the flap has a sweep angle that is equal to zero, while the outer part has a sweep angle of 16°.
The data of the flap final geometry is reported in Table 4.8.

c_{ri_f} [m]	c_{ro_f} [m]	c_{re_f} [m]	b [m]
3	3	1.5	11.2

Table 4.8 - Flap geometrical data

Once the configuration with the fixed wing is designed, the moment coefficient is evaluated at different Mach number.

SUBSONIC

The results for the subsonic regime are reported in the following figures for M=0.2, M=0.4, M=0.6 and M=0.8. Two cases are considered here: the first one, where flaps are not deflected, is shown in Figure 4.8, while the one with a flap deflection equal to -5° is reported in Figure 4.9. From these results, it is possible to see that the fixed wing configuration presents a stable behaviour in subsonic flight. During this part of the mission, the booster is supposed to fly at angles of attack that are usually below 15°. For that reason, a trimmed condition must be assured at this range of angles of attack. With this configuration, a trimmed condition can be found with a deflection of flaps that is limited to angles between 0° and -5°.

The lift coefficient, the drag coefficient and the lift to drag ratio are shown respectively in Figure 4.10, Figure 4.11 and Figure 4.12. The maximum lift to drag ratio generated by the booster with the fixed wing is limited to about 4.5 for angles of attack between 5° and 10°. It also decrease to a value lower than 4 at M=0.8. These results shows limited aerodynamic performance during subsonic. This is due to the short span used in this case.

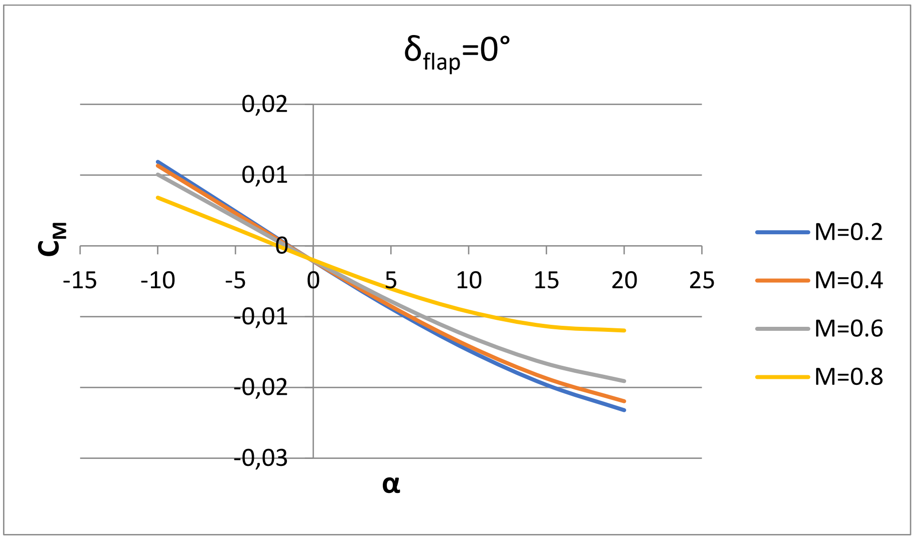

Figure 4.8 - C_M without δ_{flap}=0° (subsonic)

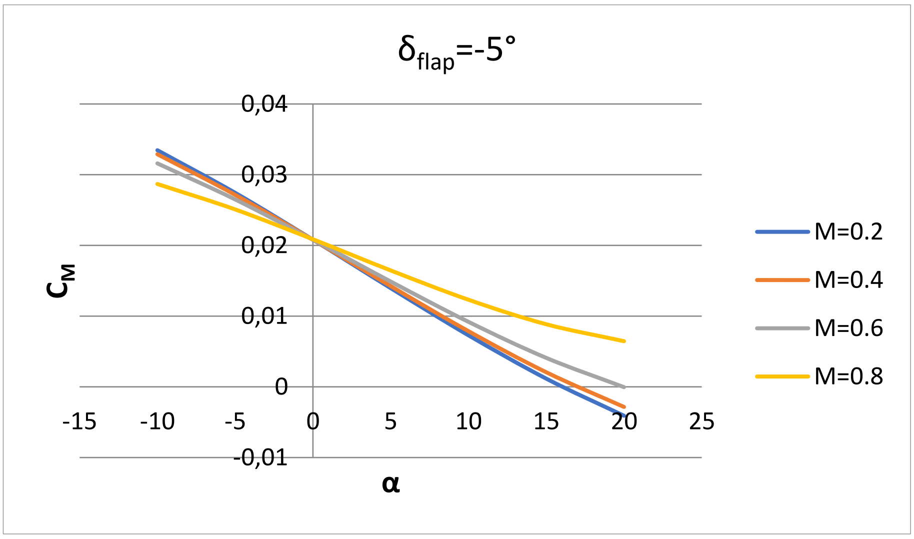

Figure 4.9 - C_M with δ_{flap}=5° (subsonic)

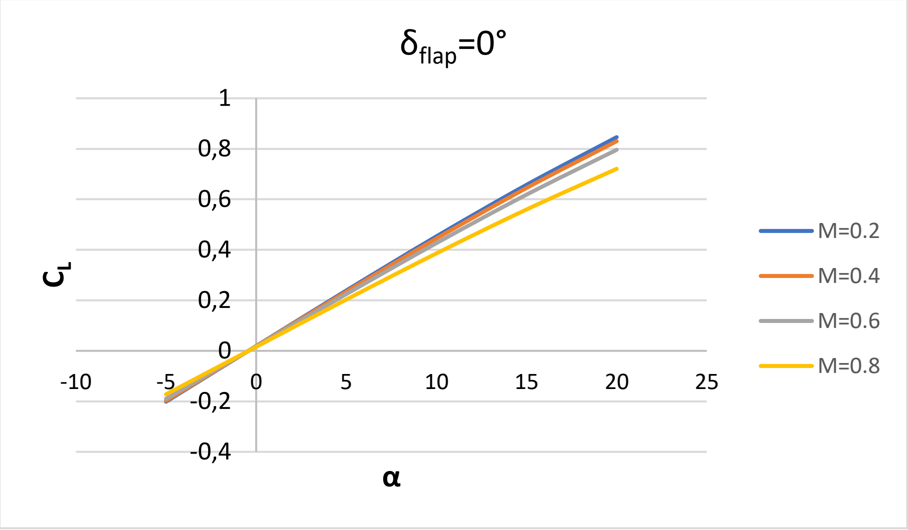

Figure 4.10 - C_L with δ_{flap}=0° (subsonic)

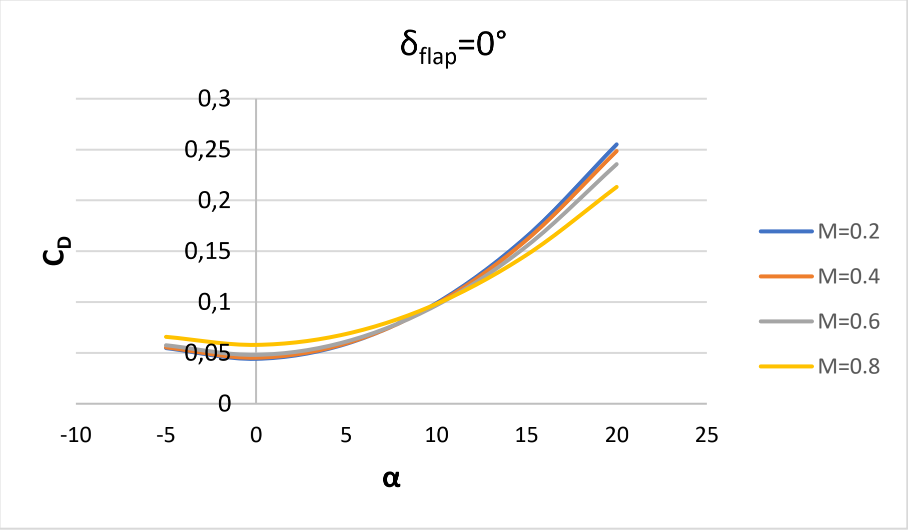

Figure 4.11- C_D with δ_{flap}=0° (subsonic)

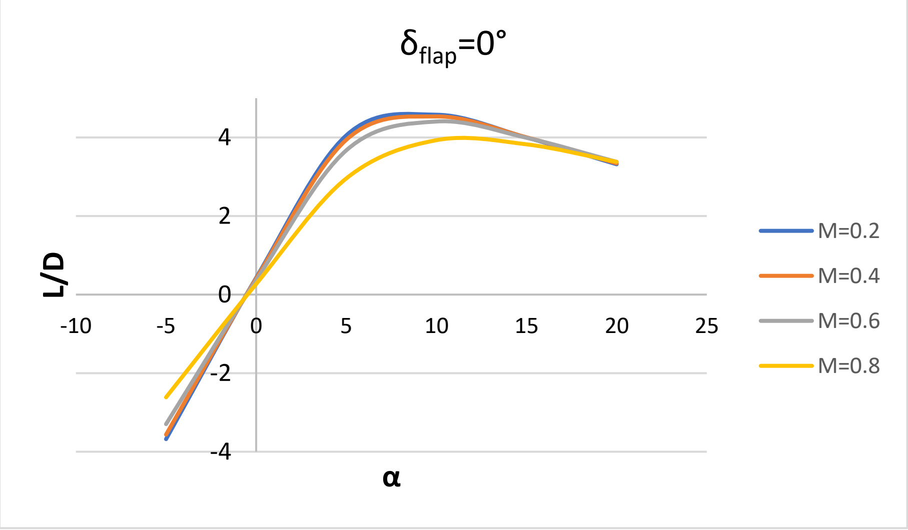

Figure 4.12 - L/D with δ_{flap}=0° (subsonic)

SUPERSONIC

The same analysis is done for the supersonic (M=3, M=3.5 and M=4) and the hypersonic (M=5, M=7, M=9, M=11 and M=13) case. The supersonic results are presented in Figure 4.13, where the flaps are not deflected, and in Figure 4.14, where the angle of flaps is equal to -15°. Figure 4.18 and Figure 4.19 show the results for the hypersonic regime, respectively with a flap deflection of -20° and 25°. In the latter case, the bodyflap is also deflected, with the same angle of the wing flaps. If the Mach number is increased to supersonic values, the results show that the configuration is still stable and trimmable for a range of angles of attack included between 0° and 20°. The latter one is the value of the angle of attack typically valid for supersonic. In this case the flap deflection is up to 15°, a value which is higher than before but still acceptable. Trends of C_L, C_D and L/D are also reported in Figure 4.15, Figure 4.16 and Figure 4.17. The maximum lift to drag ratio is now reduced to approximately 2.4 at an angle of attack of about 10°. If the angle selected for the supersonic part of the descent is considered (α=20°), L/D is reduced to 2.1.

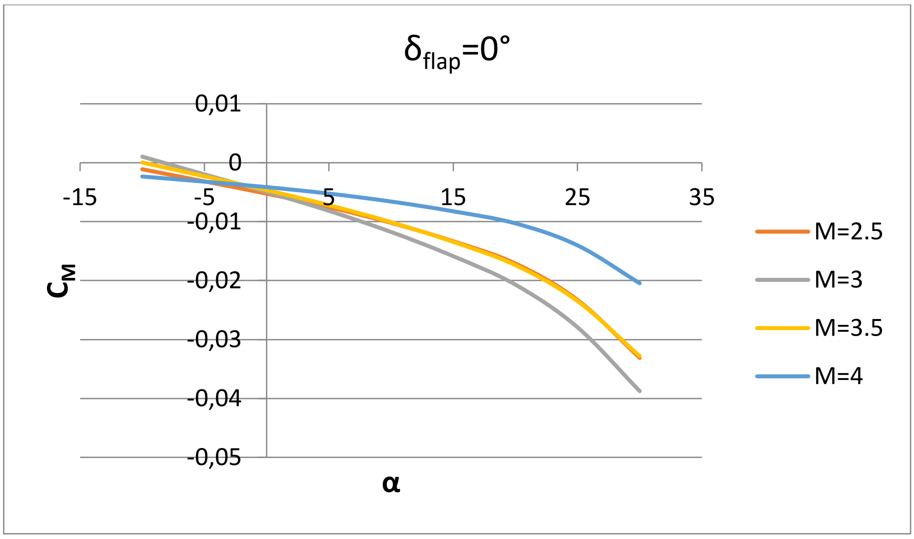

Figure 4.13 - C_M with δ_{flap}=0° (supersonic)

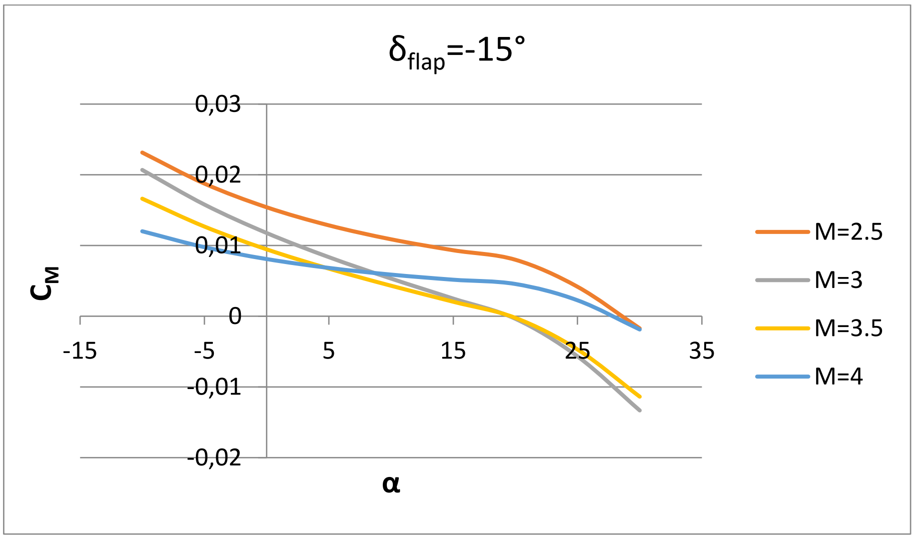

Figure 4.14 - C_M with δ_{flap} =-15° (supersonic)

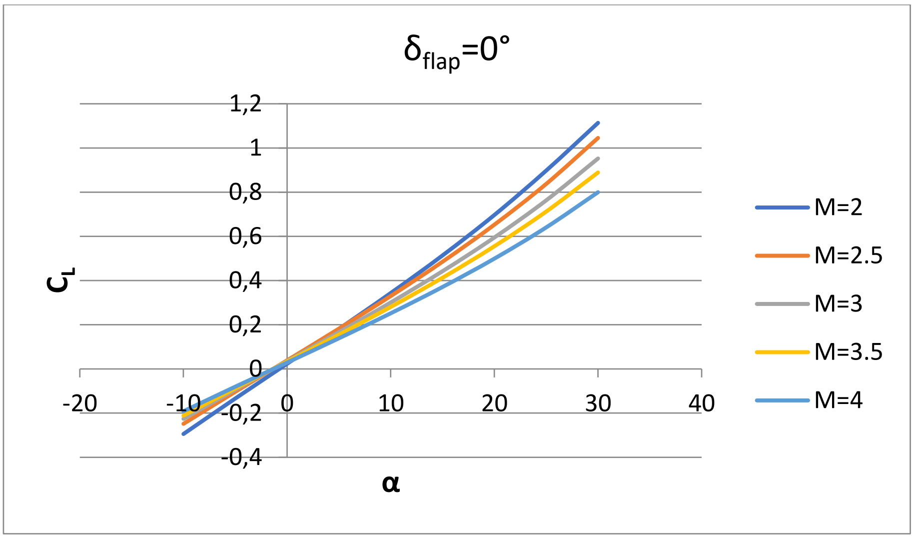

Figure 4.15 - C_L with δ_{flap}=0° (supersonic)

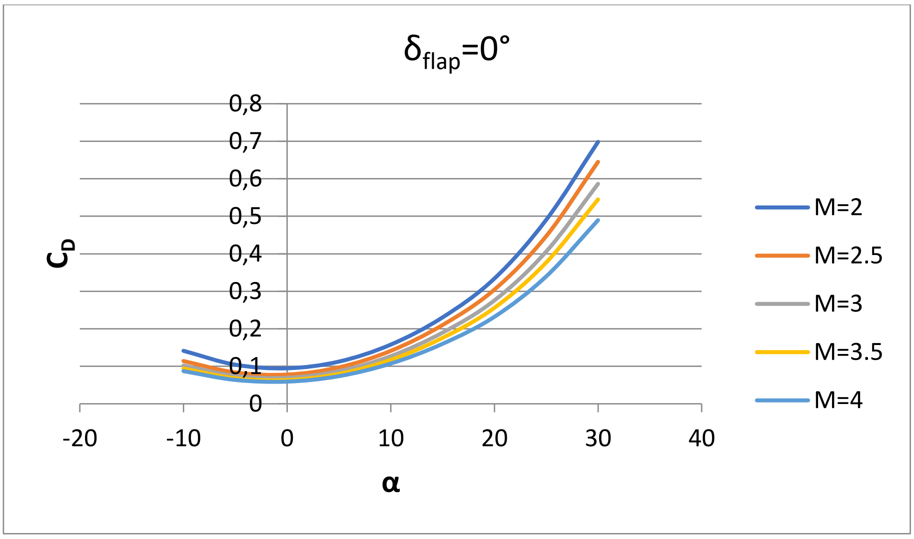

Figure 4.16 - C_D with δ_{flap}=0° (supersonic)

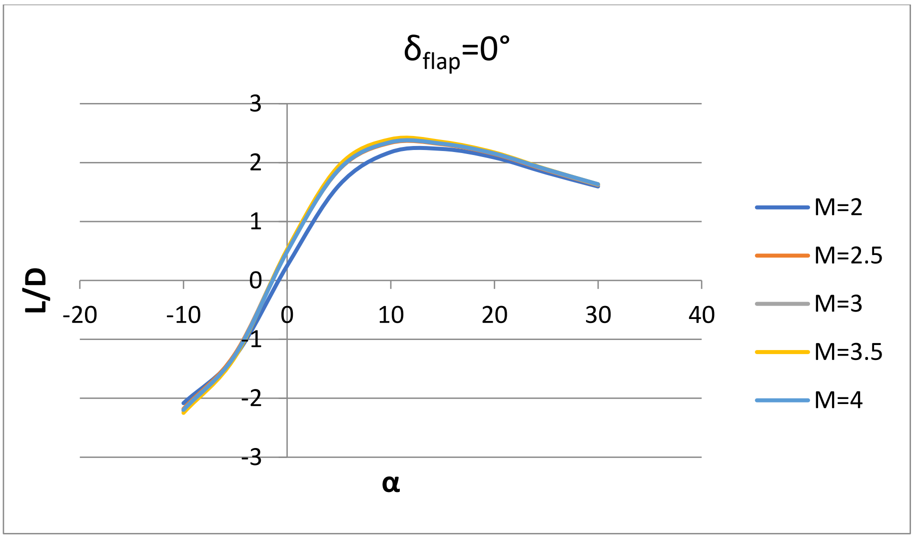

Figure 4.17 - L/D with δ_{flap}=0° (supersonic)

HYPERSONIC

Figure 4.18 and Figure 4.19 show the results for the hypersonic regime, respectively with a flap deflection of -20° and 25°. In the latter case, the bodyflap is also deflected, with the same angle of the wing flaps. Different results are found for hypersonic Mach numbers: the moment coefficient presents a positive slope (unstable) for low angles of attack, while it has a negative slope (stable) for higher α. Since during the hypersonic flight the booster is supposed to fly at high angles of attack, it is possible to assert that this configuration is stable also for this range of Mach numbers. However, this is not completely true for the lower boundary of the hypersonic regime: for M=5 and α=20° the C_M trend has a slightly positive slope. Here, the flap deflection is increasing up to 25°.

In Figure 4.20, Figure 4.21 and Figure 4.22 the results for the lift coefficient, the drag coefficient and the lift to drag ratio are displayed.

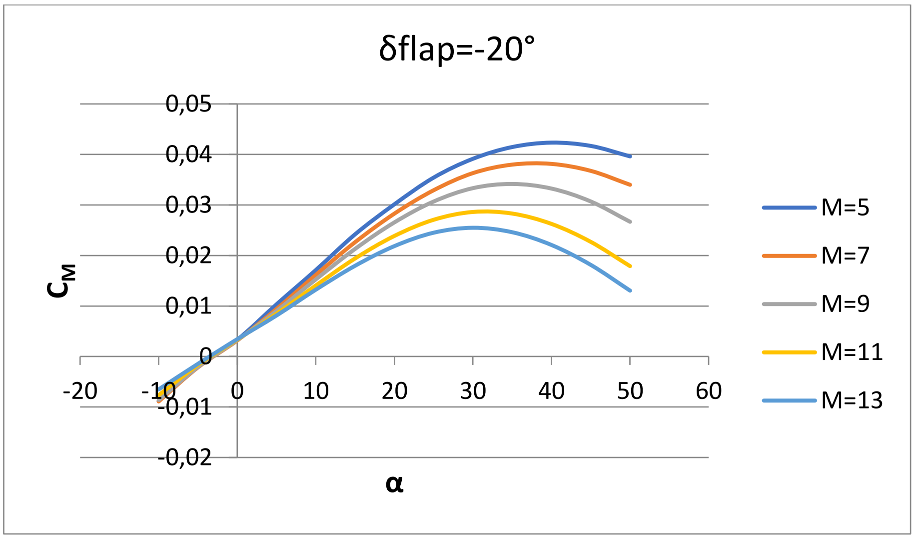

Figure 4.18 - C_M with δ_{flap}=-20° (hypersonic)

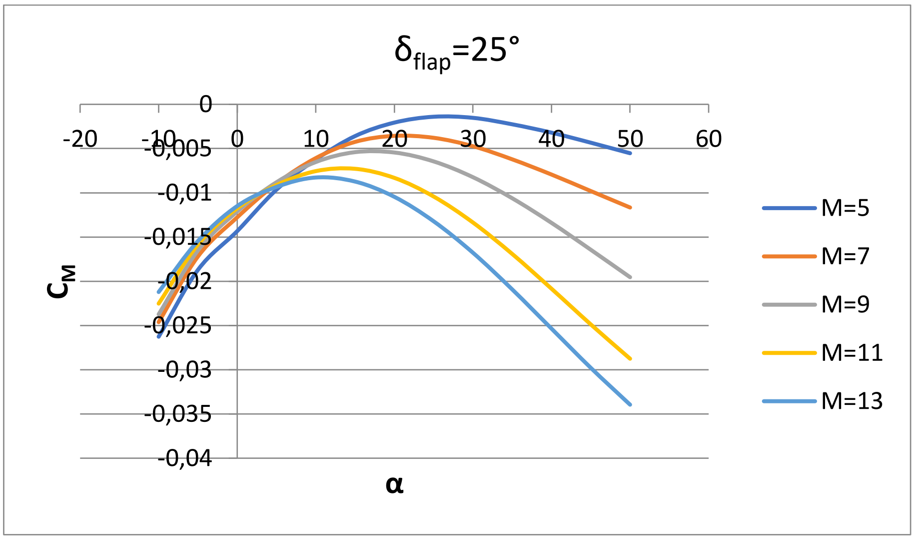

Figure 4.19 - C_M with δ_{flap}=25° (hypersonic)

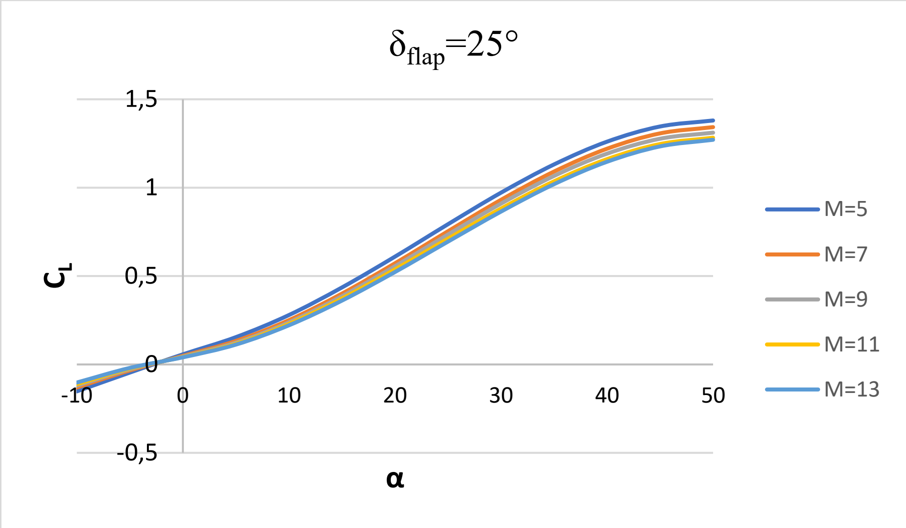

Figure 4.20 - C_L with δ_{flap}=25° (hypersonic)

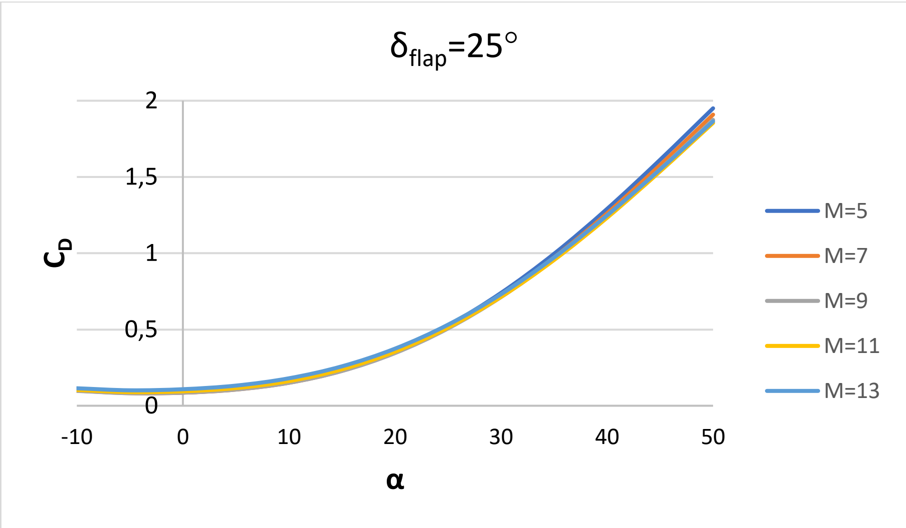

Figure 4.21 - C_D with δ_{flap}=25° (hypersonic)

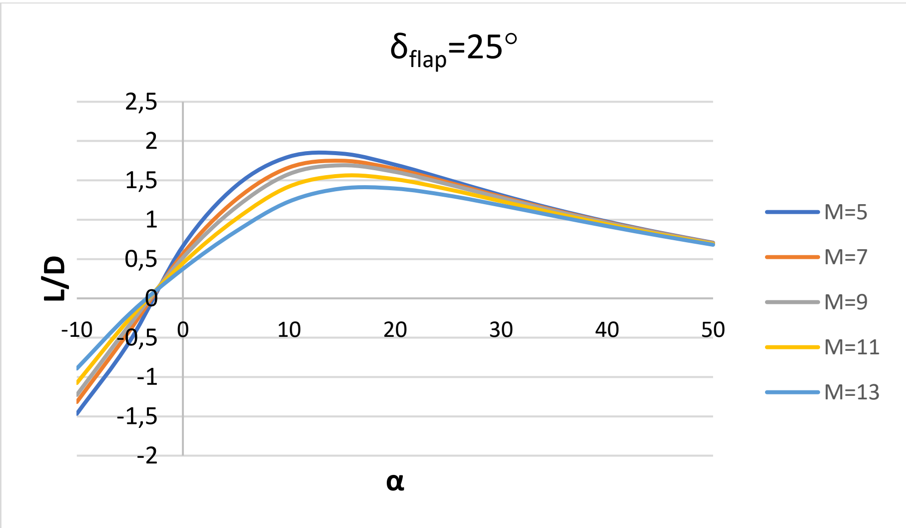

Figure 4.22 - L/D with δ_{flap}=25° (hypersonic)

4.2 Variable sweep wing configuration

Since the constraint on the maximum wing span is referred to the hypersonic flight only, a valid solution that can be adopted to overcome this limitation is represented by a variable wing. With this wing type the span can be changed throughout the mission. In particular, during hypersonic flight it is reduced to a value lower than 31 m, while for subsonic flight its value can be higher, since no limitation on the wing span exists. Moreover, a high aspect ratio is needed at low speed to improve the aerodynamic performance of the booster. This leads to choose a different wing span according to the Mach regime.

In this section, a variable sweep wing is considered. The process that leads to the definition of the wing final geometry is illustrated here. The final configuration is described later in section 4.2.1 , with particular attention on the additional constraints that arise while using a variable wing.

The variable sweep wing is composed of two parts: the inner one is fixed, while the outer is able to rotate and can be stored inside the inner part. The movable part of the wing is supposed to take only two different positions: deployed (1) or stored (2) as shown in Figure 4.23. Position 1, which is characterized by a higher span, is used during subsonic flight. Position 2, instead, is used for hypersonic flight.

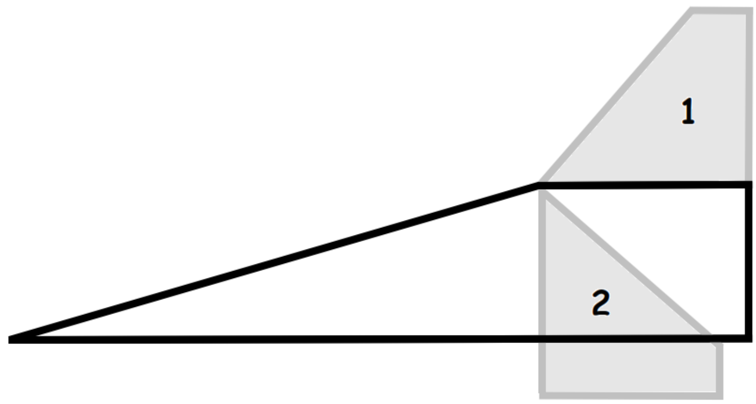

Figure 4.23 - Two wing positions

First, dimensions of both the inner and the outer part have been modified in order to achieve the best performances during the tow-back flight. A method similar to the one used for the fixed wing configurations is adopted here. The geometrical input are similar with the ones used for the fixed wing configuration. Here, two values for the wing span are defined, according to the two possible positions the wing can adopt. A scheme representing each geometric parameter is shown in Figure 4.24.

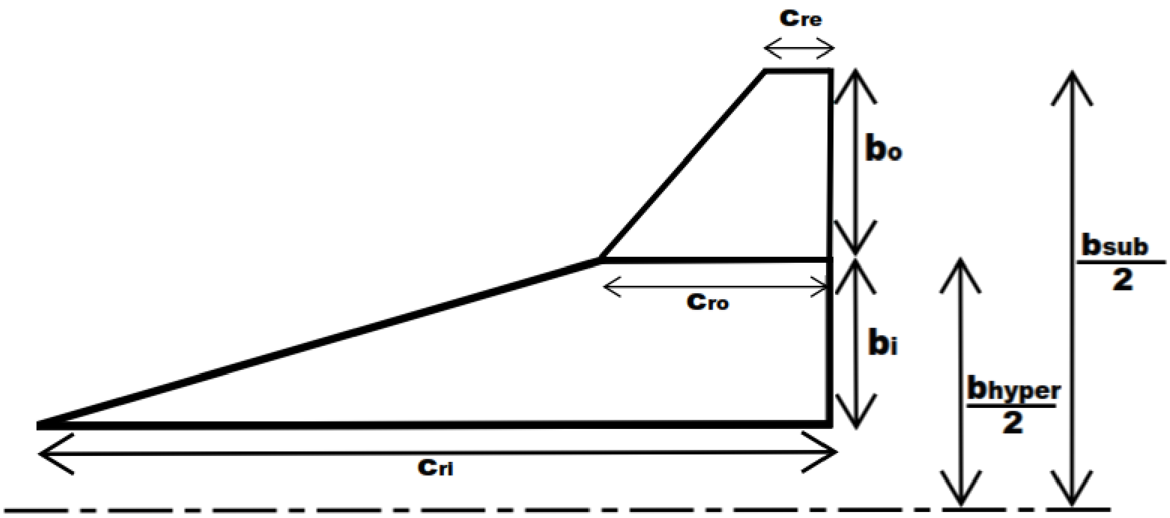

Figure 4.24 - Wing geometry

Five different configurations have been designed for what concerns the case of the variable wing. The L/D, L/W and T/D ratios are compared in Table 4.9 for five different configurations with variable wings. The nomenclature for the different configurations is similar to the one used before (Variable wing→V).

	Variable 1	Variable 2	Variable 3	Variable 4	Variable 5
L/D	9.84	10.09	9.41	9.07	9.22
L/W	0.89	0.88	1.07	1.39	1.20
T/D	3.21	3.21	2.42	1.78	2.10
m_p [kg]	126 132	122 450	133 884	141 414	138 101

Table 4.9 - Tow-back flight performances for variable wing configurations

At the beginning of the study, some wings with a very short inner part are considered. In this case the span is reduced to 20 m during hypersonic. This value is chosen to investigate the possibility to use a very short span and, as a consequence, to try to reduce the mass as much as possible. Two configurations with the same span of 20 m for hypersonic and 40 m for the subsonic are presented here, as an example.

Configuration V-1

The first configuration studied is shown in Figure 4.25 and its geometrical data are reported in Table 4.10.

Configuration	V-1
b_i [m]	5.7
b_o [m]	10.0
$b_{hypersonic}$ [m]	20.0
$b_{subsonic}$ [m]	40.0
c_{ri} [m]	31.27
c_{ro} [m]	10.00
c_{re} [m]	2.46

Table 4.10 - Geometrical data of the configuration V-1

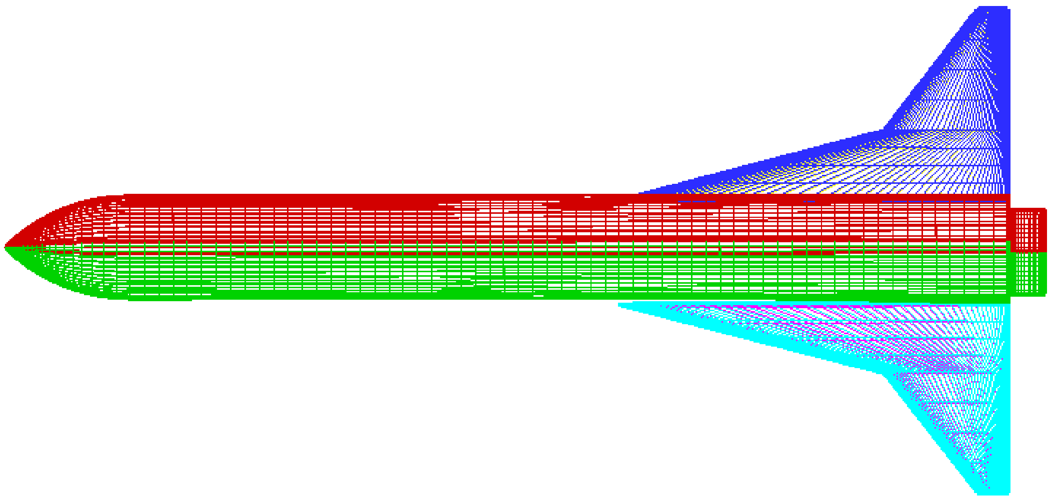

Figure 4.25 - Configuration V-1

Configuration V-2

The second configuration presents the same span of the previous one, while the geometry of the wing is slightly changed [Figure 4.26]. The only differences are the length of the root chord of the inner part and the leading edge sweep angle, as can be seen in Table 4.11. However, in both cases the resulting L/W is of approximately 0.9: for that reason a span increase is required.

	Root chord [m]	Leading edge sweep angle [°]	Tip chord [m]
V-1	31.27	75.0	10.0
V-2	27.10	72.0	10.0

Table 4.11 - Geometrical data comparison of the configurations V-1 and V-2

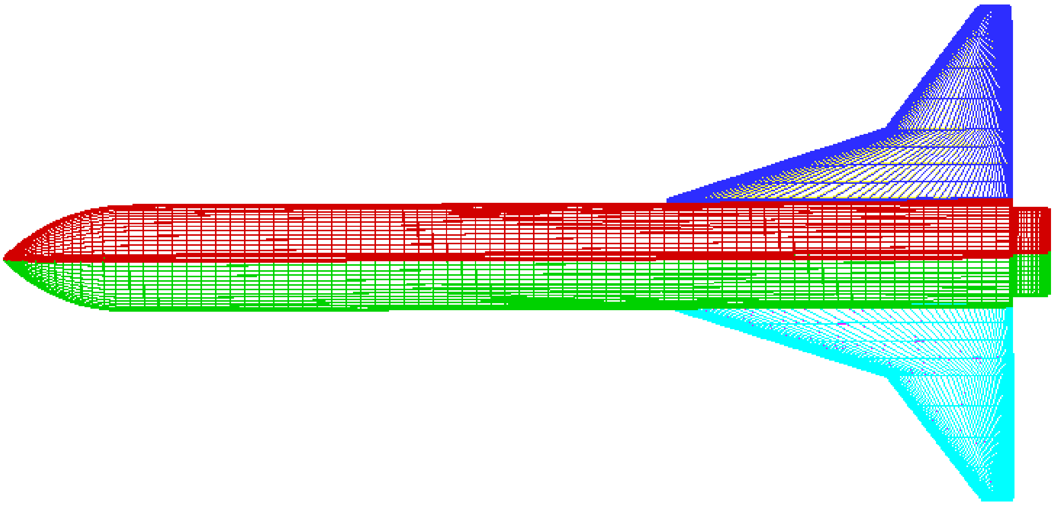

Figure 4.26 - Configuration V-2

Configuration V-3

The next configuration is renamed as V-3 and it is shown in Figure 4.27.

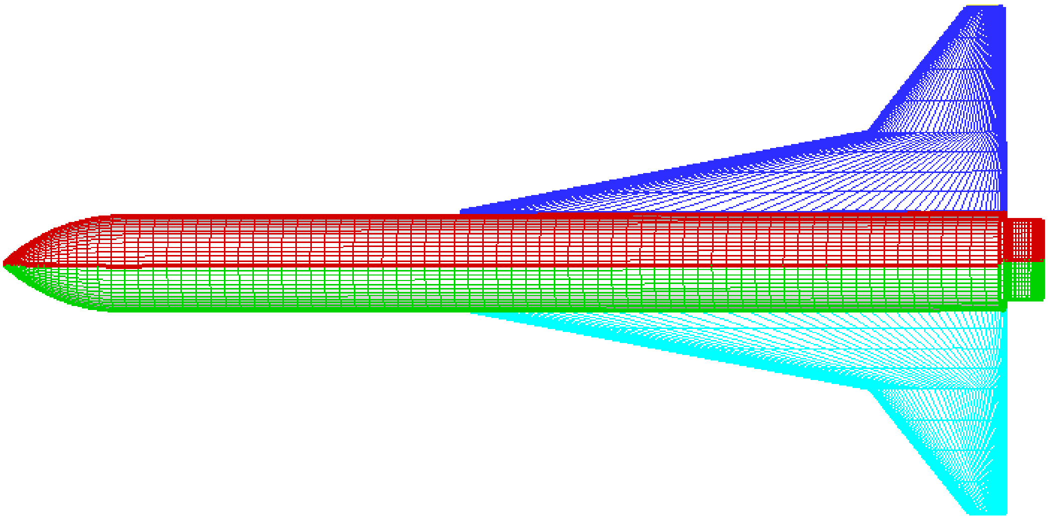

Figure 4.27 - Configuration V-3

Configuration	V-3
b_i [m]	7.0
b_o [m]	10.5
$b_{hypersonic}$ [m]	22.6
$b_{subsonic}$ [m]	44.6
c_{ri} [m]	43.93
c_{ro} [m]	11.00
c_{re} [m]	3.09

Table 4.12 - Geometrical data of the configuration V-3

The wing span is increased to 22.6 m for the inner part, while it is equal to 44.6 m for the whole wing. The complete geometrical data are presented in Table 4.12. The bigger span produces some positive effects on the lift and the L/W reaches the value of 1.07. However, the wing dimensions raise produces also an increase in drag: for that reason both L/D and T/D ratios become lower than before.

Configuration V-4

A further modification on the wingspan is carried on, in order to verify if some other improvements can be achieved. First the span is increased from 7 m to 9 m for the inner part and from 10.5 m to 12.5 m for the outer part. This is the configuration V-4, that is shown in Figure 4.28.

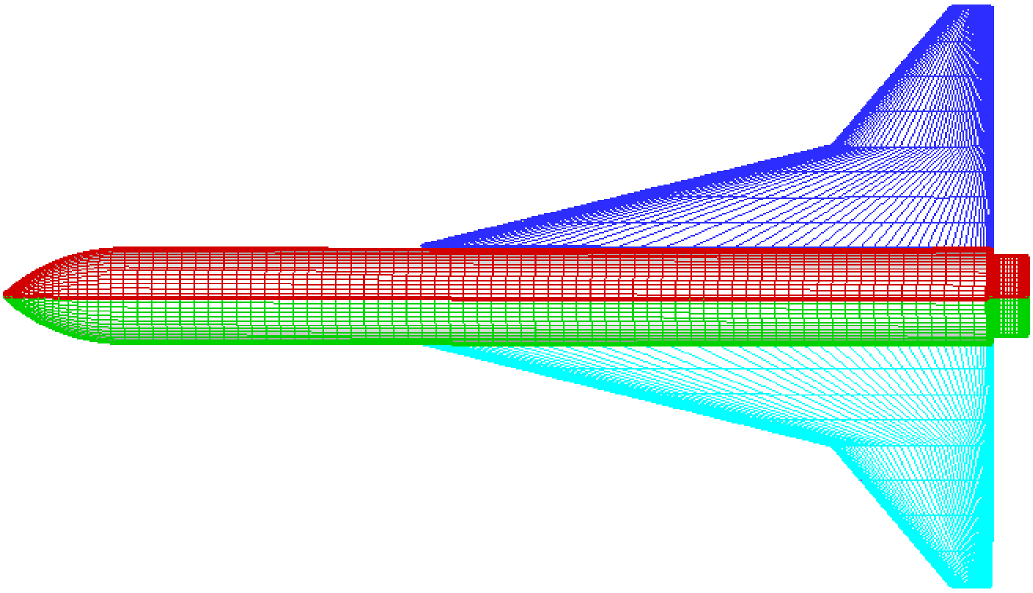

Figure 4.28 - Configuration V-4

The geometrical data are presented in Table 4.13. An even larger increase in wing dimensions is considered here and in this case L/W reaches a value of 1.39. Again, both L/D and T/D are decreasing: in particular T/D is reduced to 1.78.

Configuration	*V-4*
b_i *[m]*	*9.0*
b_o *[m]*	*12.5*
$b_{hypersonic}$ *[m]*	*26.6*
$b_{subsonic}$ *[m]*	*51.6*
c_{ri} *[m]*	*46.59*
c_{ro} *[m]*	*13.00*
c_{re} *[m]*	*3.23*

Table 4.13 - Variable 4 configuration geometrical data

Configuration V-5

The configuration V-5 presents a span that is between the values of the last two configurations considered. This configuration is shown in Figure 4.29.

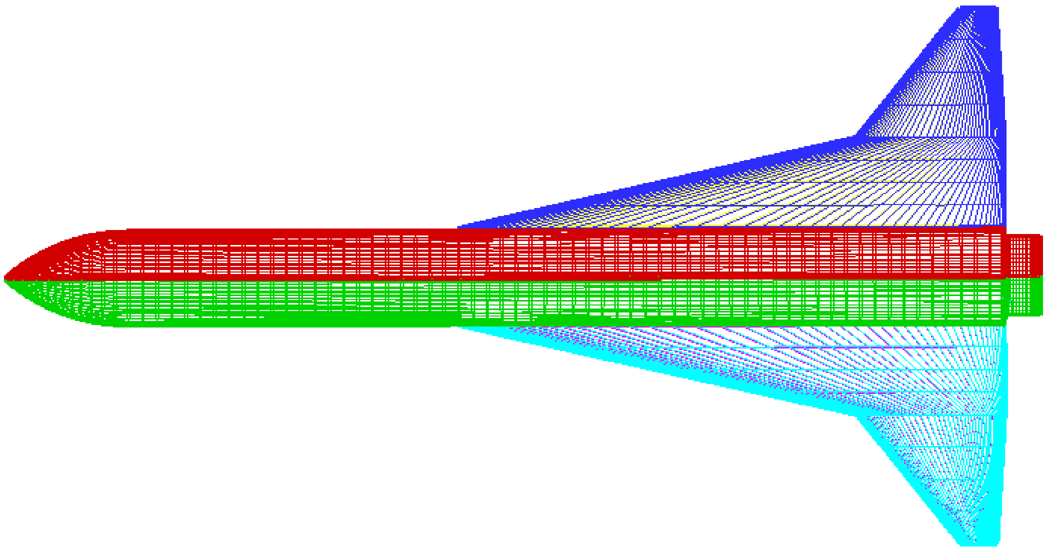

Figure 4.29 - Configuration V-5

Its geometrical data are presented in Table 4.14. The inner span is equal to 8 m, while the outer span is 11.5 m. The L/D reaches the value of 1.20 and T/D is equal to 2.10.

Configuration	Variable 5
b_i [m]	8.0
b_o [m]	11.5
$b_{hypersonic}$ [m]	24.6
$b_{subsonic}$ [m]	47.6
c_{ri} [m]	44.09
c_{ro} [m]	12.00
c_{re} [m]	2.96

Table 4.14 - Geometrical data of the configuration V-5

Since the last three configurations show good performance characteristics during the tow-back flight, some other considerations need to be done in order to choose the best one among them. V-3 is the smallest one and it guarantees a saving in terms of mass, but it provides the lowest performances for what concerns L/W. The opposite can be said about V-4, which has the highest L/W, but its wing is quite large with respect to the other configuration. The performances of the configuration V-5, instead, presents a value of L/D that is included between the values of the other two configurations. Since there is the need to keep the mass as lower as possible, configuration V-4 is not taken into account for further analysis. For that reason, the pitching moment coefficient is studied only for the two configurations V-3 and V-5.

The analysis of the moment coefficient is presented here, for both the configurations that have been selected previously. First the configuration V-3 is studied. Its flap geometric data are reported in Table 4.15.

Root chord length [m]	*Tip chord length [m]*	*Span [m]*
5	*5*	*7*

Table 4.15 - Variable 3 configuration flap data

SUBSONIC

The moment coefficient is evaluated for the subsonic regime at M=0.2, M=0.4, M=0.6 and M=0.8. The results are shown in Figure 4.30 and Figure 4.31. This configuration is stable during subsonic flight and a trimmed condition is guaranteed for angles of attack below 15°. Indeed, if a flap deflection of 5° is selected, the trimmed condition is verified for $\alpha \approx -5°$, while if $\delta_{flap} = -15°$ the trimmed condition is found for $\alpha \approx 15°$.

Flaps used for the configuration V-5 have the same chord of the previous case. However, since this configuration is bigger than the other, their span is higher and equal to 8 m. Once the flaps are defined, the moment coefficient is evaluated and the results are illustrated in Figure 4.32 and Figure 4.33. It can be seen that this configuration is also stable, with a trend of the moment coefficient that is similar to the one found before. The same range of flap deflections is needed to find a trimmed condition at $\alpha < 15°$.

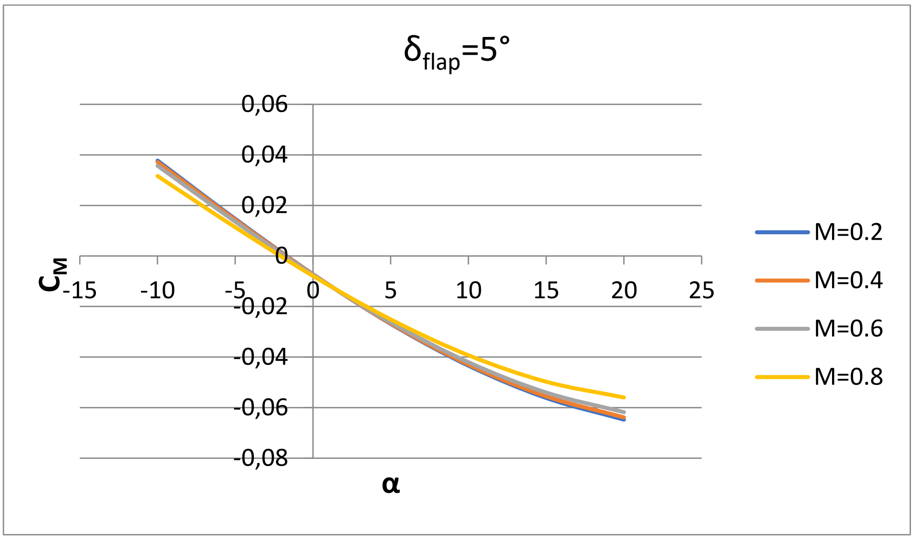

Figure 4.30 - C_M with δ_{flap}=5° (Subsonic – V-3)

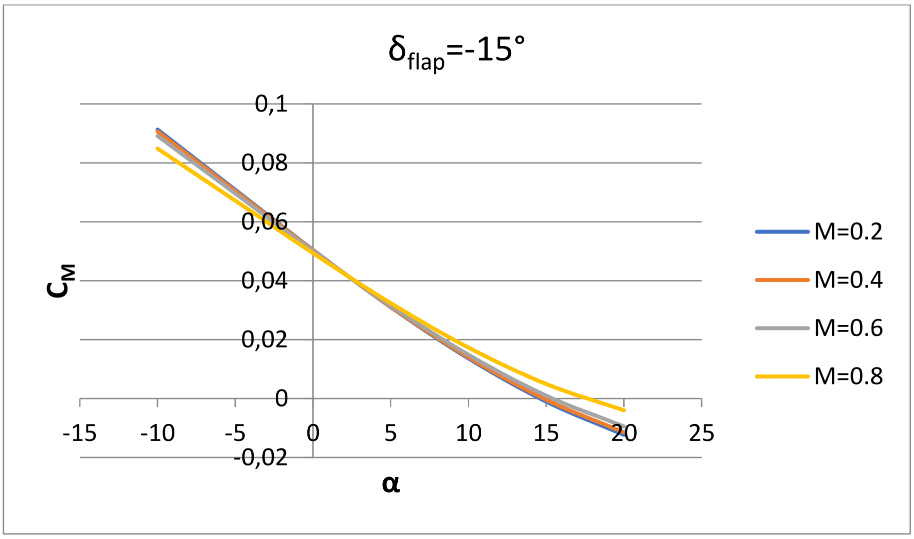

Figure 4.31 - C_M with δ_{flap}=-15° (Subsonic – V-3)

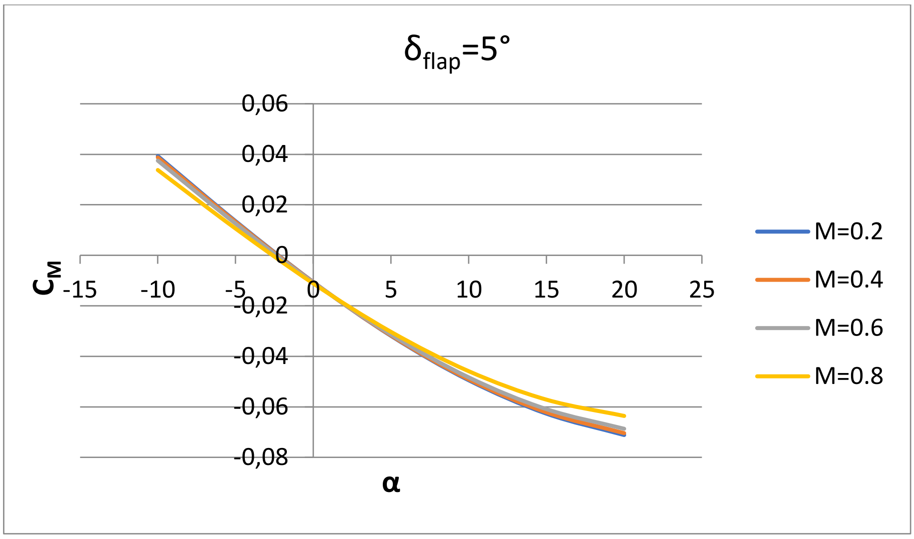

Figure 4.32 - C_M with δ_{flap}=5° (Subsonic – V-5)

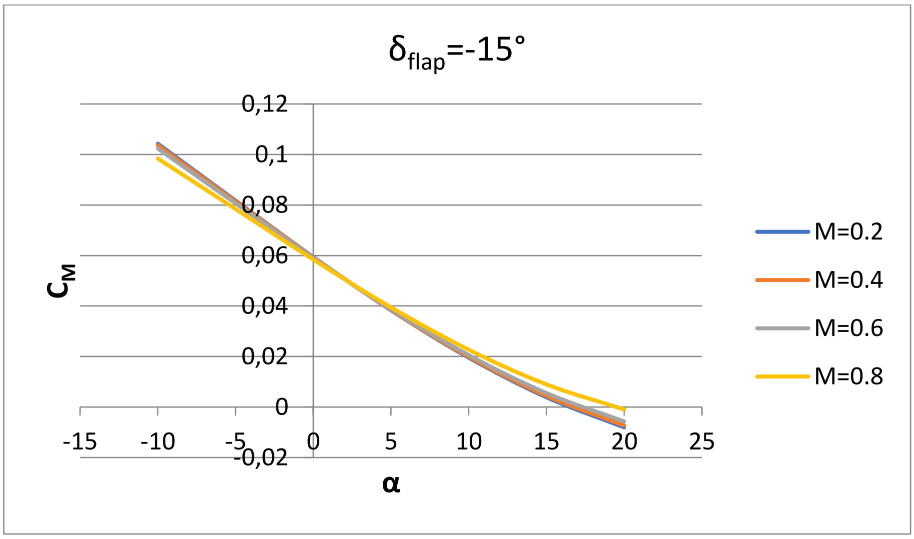

Figure 4.33 - C_M with δ_{flap}=-15° (Subsonic – V-5)

SUPERSONIC

A similar analysis is done for the supersonic speed range. The results obtained for the configuration V-3 are shown in Figure 4.34 and Figure 4.35. In this case, it is possible to find a trimmed condition for angles of attack of about 20°, with a flap deflection between 5° and 15°. The trend of the moment coefficient is different with respect to the subsonic regime, since this configuration presents an almost neutral behaviour during supersonic flight. A stable condition, indeed, cannot be found even if the flap dimension is increased. Similar results are found for the other configuration (V-5). The only major difference is that smaller flap deflections ($0° < \delta_{flap} < 5°$) are required to have C_M=0.

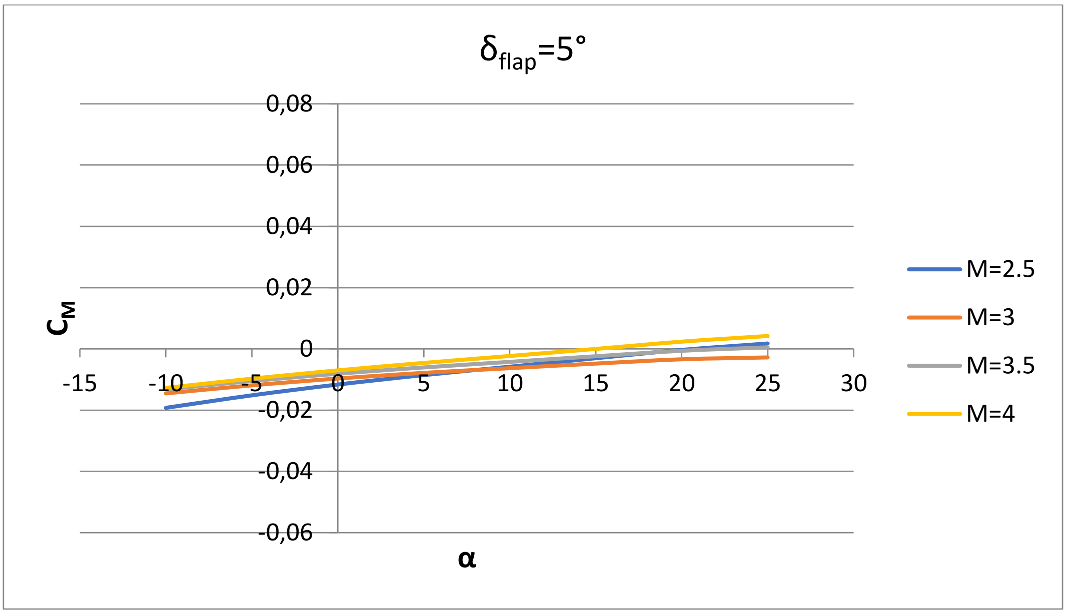

Figure 4.34 - C_M with δ_{flap}=5° (Supersonic – V-3)

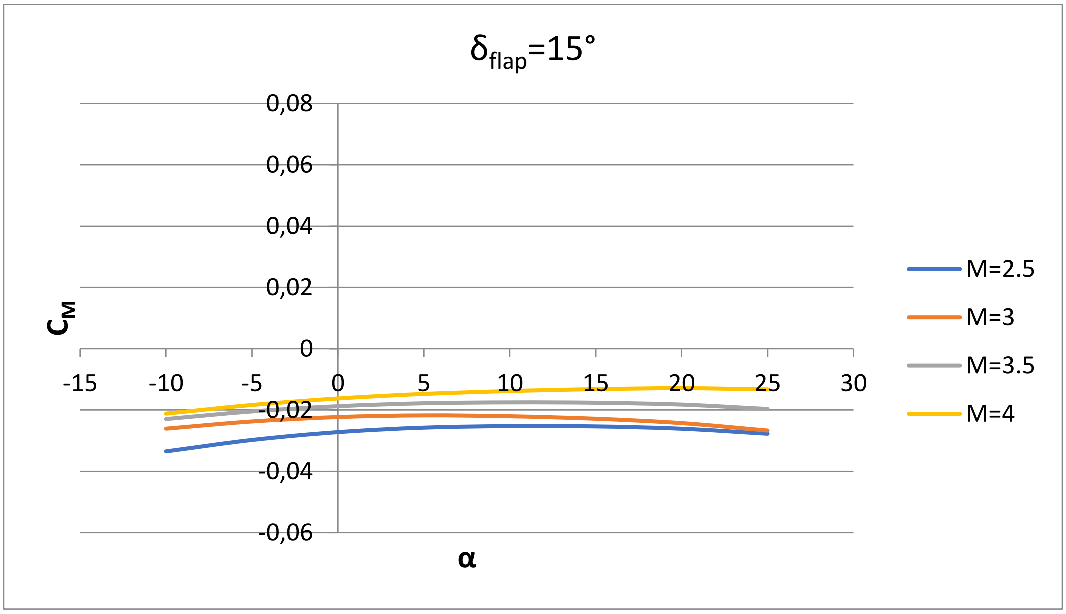

Figure 4.35 - C_M with δ_{flap}=15° (Supersonic – V-3)

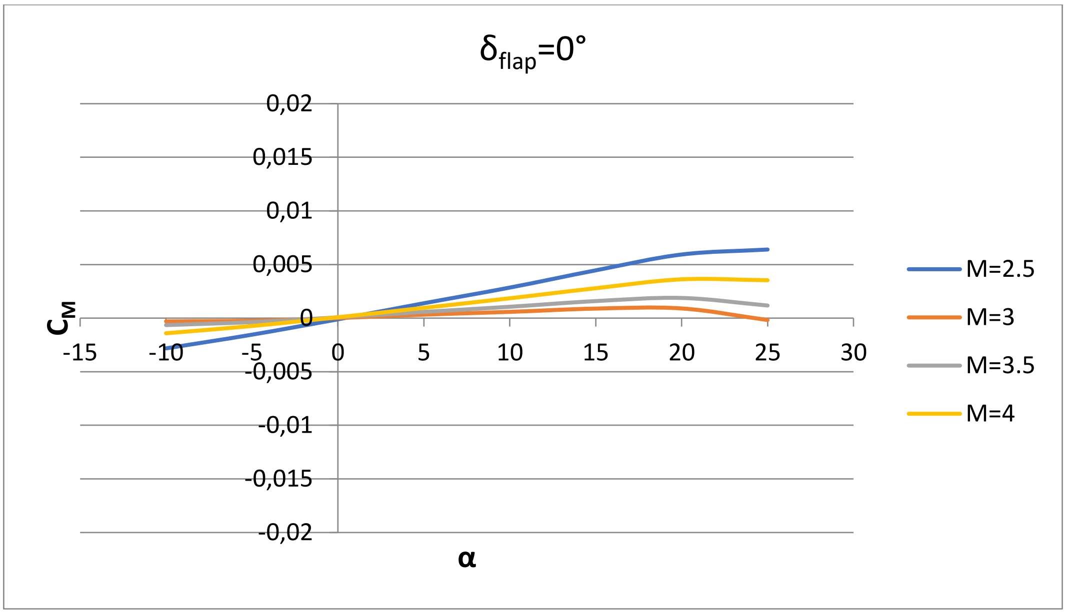

Figure 4.36 - C_M with δ_{flap}=0° (Supersonic – V-5)

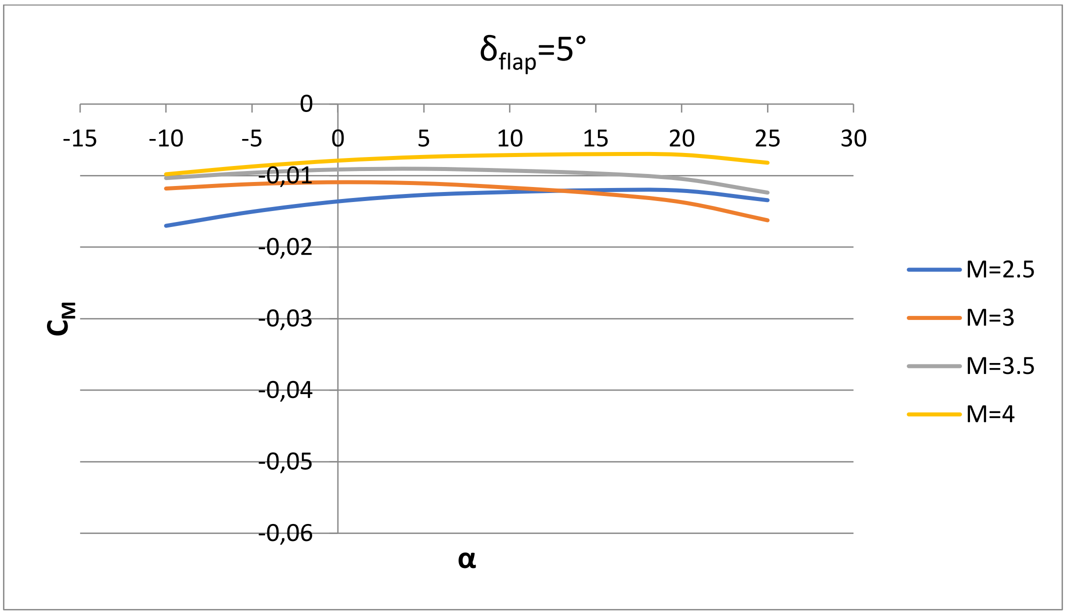

Figure 4.37 - C_M with δ_{flap}=5° (Supersonic – V-5)

HYPERSONIC

For the hypersonic speed range the trend of the moment coefficient is different. The curve representing the C_M has a positive slope and an unstable behaviour for low angles of attack, while it presents a negative slope for higher α. However, the booster is supposed to flight at angles of attack that are included between 20° and 50° during this part of the mission. For that reason, it is possible to say that both configurations V-3 and V-5 have a trimmed and stable condition for M≥5.

Here, the flap deflection needed is increasing up to 25°. For δ_{flap}>0°, it must be highlighted that the bodyflap is also deflected during hypersonic flight, as an additional control surface. In Figure 4.38 and Figure 4.39 the results found with V-3 are reported, while in Figure 4.40 and Figure 4.41 the results valid for V-5 are shown.

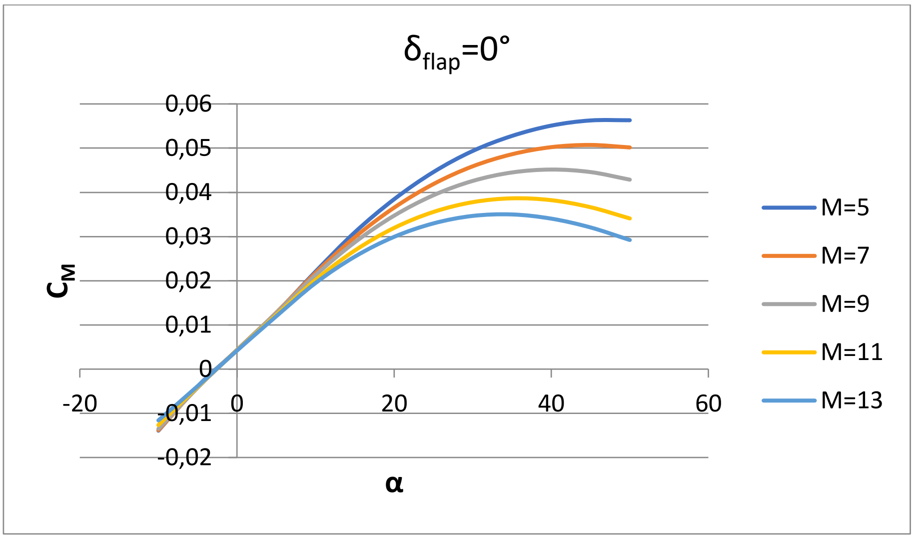

Figure 4.38 - C_M with δ_{flap}=0° (Hypersonic – V-3)

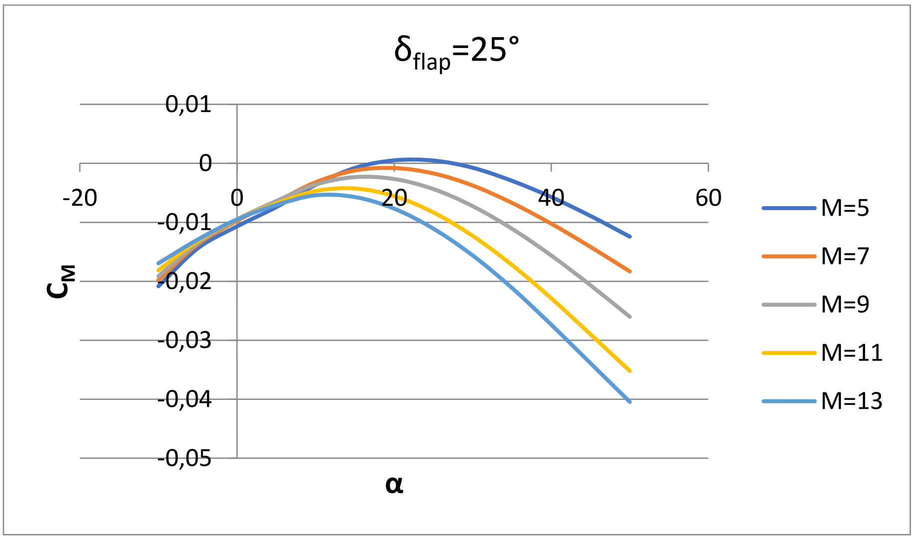

Figure 4.39 - C_M with δ_{flap}=25° (Hypersonic – V-3)

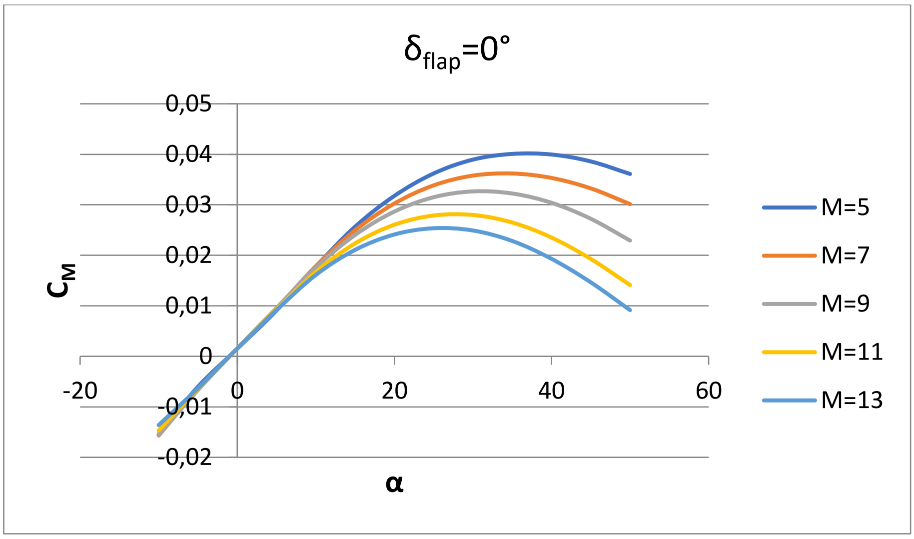

Figure 4.40 - C_M with δ_{flap}=0° (Hypersonic – V-5)

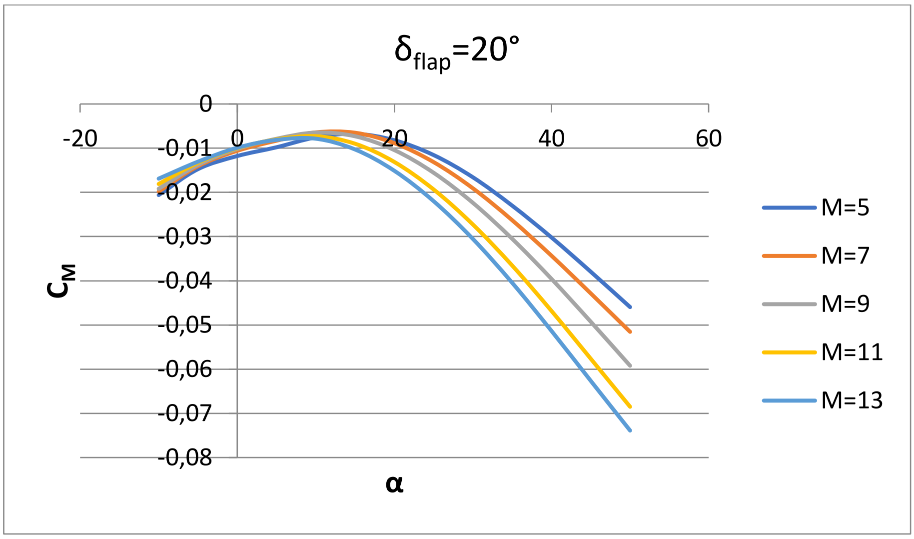

Figure 4.41 - C_M with δ_{flap}=20° (Hypersonic – V-5)

4.2.1 Final variable wing configuration

No major differences arise from the comparison between the moment coefficient of these two configurations. However, since Variable 3 presents the advantage of a lower mass and a smaller geometry, it has been selected as the best one between the two studied here.

Once the configuration with variable wing is defined, it is possible to evaluate its trajectories and its thermal protection system. This part of the study is described in detail in the next chapter of this thesis. However, it is important to highlight here that these results have an impact on the geometry of the wing. Once the TPS is computed, indeed, it can have an effect on the position of the centre of gravity and consequently on the moment coefficient. This is exactly what it is found in this case: the centre of gravity shifts to a rearward position and a trimmed and stable condition is no more guaranteed during hypersonic flight. For that reason some modifications on the wing geometry are needed and it has been further modified to fulfil this requirement.

The final geometry is described here, with particular attention on the additional issues and constraints that arises if a variable wing is used. This configuration has been renamed as SpaceLiner Booster 8-3.

Wing structure

A general description of the wing structure is presented in this section. The wing is divided into two parts:

1. Inner part which is fixed;
2. Outer part which is able to rotate;

The geometric data of both the inner and the outer part of the wing are presented respectively in Table 4.16 and Table 4.17. In Figure 4.42 a plan view of the wing is shown.

Root chord [m]	Semi-span [m]	Leading edge sweep angle [°]	Tip chord [m]
41.93	8.90	73.60	11.69

Table 4.16 - Geometrical data of the variable wing (inner part)

Root chord [m]	Semi-span [m]	Leading edge sweep angle [°]	Tip chord [m]
11.69	10	40	3.30

Table 4.17 - Geometrical data of the variable wing (outer part)

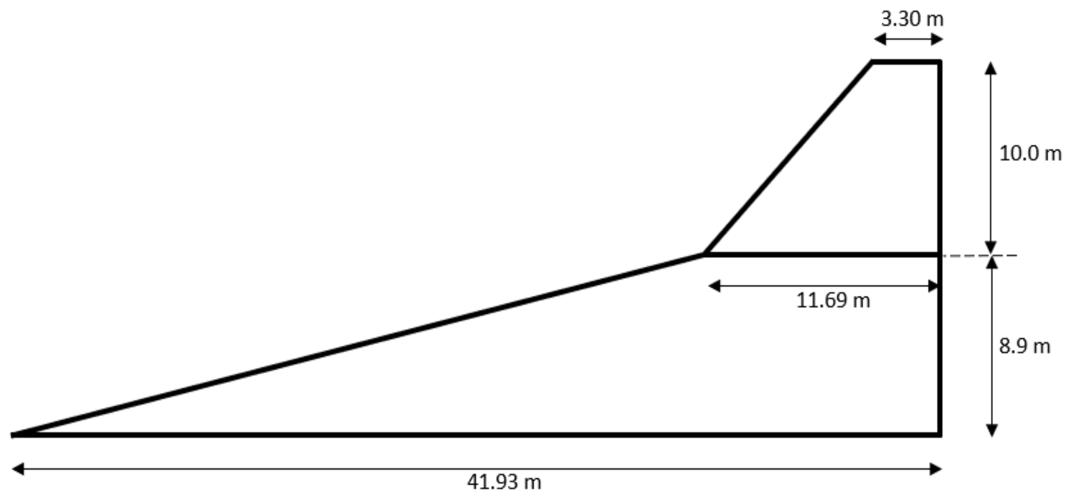

Figure 4.42 - Plan view of the wing

Two positions for the variable wing are identified, one for the subsonic flight and the other one for the supersonic/hypersonic flight. The rotation of the outer part is shown in Figure 4.43, Figure 4.44 and Figure 4.45.

Since there are no limitations on span during subsonic flight, the wing can be fully deployed as can be seen in Figure 4.46. The wingspan is now equal to 46.4 m: the very large surface of the wing, with respect to the dimension of the inner part only, provides better performances for this flight regime. The subsonic performances for the tow back flight are evaluated again and they are reported in Table 4.18:

L/D	L/W	T/D
8.81	1.48	1.64

Table 4.18 - Tow-back flight performances

Even if the wing has been modified, L/D, L/W and T/D ratios still presents acceptable value. In particular, while the L/W is increasing thanks to the bigger wing surface, the T/D is reduced due to the increased drag.

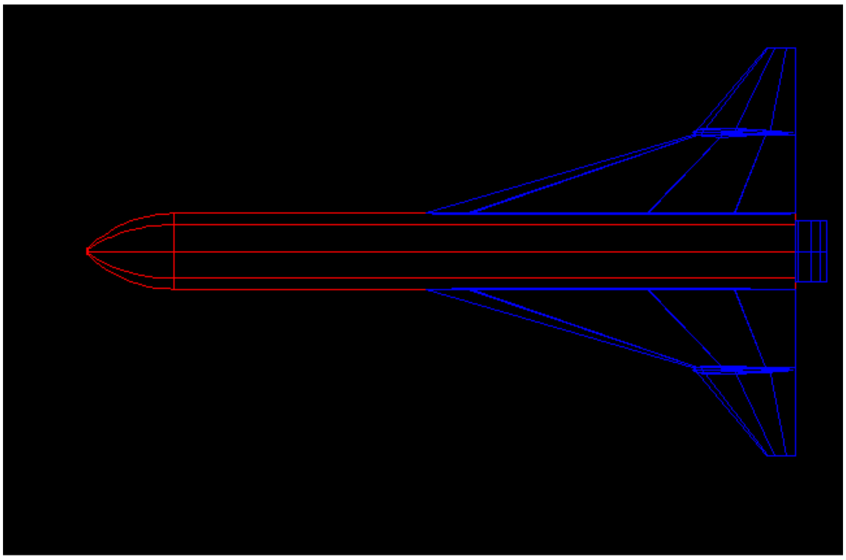

Figure 4.43 - Outer part rotation (deployed)

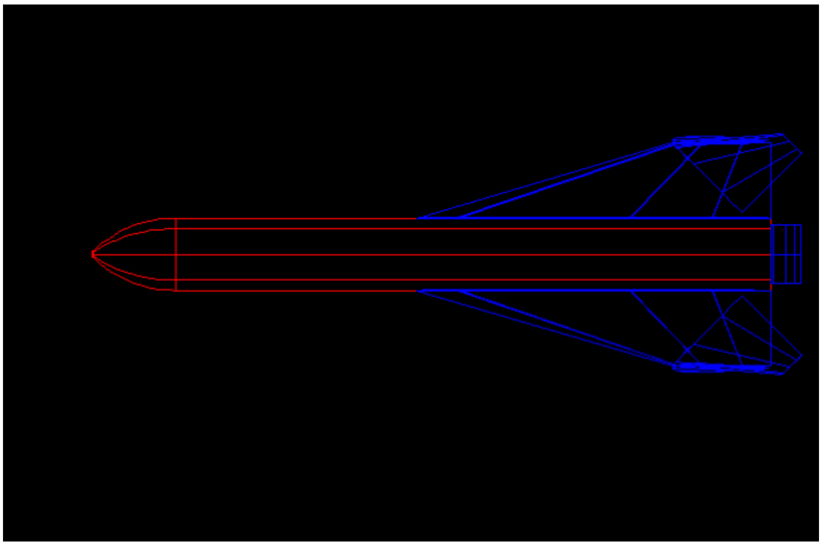

Figure 4.44 - Outer part rotation (45°)

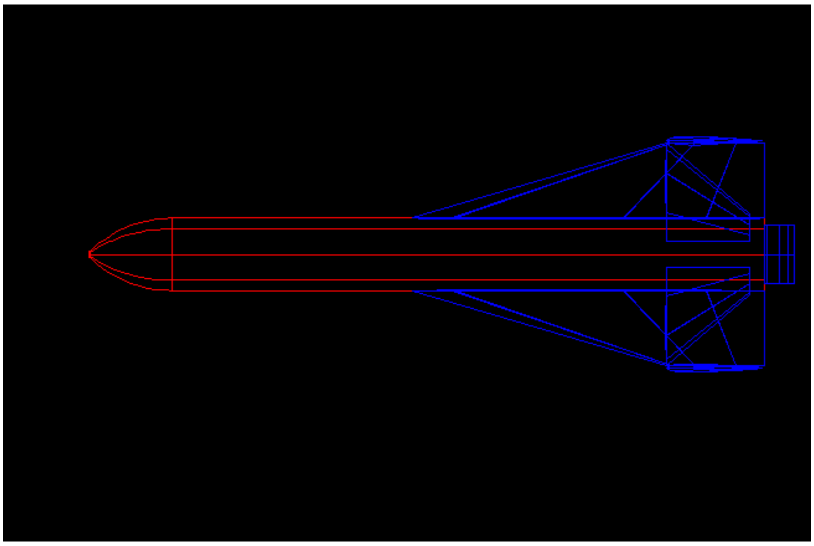

Figure 4.45 - Outer part rotation (stored inside)

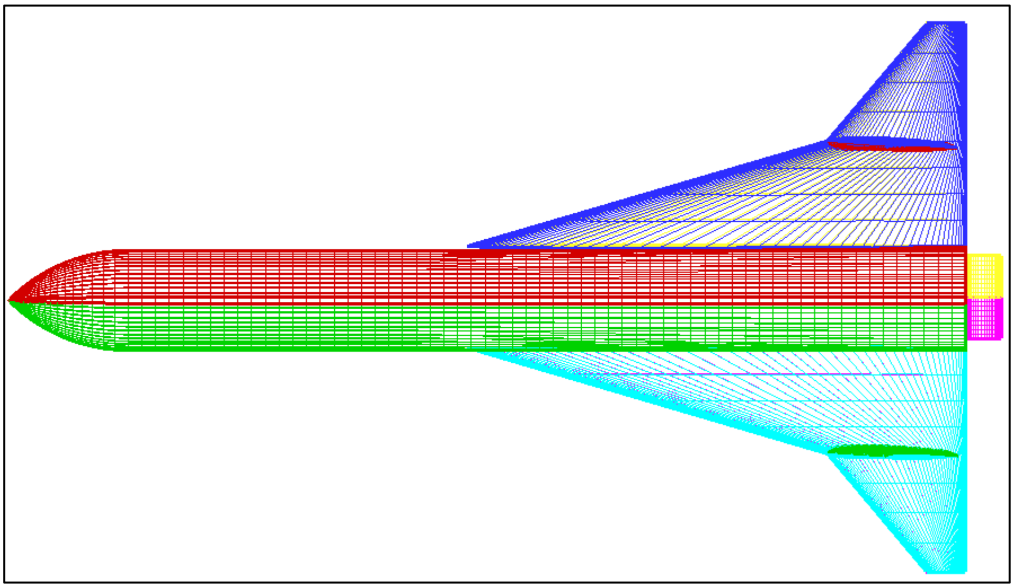

Figure 4.46 - Subsonic configuration

During the remaining part of the flight, the outer section of the wing is stored inside the inner part. With this solution the wingspan is reduced to 26.4 m, as can be seen in Figure 4.47.

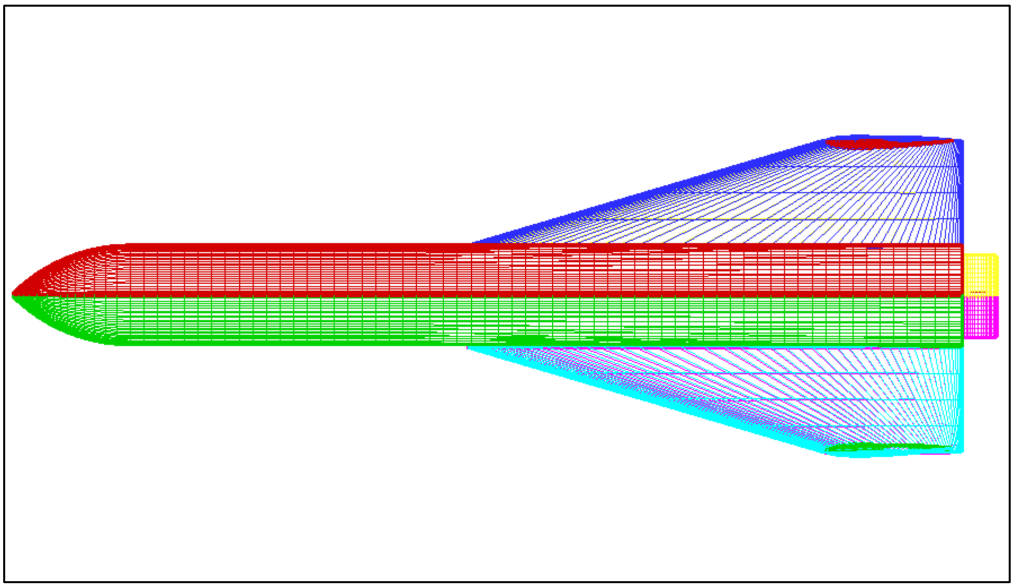

Figure 4.47 - Supersonic and hypersonic configuration

The general coordinates for the starting point of the wing root leading edge are reported in Table 4.19 and Figure 4.48.

x - coordinate	y - coordinate	z - coordinate
38.57	4.3	-4.7

Table 4.19 - Wing coordinates

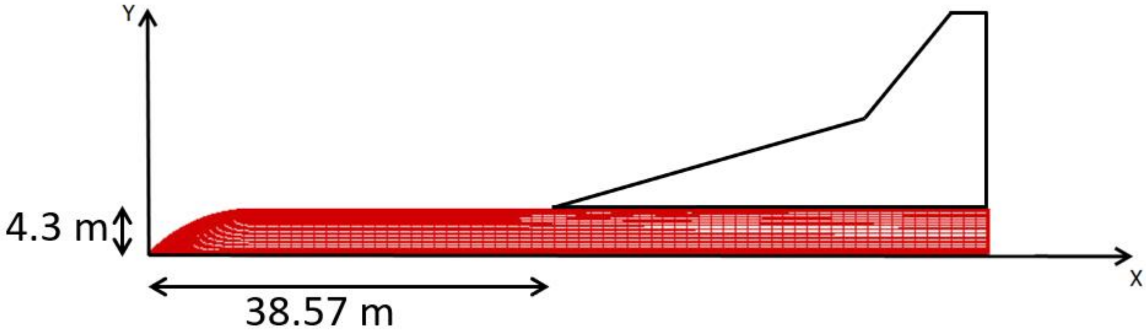

Figure 4.48 - X and Y wing starting point coordinates

A major constraint concerning the variable wing is related to the position of the wing along the vertical z-axis. The previous fixed configuration has a wing that is placed in proximity of the middle of the fuselage. If the same solution is adopted here, the space available for the storage of the outer part is limited. The available space stretches from the external part of the fuselage to the tip of the wing inner part. The internal segment of the fuselage, indeed, cannot be used for this purpose, because it is already occupied by the LH2 tank.
For this reason, the position of the wing is changed and it is moved to a lower one. The wing is now placed below the fuselage, so that the space available for storage is maximized. With this solution, this space is included between the centre line of the booster and the tip of the inner wing, as shown in Figure 4.49.

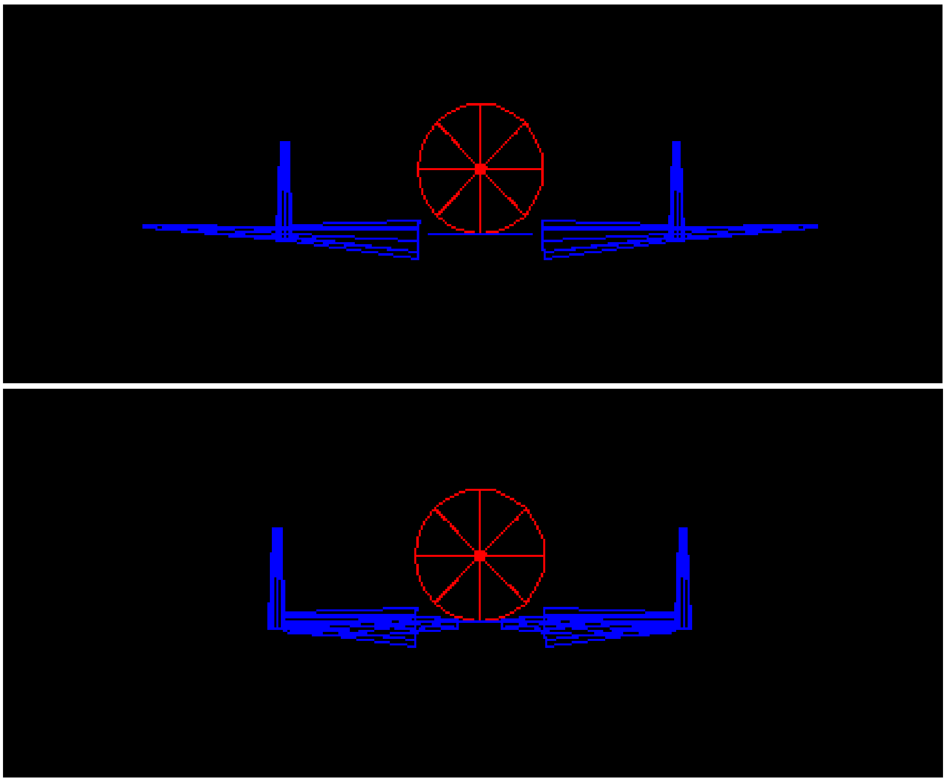

Figure 4.49 - Outer part rotation (rearview)

The geometry of the outer part of the wing is designed taking into account for this available space. However, since only a preliminary geometry is considered, a conservative approach has been used here. For that reason, some empty space has been left free between the wing in the stored position and the limits of the fuselage:

1. 1.69 m → The distance between the rearward point of the wing movable part and the back of the fuselage.
2. 1.51 m → The distance between the internal point of the wing movable part and the center line of the fuselage.

Figure 4.50 shows the outer part of the wing in the stored position and highlights the two distances described before.

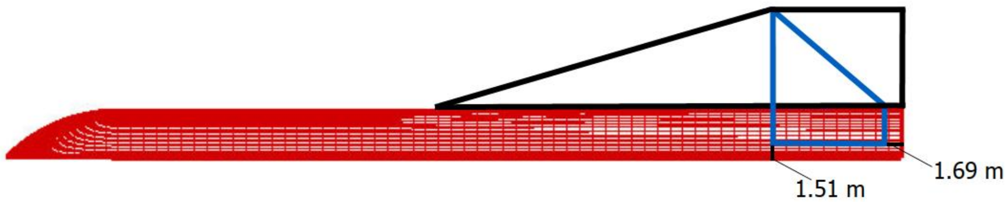

Figure 4.50 - Wing in stored position

However, it must be considered that a simple geometry has been used here: the wing is rotating around a pivot placed exactly on the wing root leading edge. In reality this pivot would be somewhere else inside the inner part, so the available space would be less than in this simplified case. That is another reason why some space has been left empty between the stored wing and the fuselage.

Flap configuration

The flap geometry has been briefly described previously in this report. Here, however, a detailed description is presented. The main issue linked to the design of flaps concerns the wing type: since the outer wing is assumed to rotate inside the inner part, a typical flap configuration cannot be used. For that reason, different solutions have been taken into account.

In a first assessment, a configuration involving canards, which were placed in a forward position, has been considered. However, this configuration has been immediately rejected since these canards would interact with the shock wave arising from the fuselage nose during hypersonic flight.

The selected solution presents two distinct flaps similar to spoilers, that are placed one on the upper and one on the lower side of the wing, as shown in Figure 4.51.

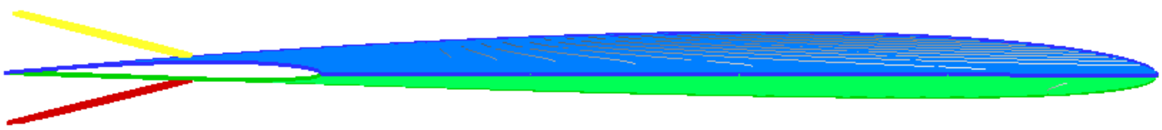

Figure 4.51 - Flaps both deflected

If this solution is adopted, the outer part of the wing has the possibility to rotate inside the inner part, without any interference between flaps and the moving wing. The two different flaps are both deflected when this rotation occurs, so that there is enough space for the wing to move between them. When the outer part is not rotating, the flaps can be used for control and they can be individually turned according to the type of deflection that is needed.
The next step consists in the definition of flaps geometry: they have to be designed in order to guarantee that a trimmed condition exists during the mission. The data are presented in Table 4.20 and a plan view of the wing with flaps is shown in Figure 4.52.

Root chord [m]	Tip chord [m]	Span [m]
6.5	6.5	8.9

Table 4.20 - Flap geometry data

Figure 4.52 - Flap geometry

Mass estimation

The use of a variable wing configuration involves an increment in mass, due to the presence of the mechanism that allows the wing rotation. In this study, a detailed analysis on this additional mass has not been performed. However, if one wants to complete a correct computation of the masses and of the centre of gravity, this increment must be taken into account. The approach used to estimate the increase in mass is described here.
To explain this method, some considerations on the different ways to define the wing in the STSM input file are done. The wing mass estimation depends on the following parameters:

- Structural wing span
- Wing area
- Maximum airfoil thickness

First, the mass of the SpaceLiner booster is computed without taking into account any addition for the sweeping mechanism. In the STSM input file the wing is defined as a single component and the three parameters described previously are referred to the entire wing.

The mass obtained with this computation is exactly the same mass that one would have in the case of a fixed wing.
Then, for a second computation, the wing is divided into two separate wings: the first one corresponds to the inner part, while the other one corresponds to the outer part. The three input parameters are defined twice, both for the inner and the outer wing. The sum of the two wing spans and two areas of each part is equal to the value of the entire wing. Something more must be said for what concerns the thickness. While in the previous case only one value of maximum thickness is required, now this parameter is defined for both the wing parts. The thickness of the inner part is greater than the one of the outer part, so that the latter one can be able to fit inside the inner one.
It is also important to highlight that, since in STSM each wing is supposed to be able to carry the full load, the value of the overall mass of the wing is higher than in the previous case.
The values of the wing structure mass that have been found are presented in Table 4.21.
This mass difference is taken as a first estimation of the sweeping mechanism of the variable wing configuration.

2 components	23 605 Kg
1 component	21 615 Kg
Difference	**1 990 Kg**

Table 4.21 - Wing mass estimation

Later in this analysis, the mechanism mass is updated taking as a reference a previous study carried on at DLR [15]. Here, the mass of the mechanism is of about 1250 Kg on each side of the wing. The configuration considered is quite different with respect to the SpaceLiner booster, since its wing has a smaller surface and a greater aspect ratio. For that reason, this mechanism mass represents only a reference value and cannot be taken as a precise estimation of the mass for the SL case.

Vertical fins

At the beginning of this study the design of the vertical fins has not been carried out. However, since some kind of vertical fins must be considered for the booster, the previous SpaceLiner configuration is taken as a reference: the area of the vertical fins is kept constant and the geometry is adapted to the new configuration. The geometric data are presented in Table 4.22.

Root chord [m]	Tip chord [m]	Span [m]	Leading edge sweep angle [°]
10	6	6.5	40

Table 4.22 - Vertical fins geometric data

However, it must be highlighted that the fins geometry is updated at the end of this study, once some data for the yaw moment coefficient are estimated.

4.2.2 Aerodynamic coefficients analysis

SUBSONIC

With the new variable wing configuration the moment coefficient is evaluated again for the entire Mach range. The results for subsonic flight are reported in Figure 4.53 and Figure 4.54. With flap deflection angles between 0° and -15° it is possible to find a trimmed condition for angles of attack included between 0° and 15°. This trend is quite similar to the one found with the configuration V-3, which is the one this final configuration is derived from.

C_L, C_D and L/D are reported in Figure 4.55, Figure 4.56 and Figure 4.57. If the plot of the lift to drag ratio is analysed, it can be seen that this configuration presents a maximum value of approximately 7 for angles of attack between 5° and 10°. L/D is reduced to about 6 for M=0.8.

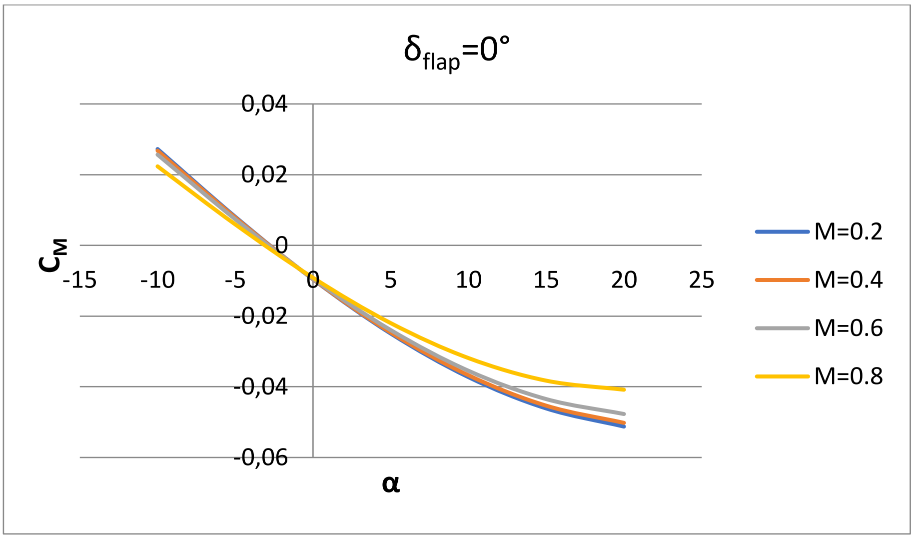

Figure 4.53 - C_M with δ_{flap}=0° (subsonic)

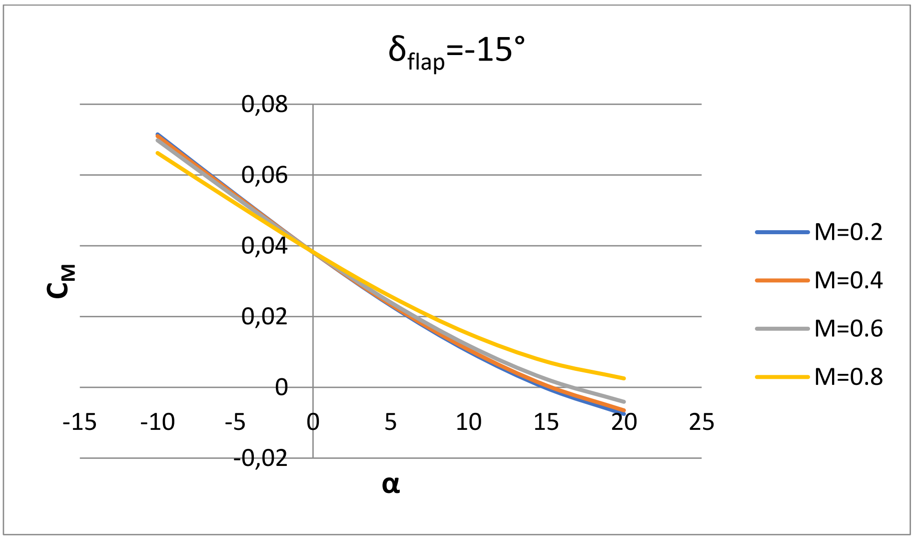

Figure 4.54 - C_M with δ_{flap}=-15° (subsonic)

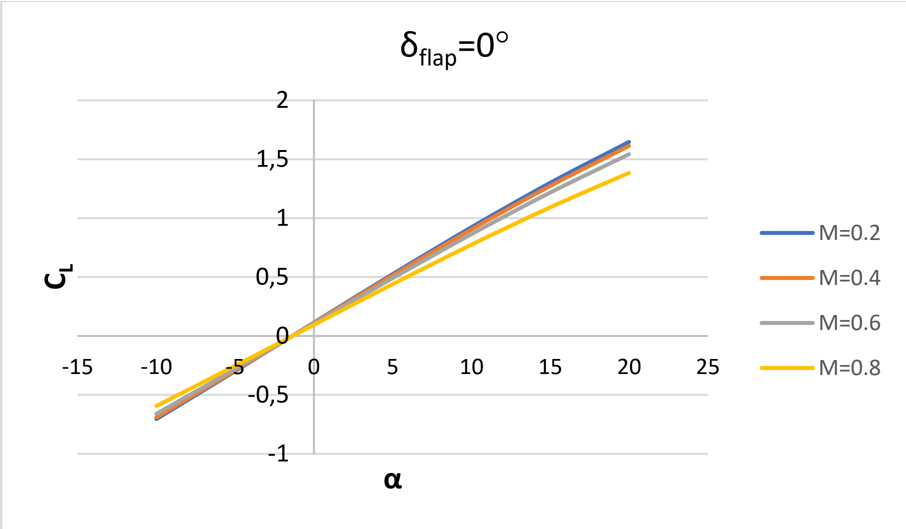

Figure 4.55 - C_L with δ_{flap}=0° (subsonic)

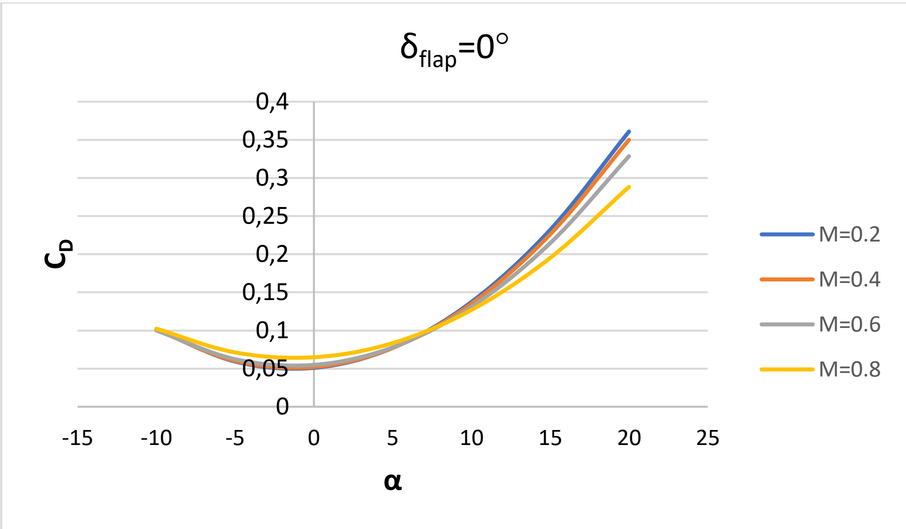

Figure 4.56 - C_D with δ_{flap}=0° (subsonic)

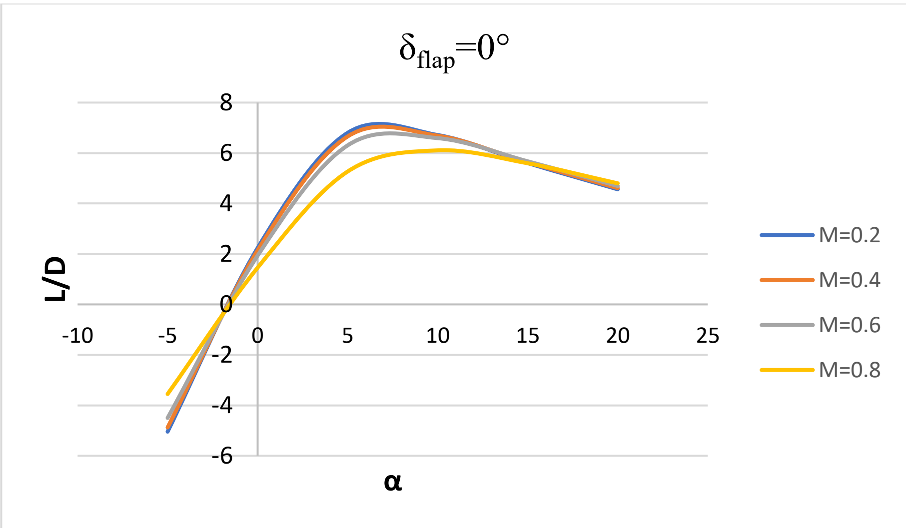

Figure 4.57 - L/D with δ_{flap}=0° (subsonic)

SUPERSONIC

The moment coefficient curve has a slightly positive slope, suggesting an almost neutral behaviour in supersonic. For α=20° a trimmed condition is found with a flap deflection between 0° and 5°. The results are shown in Figure 4.58 and Figure 4.59. The lift and drag coefficient are also reported in Figure 4.60 and Figure 4.61 for δ_{flap}=0°. The maximum value of the lift to drag ratio is now reduced to approximately 2.5, as can be seen in Figure 4.62.

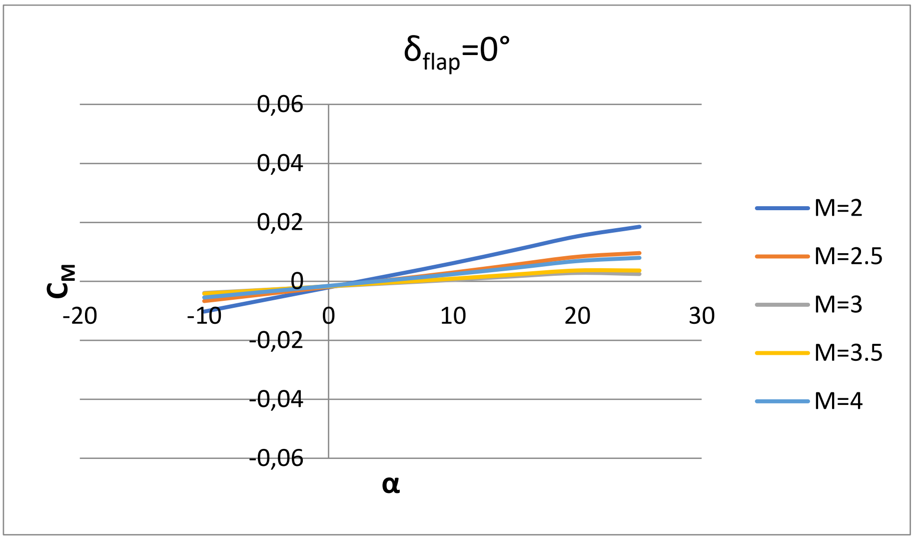

Figure 4.58 - C_M with δ_{flap}=0° (supersonic)

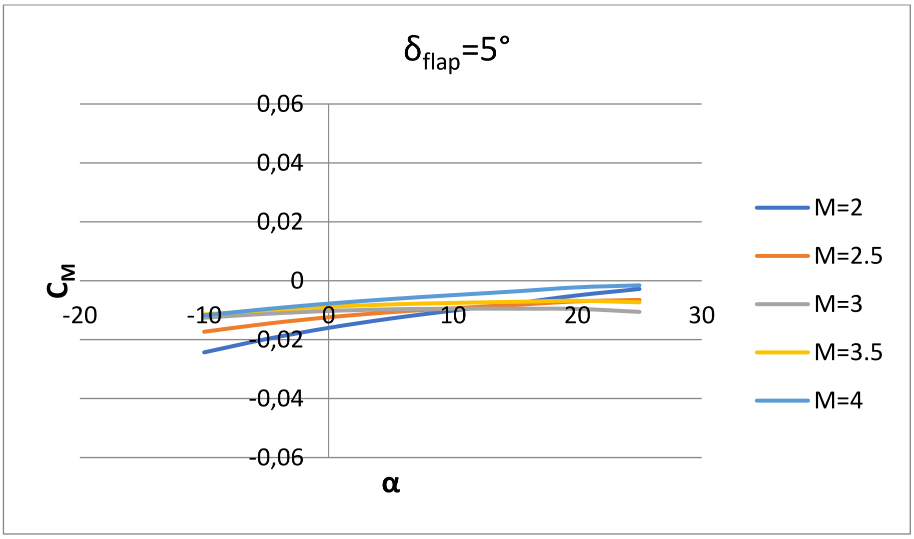

Figure 4.59 - C_M with δ_{flap}=5° (supersonic)

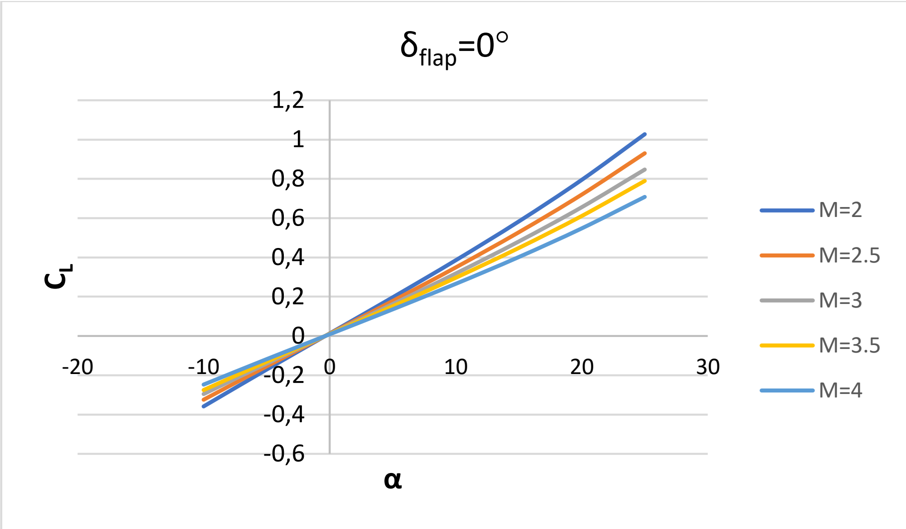

Figure 4.60 - C_L with δ_{flap}=0° (supersonic)

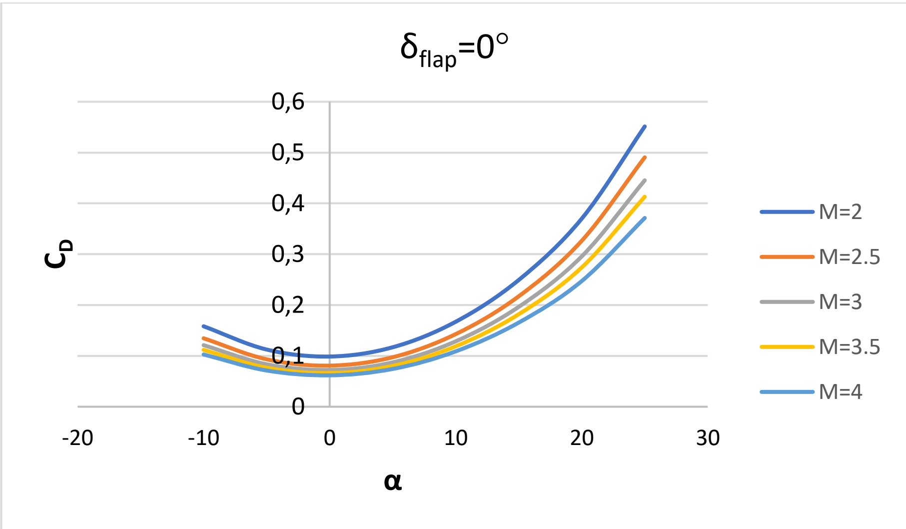

Figure 4.61 - C_D with δ_{flap}=0° (supersonic)

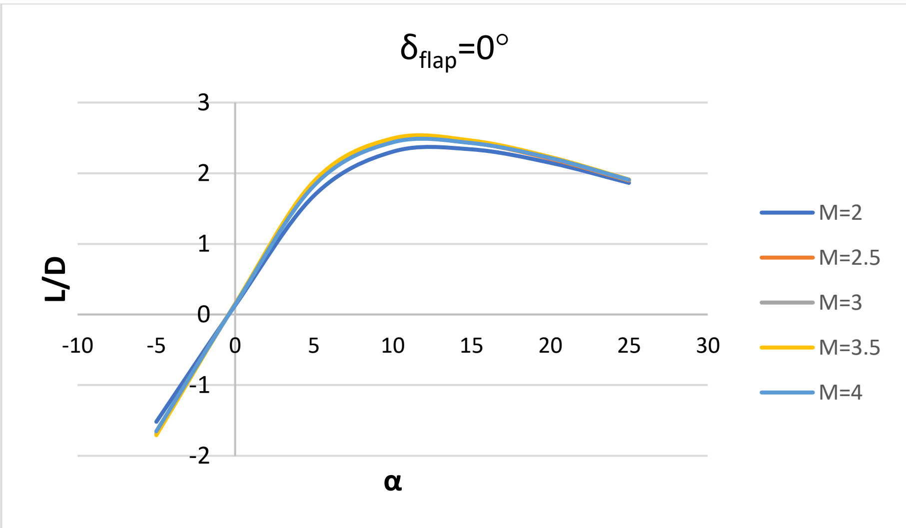

Figure 4.62 - L/D with δ_{flap}=0° (supersonic)

HYPERSONIC

The C_M trend for hypersonic Mach number is similar to the previous configurations and it is shown in Figure 4.63 and Figure 4.64. For a range of angles of attack between 20° and 50° different trimmed points can be found with flap deflection angles between -15° and 15°. Here, for δ_{flap}>0° the bodyflap is also deflected as an additional control surface, with an angle that is equal to the one used for flaps.

Lift coefficient, drag coefficient and lift to drag ratio are reported in Figure 4.65, Figure 4.66 and Figure 4.67.

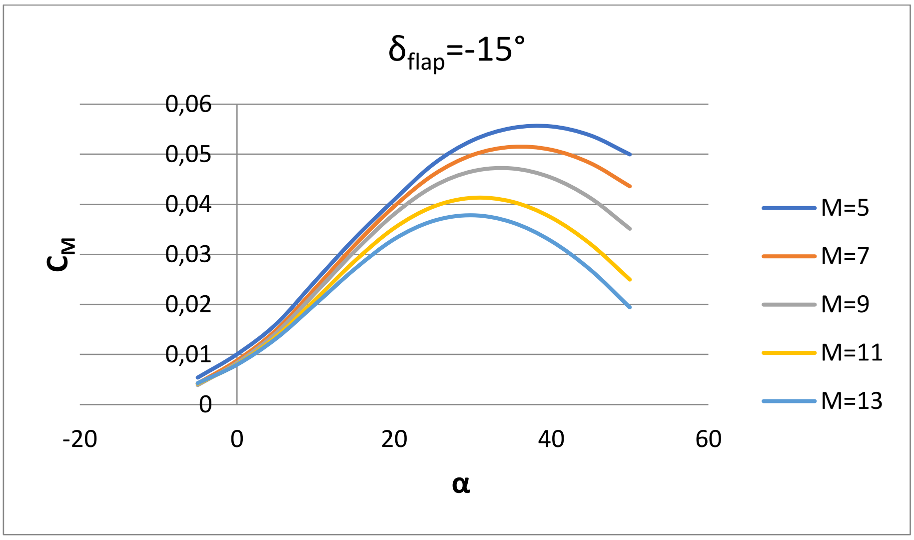

Figure 4.63 - C_M with δ_{flap}=-15° (hypersonic)

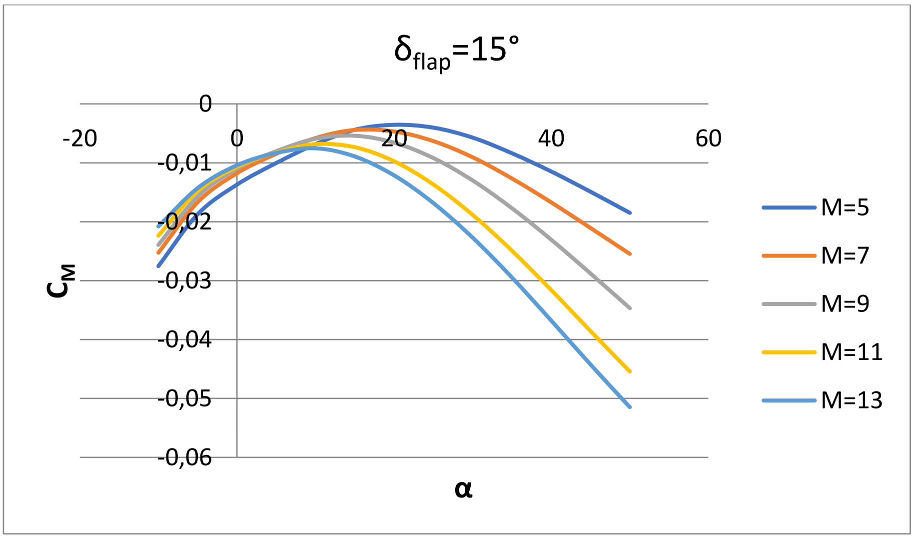

Figure 4.64 - C_M with δ_{flap}=15° (hypersonic)

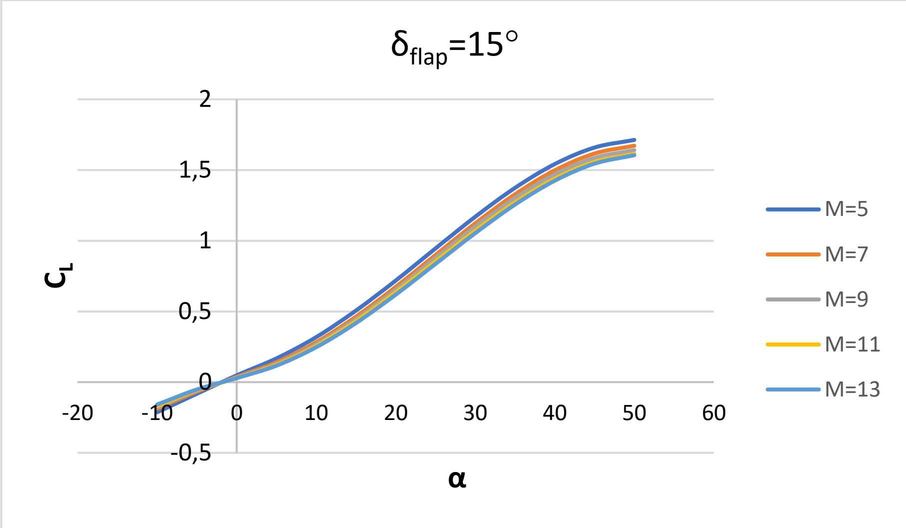

Figure 4.65 - C_L with δ_{flap}=15° (hypersonic)

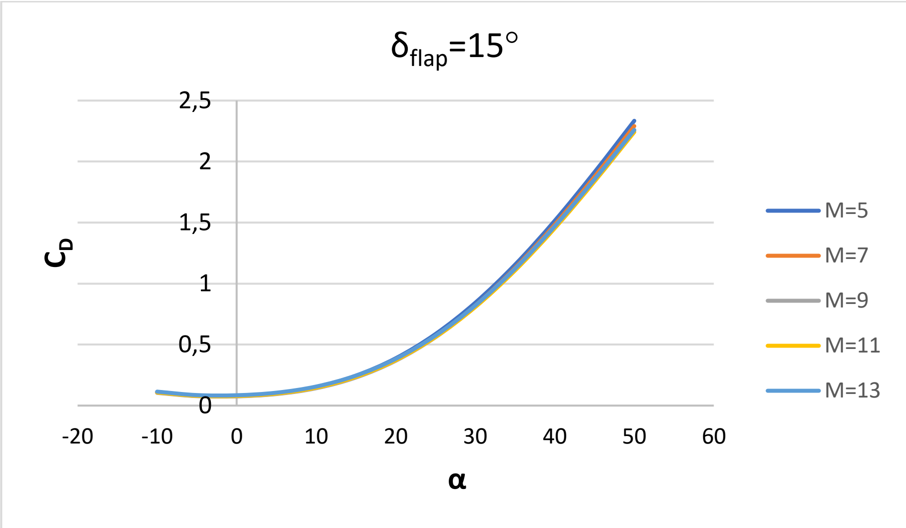

Figure 4.66 - C_D with δ_{flap}=15° (hypersonic)

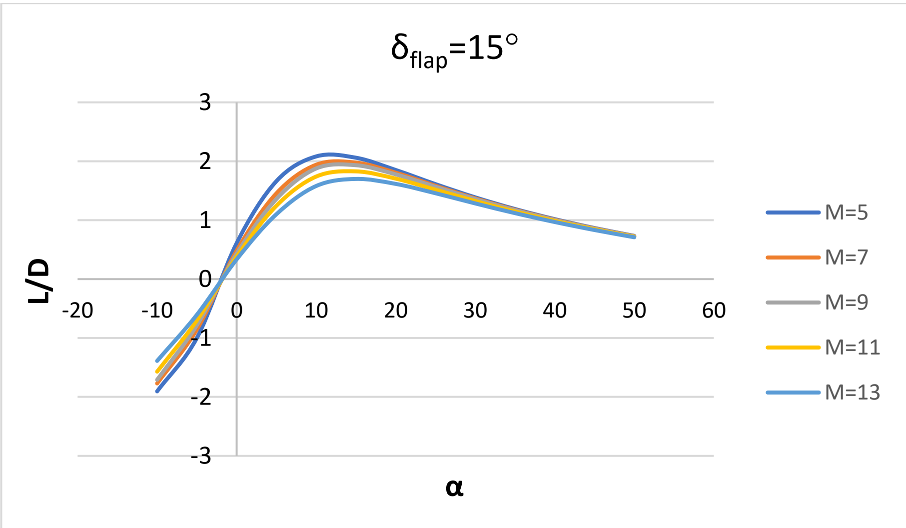

Figure 4.67 - L/D with δ_{flap}=15° (hypersonic)

4.3 Foldable wing configuration

A different kind of variable configuration is now studied, as a possible alternative to the variable sweep wing. The third configuration analysed is represented by the foldable wing. In this case the outer part of the wing is able to rotate around a horizontal axis that coincides with its root chord, as can be seen in Figure 4.68.

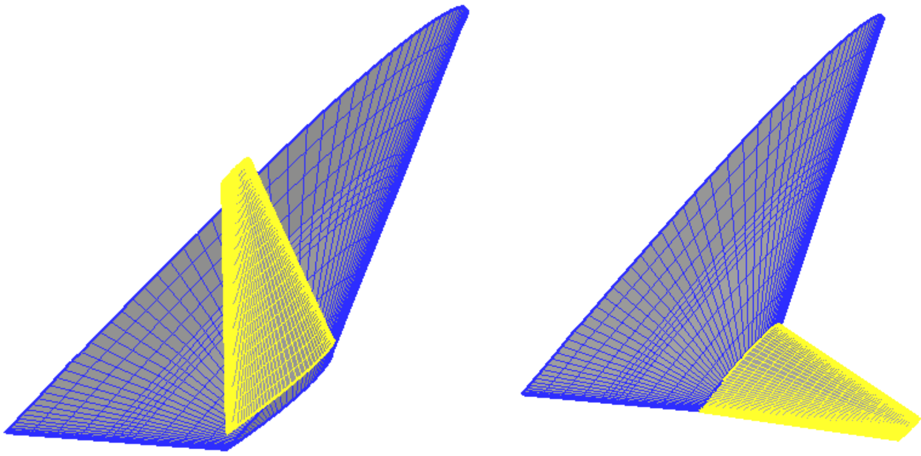

Figure 4.68 - Foldable wing

Again, two positions are identified: the first one in Figure 4.68 is chosen for supersonic and hypersonic flight, while the other one having the bigger span is used for the subsonic regime.

The complete booster configuration with foldable wing is showed in Figure 4.70. The wing is divided into two parts having the geometrical data reported in Table 4.23 and Table 4.24.

Root chord [m]	Tip chord [m]	Span [m]	Leading edge sweep angle [°]
41.5	9.41	8	76

Table 4.23 - Geometrical data of the foldable wing (inner part)

Root chord [m]	Tip chord [m]	Span [m]	Leading edge sweep angle [°]
9.41	2.38	9	38

Table 4.24 - Geometrical data of the foldable wing (outer part)

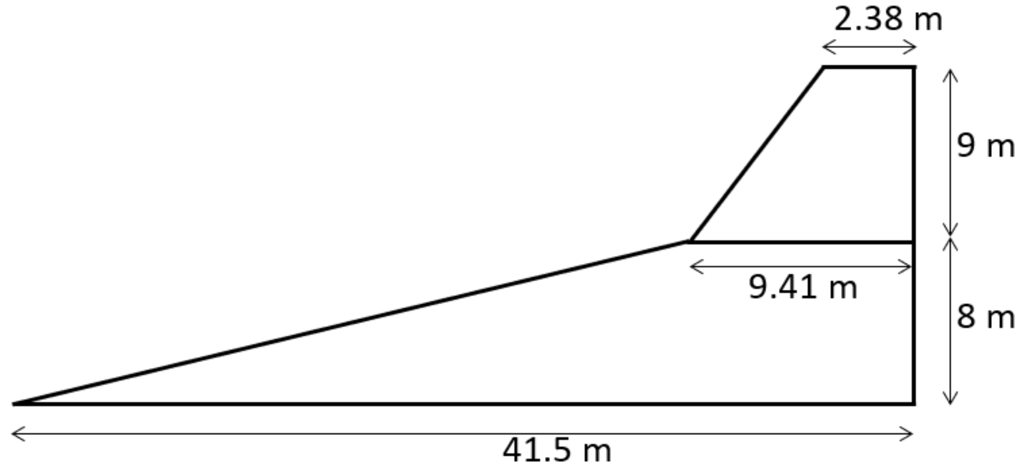

Figure 4.69 - Foladable wing geometry data

Since some kind of directional control is needed during the whole flight, a pair of vertical fins is added to guarantee it. They are placed in the middle of the inner part of the wing, in order to allow the outer part to be folded and to avoid any interference. However, this solution involves the presence of two vertical fins on each side of the wing when the outer part is in folded position, creating the configuration shown in Figure 4.71.

Once the wing and the vertical fins are designed, some flaps are added for booster control. In this case it is not possible to have a single flap on the inner wing trailing edge, because the vertical fins would interfere with it. For that reasons two flaps are placed on each side of the wing:

1. One flap is included between the fuselage and the vertical fin;
2. The other flap is included between the vertical fin and the tip of the inner part of the wing;

Once the configuration is designed, it is possible to evaluate the performances during the tow-back flight. These results are reported in Table 4.25. It can be seen that, also with the foldable wing configuration, the L/D, L/W and T/D have value that are higher than one.

L/D	*L/W*	*T/D*	m_p *[kg]*
9.22	*1.20*	*2.10*	*137 513*

Table 4.25 - Tow-back flight performances

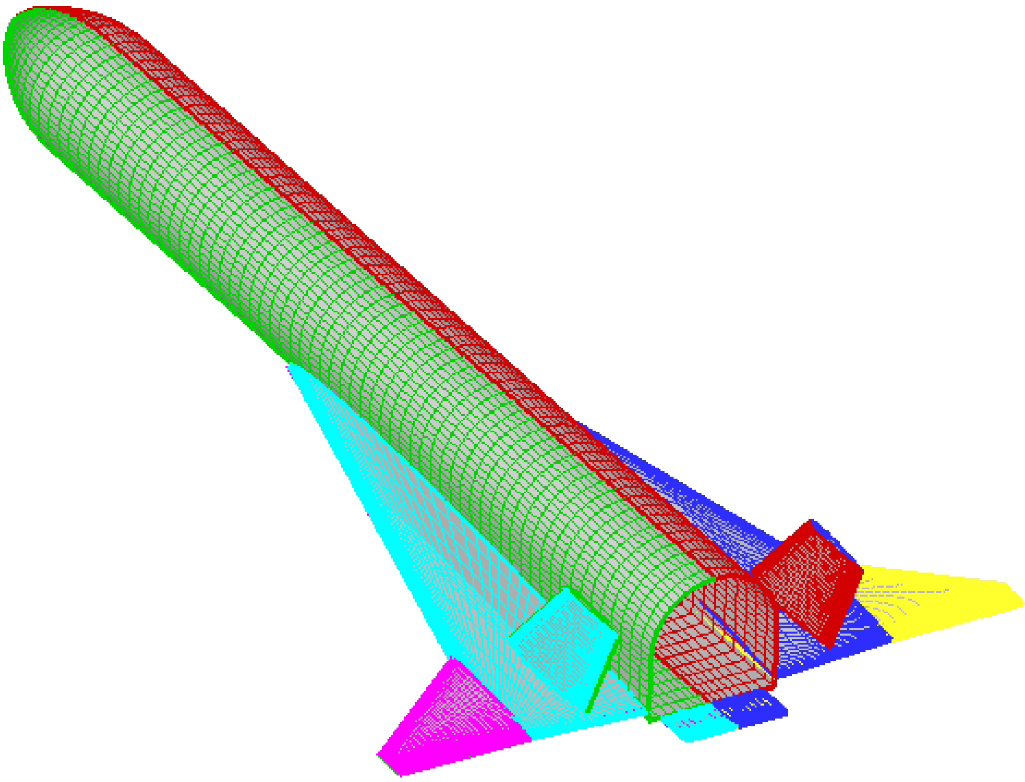

Figure 4.70 - Foldable wing - subsonic configuration

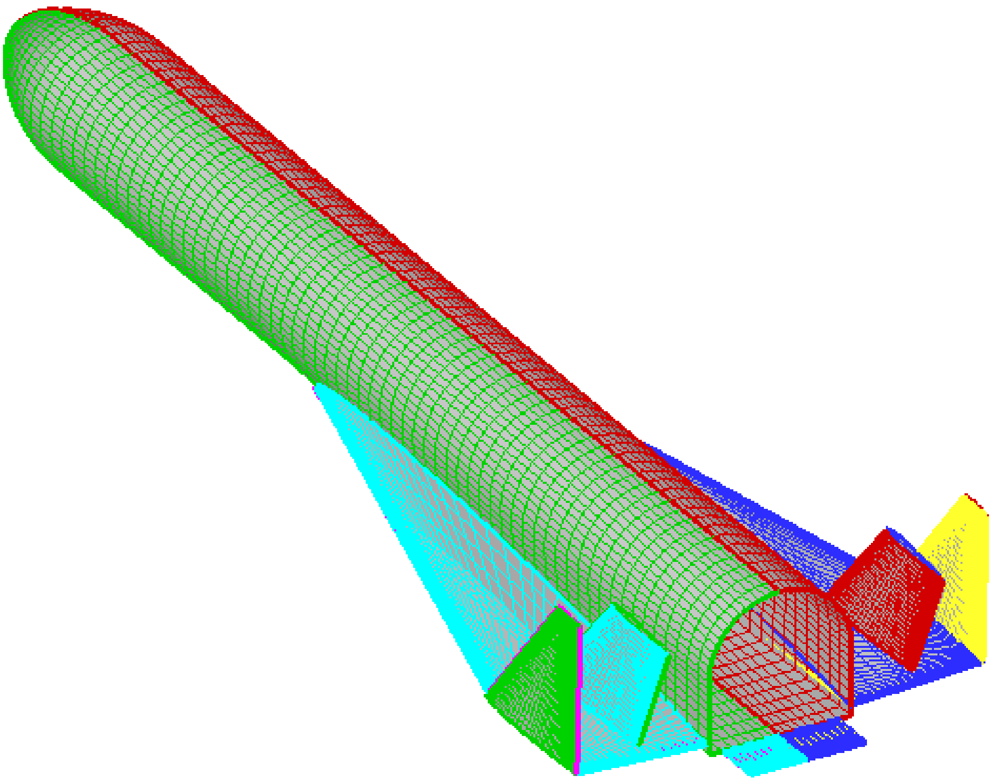

Figure 4.71 - Foldable wing - hypersonic configuration

SUBSONIC

The moment coefficient is then evaluated at different Mach numbers. The results for the subsonic regime are shown in Figure 4.72 and Figure 4.73. It can be seen that the configuration is stable for this range of speeds and a trimmed condition is found for angles of attack between 0° and 10°. However, it is also possible to notice that a much bigger flap deflection (up to 25°) is needed to find a trimmed condition, with respect to the previous cases.

The lift to drag ratio is evaluated also in this case and it is reported in Figure 4.76. The maximum value is now slightly higher than 6 for $M \leq 0.6$, while it is of about 5.7 for M=0.8.

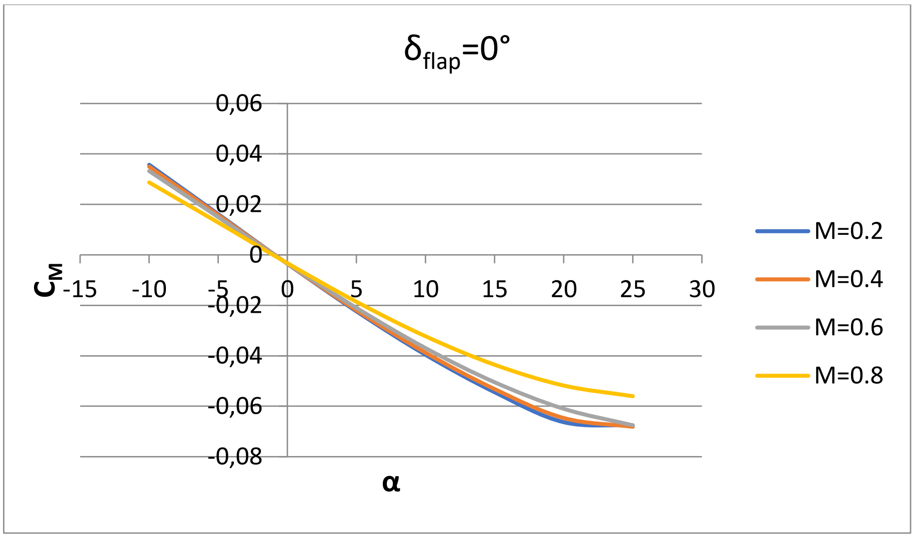

Figure 4.72 - C_M with δ_{flap}=0° (Subsonic)

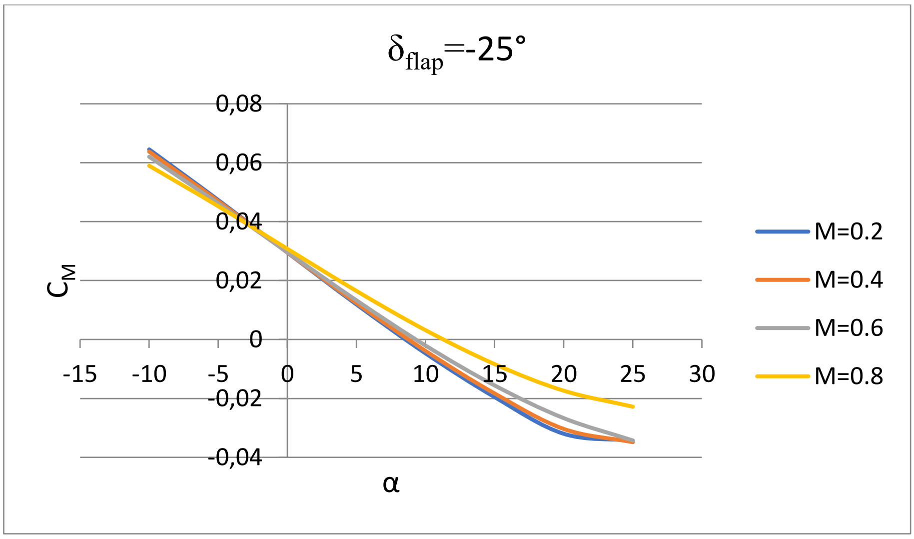

Figure 4.73 - C_M with δ_{flap}=-25° (Subsonic)

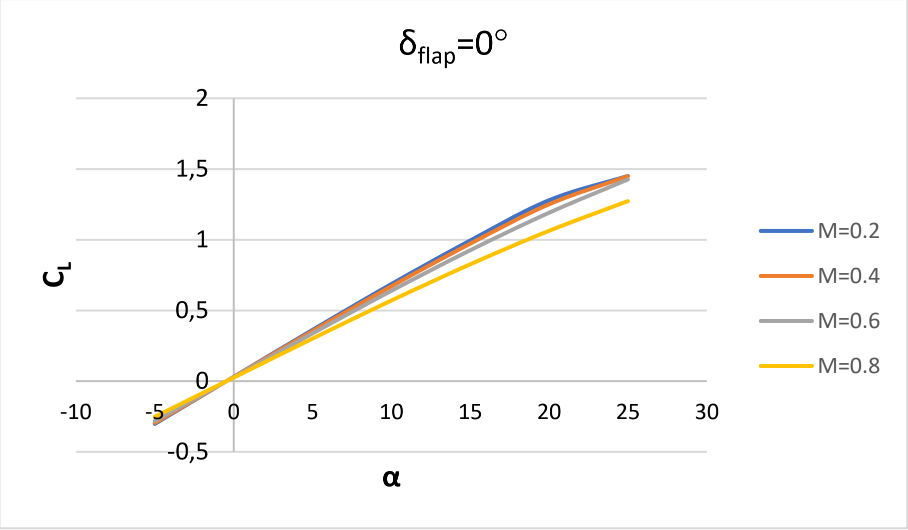

Figure 4.74 - C_L with δ_{flap}=0° (subsonic)

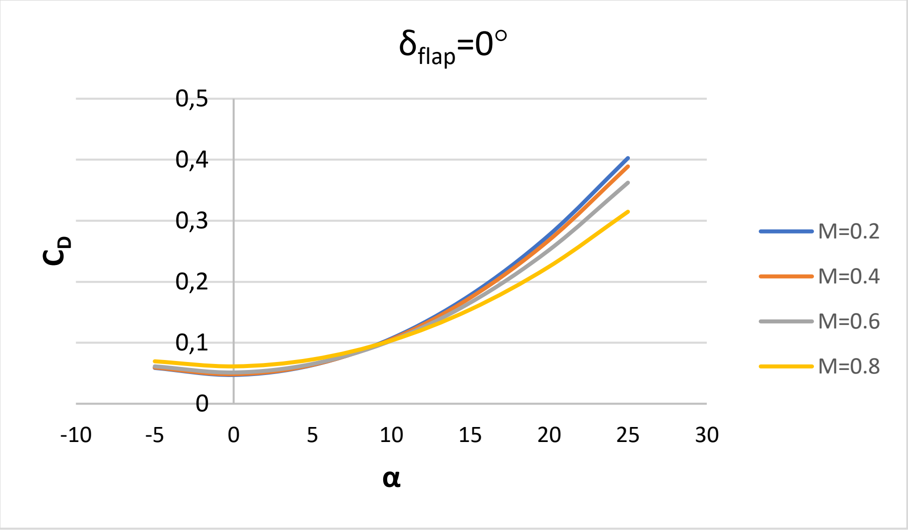

Figure 4.75 - C_D with δ_{flap}=0° (subsonic)

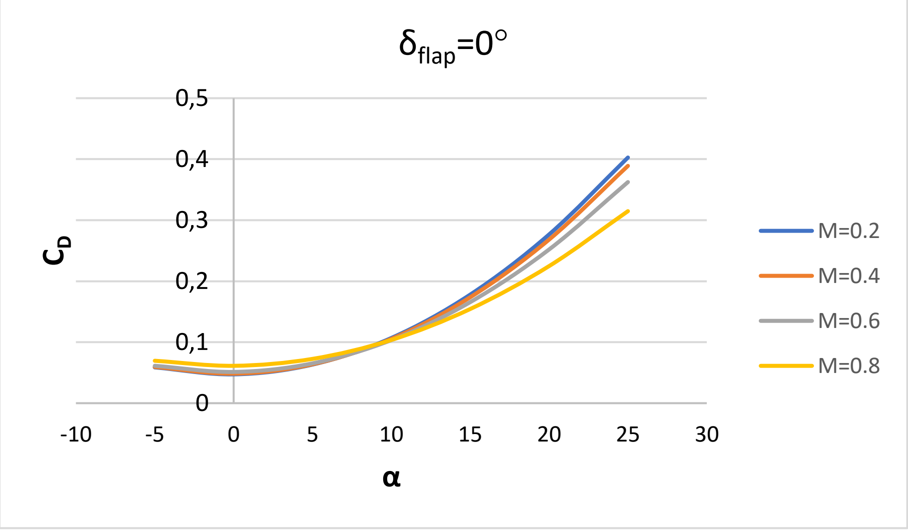

Figure 4.76 - L/D with δ_{flap}=0° (subsonic)

SUPERSONIC

The C_M is now studied for the supersonic Mach range. Here, the foldable configurations has an almost neutral behaviour, with a slight trend to be unstable. The flap deflection required is limited and it is included between -5° and 5° [Figure 4.77 and Figure 4.78].

Figure 4.79, Figure 4.80 and Figure 4.81 show the trend of the lift coefficient, drag coefficient and lift to drag ratio. During supersonic regime, the maximum L/D is of about 2.

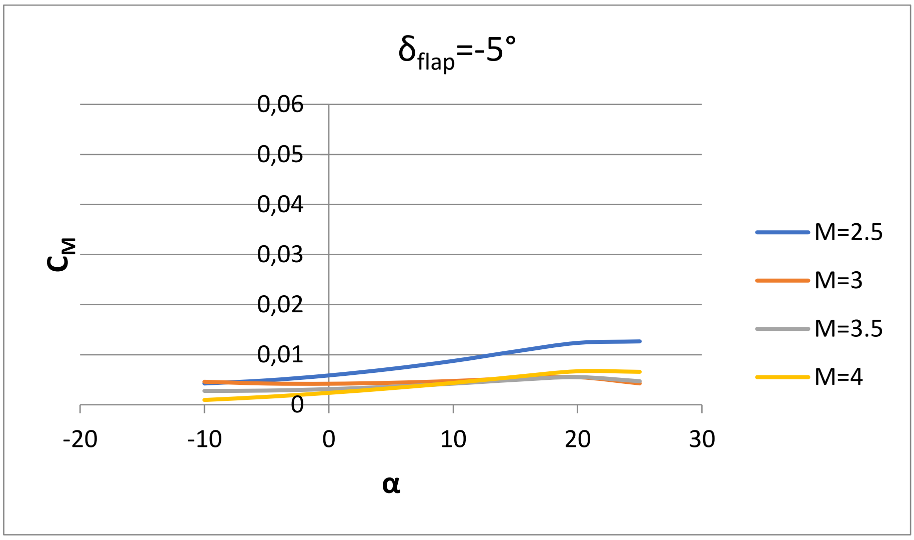

Figure 4.77 - C_M with δ_{flap}=-5° (supersonic)

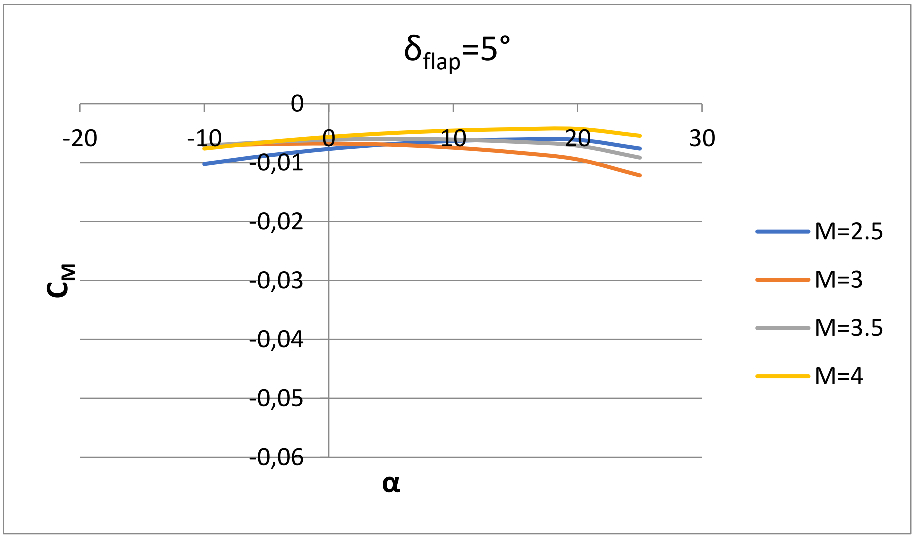

Figure 4.78 - C_M with δ_{flap}=5° (supersonic)

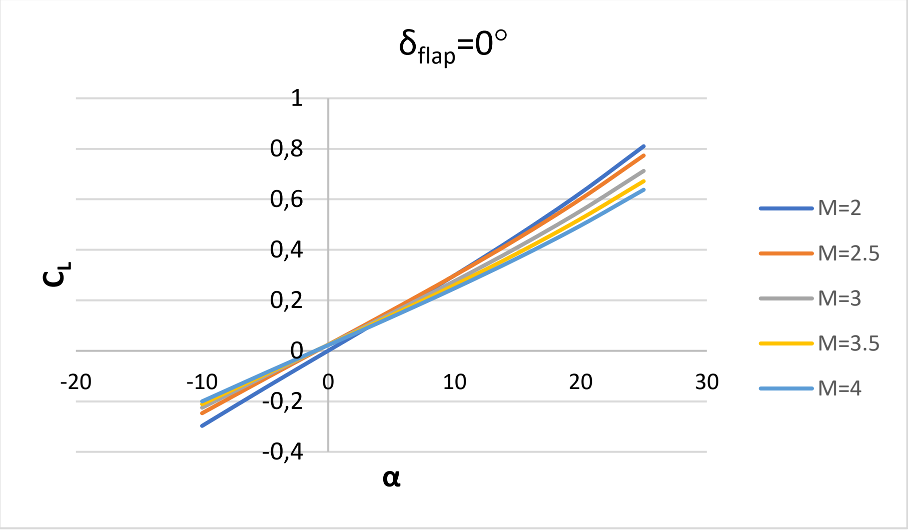

Figure 4.79 - C_L with δ_{flap}=0° (supersonic)

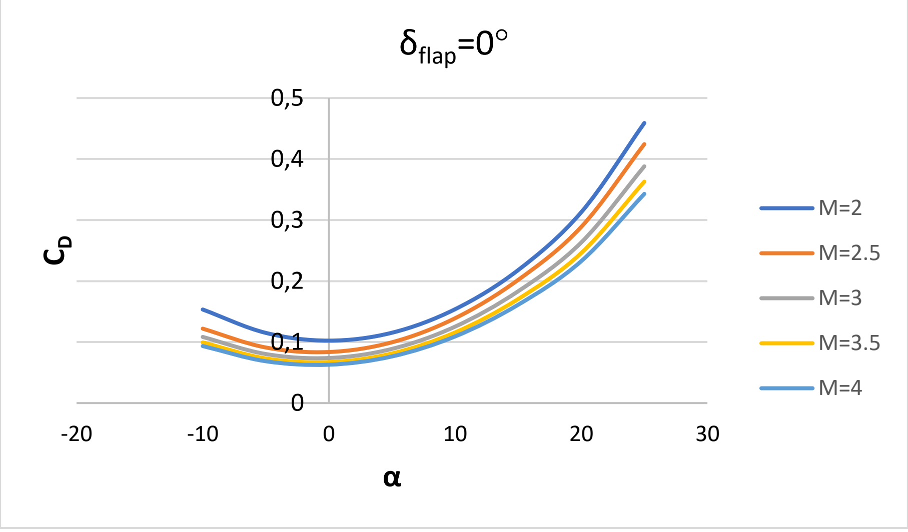

Figure 4.80 - C_D with δ_{flap}=0° (supersonic)

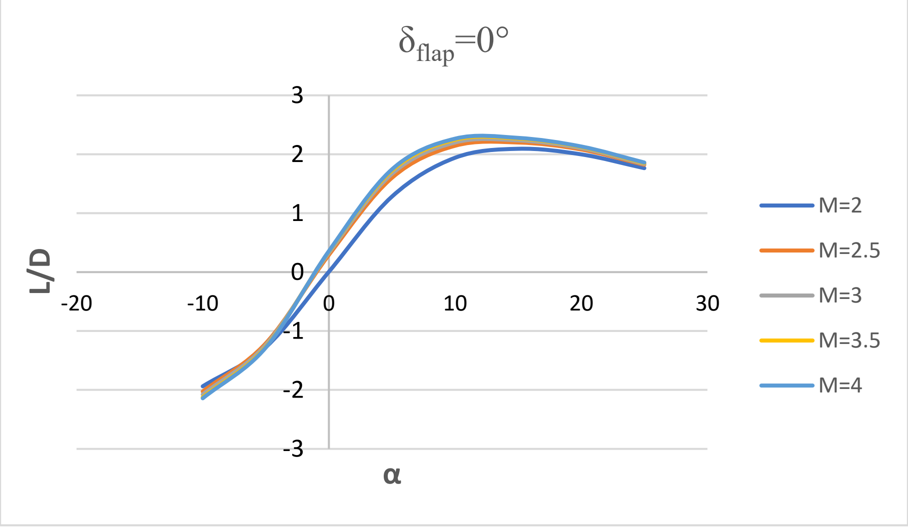

Figure 4.81 - L/D with δ_{flap}=0° (supersonic)

HYPERSONIC

The moment coefficient is now analysed for the hypersonic regime. The same trend that was found with the other configurations, is also found here if no flaps are used. The C_M trend shows a negative slope for high angles of attack (α ≈50°) and M>9. If the flap deflection is increased, a trimmed condition for lower angles of attack (α≈20°) and M<7 is also found. In this case, however, the curve slope becomes positive and the configuration is unstable, as can be seen in Figure 4.83.

Trends of lift coefficient, drag coefficient and lift to drag ratio are reported respectively in Figure 4.84, Figure 4.85 and Figure 4.86.

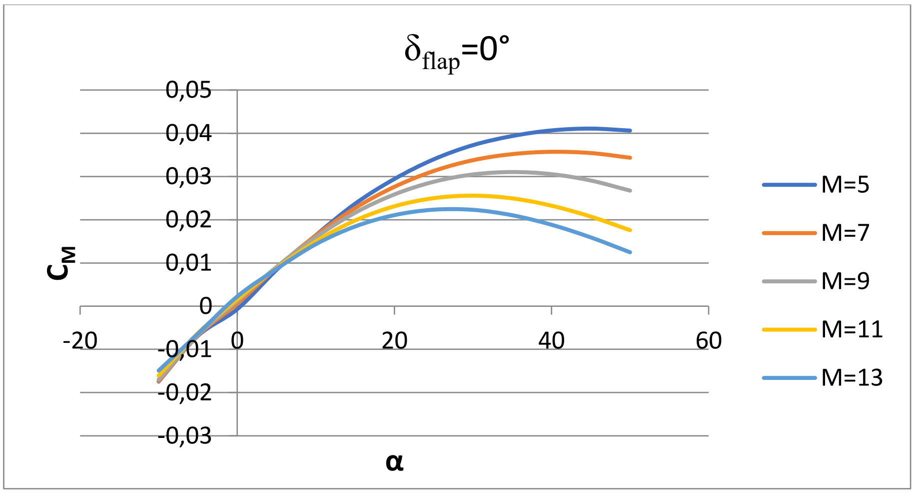

Figure 4.82 - C_M with δ_{flap}=0° (hypersonic)

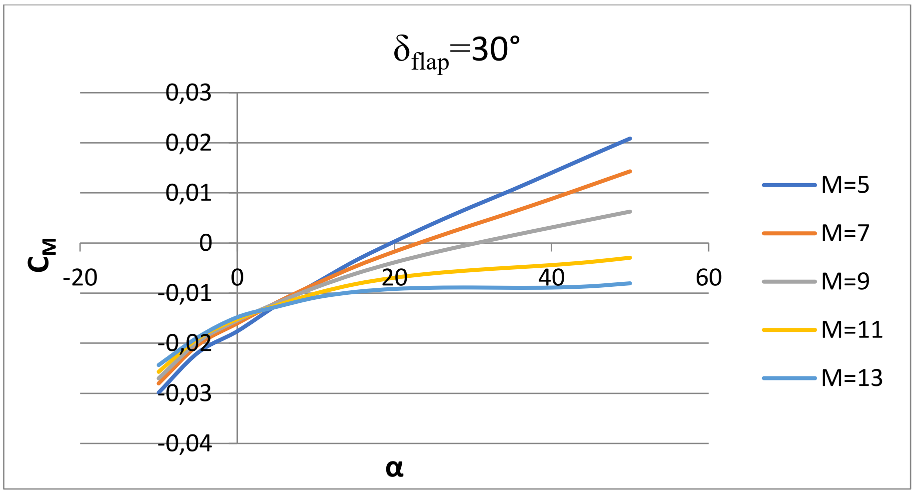

Figure 4.83 - C_M with δ_{flap}=30° (hypersonic)

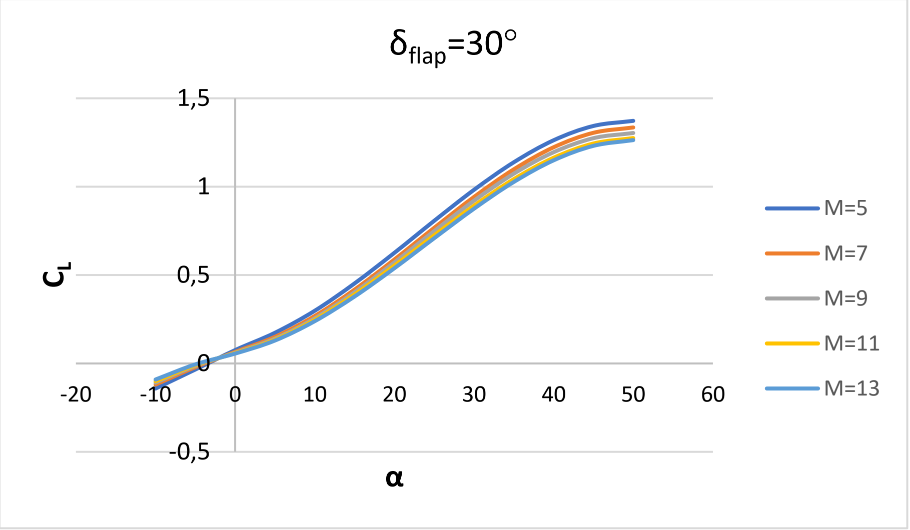

Figure 4.84 - C_L with δ_{flap}=30° (hypersonic)

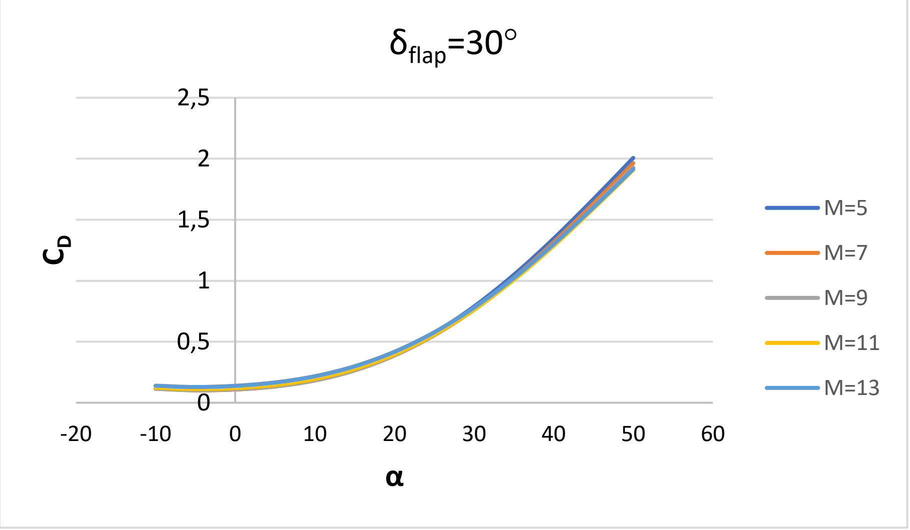

Figure 4.85 - C_D with δ_{flap}=30° (hypersonic)

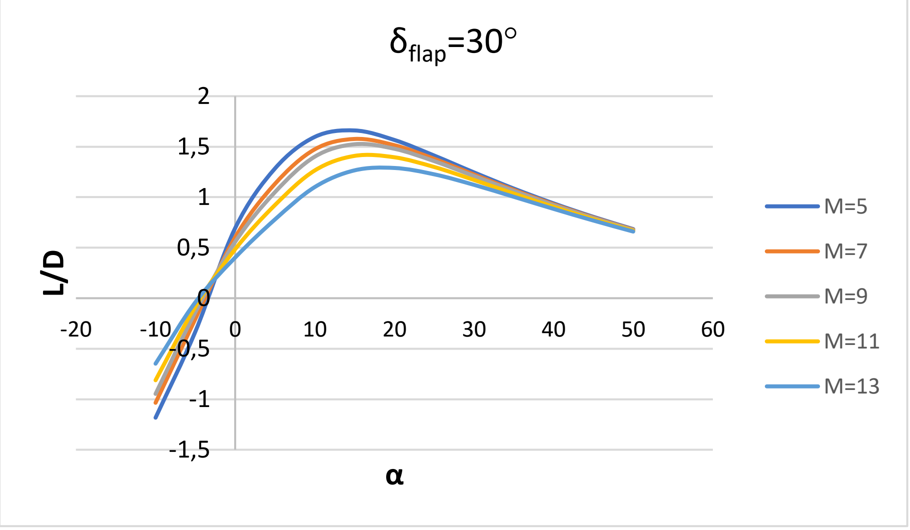

Figure 4.86 - L/D with δ_{flap}=30° (hypersonic)

As described in this section, the foldable configuration presents two main issues that must be considered when comparing this solution to the other previously studied:

1. Two vertical fins are present on each side of the wing during supersonic and hypersonic flight. With this solution, the air flow could present some interactions, which makes the evaluation of the aerodynamic coefficients and performances more difficult.
2. This configuration needs much higher flap deflection angles to reach a trimmed condition both in subsonic and hypersonic. It is also unstable in hypersonic flight.

Those are the main reasons why this configuration is rejected and it is not considered for further analysis.

Chapter 5 Trajectories

The mission taken as a reference in this study is the SpaceLiner TSTO mission. In this case, the main objective of the mission is to deliver a certain payload to GTO (or a different target orbit). The launch site is Kourou, French Guyana. The lift-off and ascent configuration involves both the booster and the orbiter, the latter attached on top of the booster. At the end of the ascent, the two stages separate: the booster starts its descent while the orbiter continues its flight to the final orbit. The separation occurs at an altitude of about 60 km and at a velocity of about 3.7 km/s. During the descent, the booster is in-air captured by a towing aircraft and returns to the launch site for the autonomous landing.

In this study both the ascent and the descent trajectory are computed. In the first case, the mated configuration is considered, with the orbiter attached on top of the booster. For what concerns the descent, instead, only the trajectory of the booster is analysed.

This process is not straightforward and an iterative method is required. Some inputs for the evaluation of the ascent trajectory are derived from the output of the descent calculations and vice versa. The first step is the determination of the descent trajectory. However, it is important to specify that only the supersonic and the hypersonic part of the descent is analysed here. There are two reasons for that choice. The first one is linked to the aerodynamic input file that is used for TOSCA simulation. This file includes the aerodynamic data, that are computed for the entire Mach range: it is made up of a CAC and a HOTSOSE file united together. However, since the configuration with the variable wing in subsonic differs from the one in supersonic, a single CAC file cannot be used to simulate both the conditions. The other reason is linked to the mission itself: during subsonic flight, indeed, the booster is supposed to be towed by an aircraft and this condition cannot be simulated here.

Since the initial parameters are not known, the conditions valid for the SLB7 are used here for a first estimation. Those values will be updated later, once the ascent is computed. The parameters are shown in Table 5.1.

Altitude [Km]	Longitude [°]	Latitude [°]	Velocity [m/s]	Flight path angle [°]	Azimuth [°]	Inclination [°]
69.447	-50.336	5.182	3816.5	4.865	-1.534	5.359

Table 5.1 - Initial parameters for the descent

The selected values for the angle of attack during descent are presented in Figure 5.1.

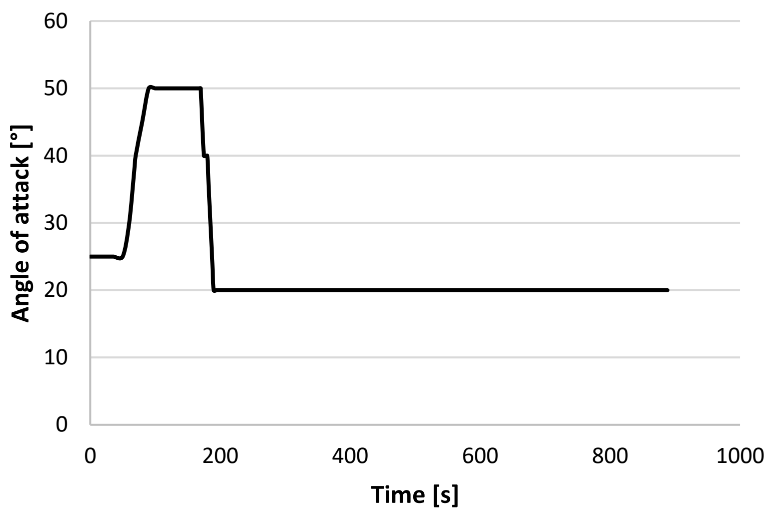

Figure 5.1 - Angle of attack during descent (α_{max}=50°)

The output data of this first descent trajectory, simulated with TOSCA, are reported in Figure 5.2. In this phase, the main focus is placed on the analysis of the descent output data. In particular, three parameters are analysed:

- Dynamic pressure
- Acceleration n_z
- Stagnation point heat flux

The stagnation heat flux is evaluated for a nose radius of 0.5 m.

First, it can be seen that the maximum value of the dynamic pressure is of around 5 kPa. This value is well below the structural limits of the booster and it is considered as acceptable. The other two parameters present tolerable values, but a further reduction could be advantageous. To fulfil this purpose, a manual adjustment of the selected angles of attack during the descent is done.

In the first case the maximum angle of attack is 50°, while in a second calculation this angle is reduced to 45° and then to 40°. The results obtained are shown in Figure 5.3 and Figure 5.4.

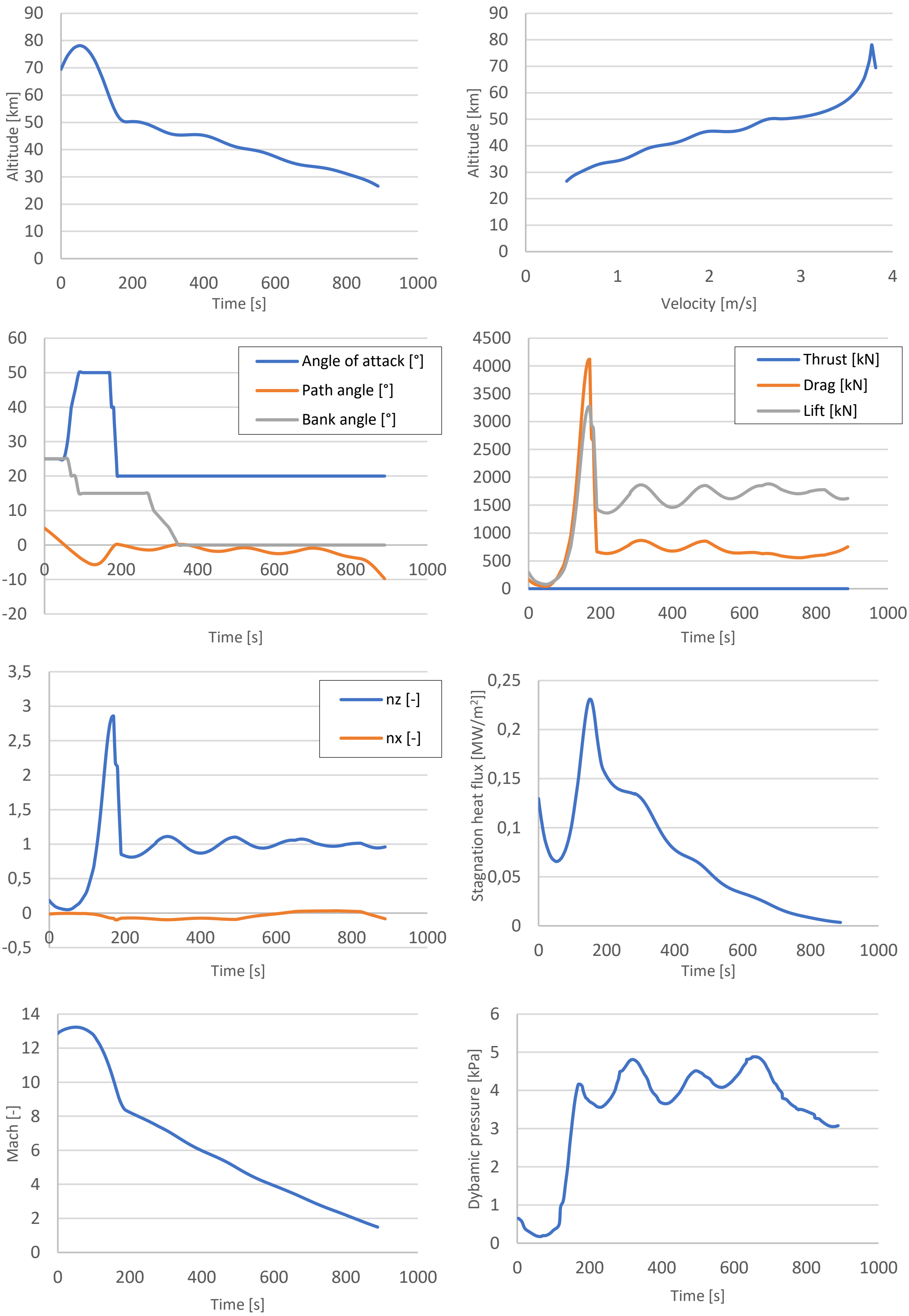

Figure 5.2 - Output data for descent (α_{max}=50°)

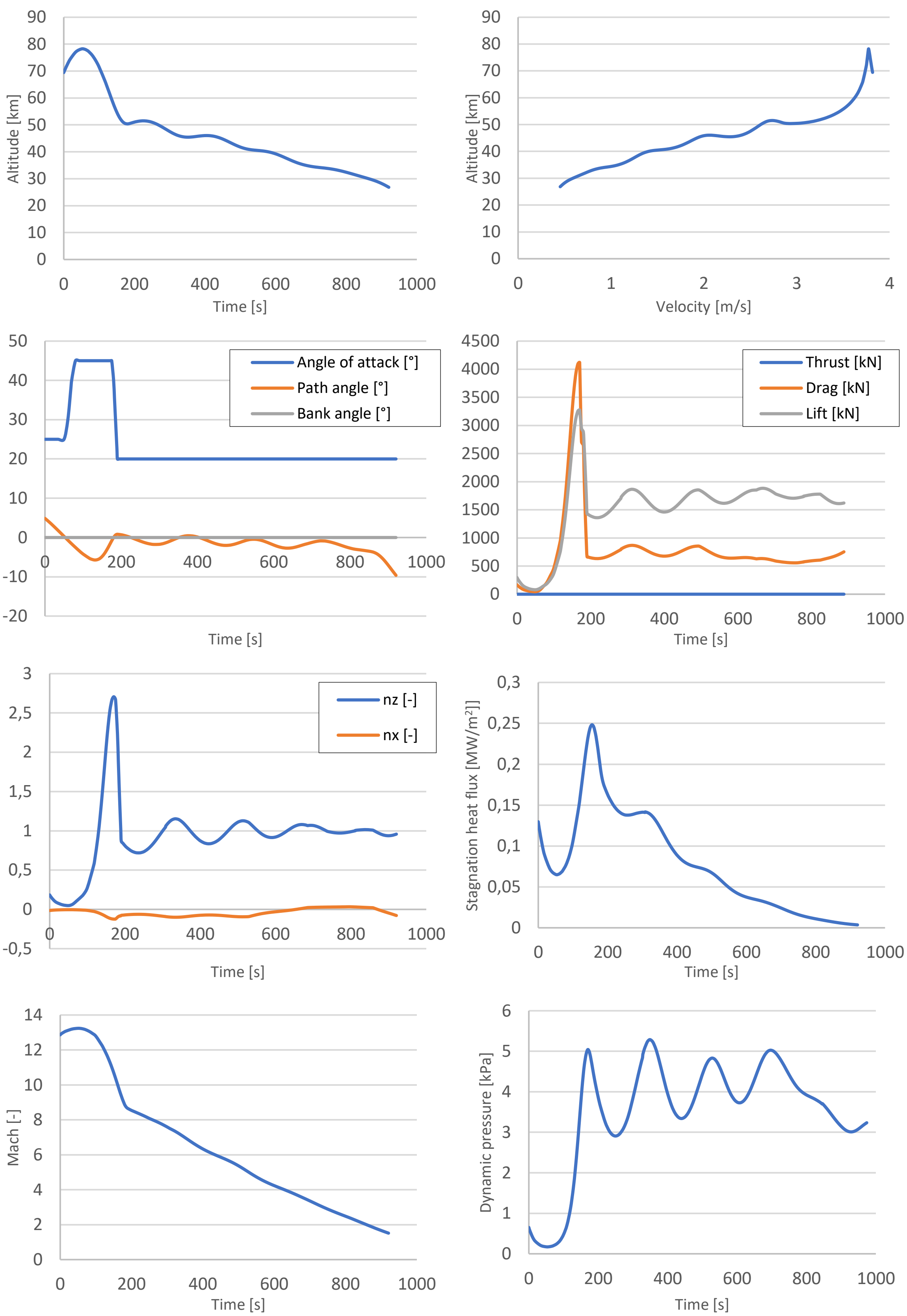

Figure 5.3 - Output data for descent (α_{max}=45°)

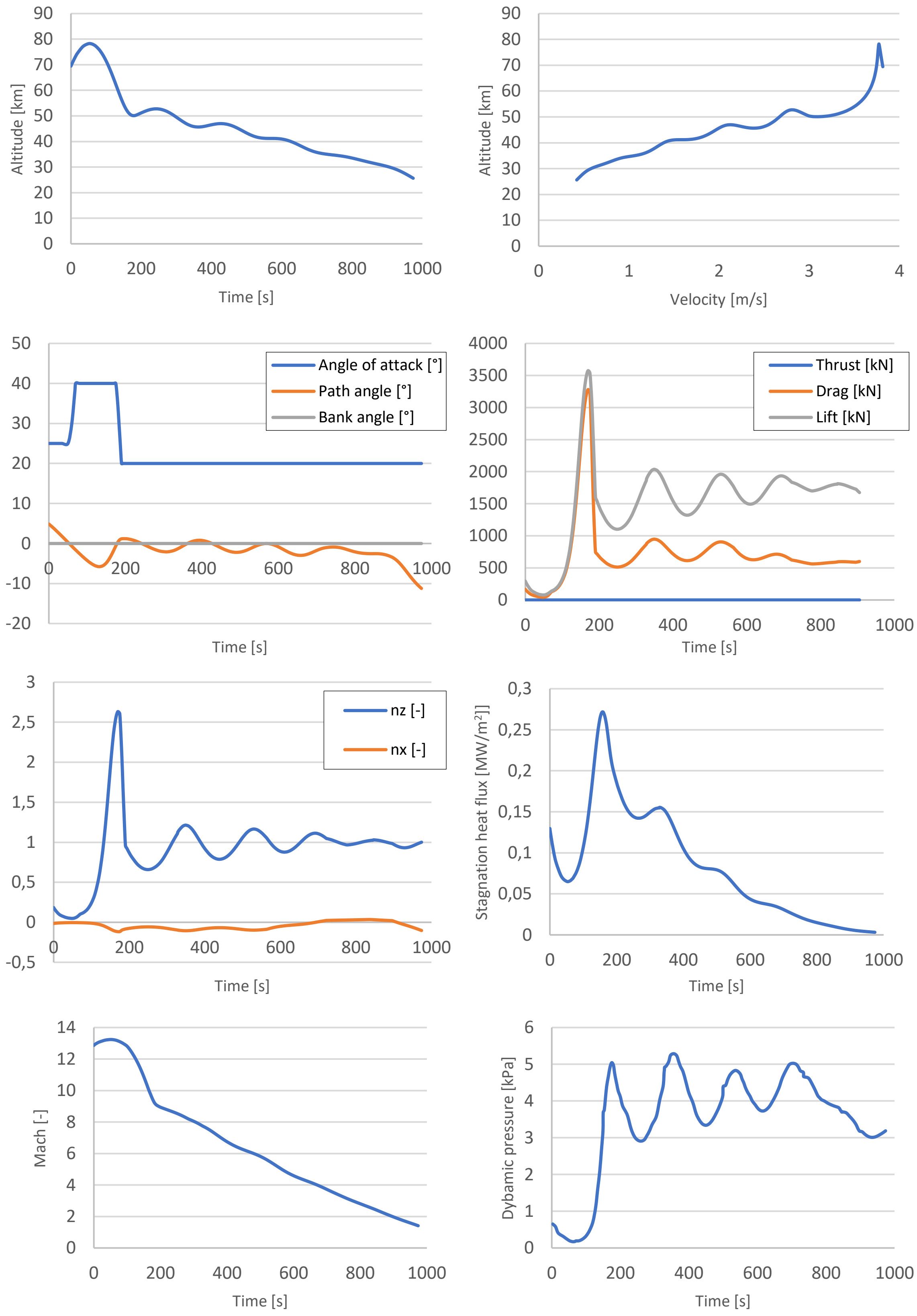

Figure 5.4 - Output data for descent (α_{max}=40°)

The reduction of the maximum angle of attack leads to a variation of both the acceleration and the stagnation point heat flux. However, while the acceleration n_z is reduced, the stagnation point heat flux increases. The dynamic pressure instead remains almost constant for the three cases.

	α_{max}=50°	α_{max}=45°	α_{max}=40°
Dynamic pressure [kPa]	5	5.2	5.2
Acceleration n_z	2.69	2.67	2.62
Stagn. Pt. heat flux [MW/m^2]	0.23	0.25	0.27

Table 5.2 - Output values for different angles of attack

In a second step the angle of attack has been kept constant for the entire first part of the flight and three different estimation have been done with α=40°, α=45° and α=50°. The case with α=40° is presented in Figure 5.5.

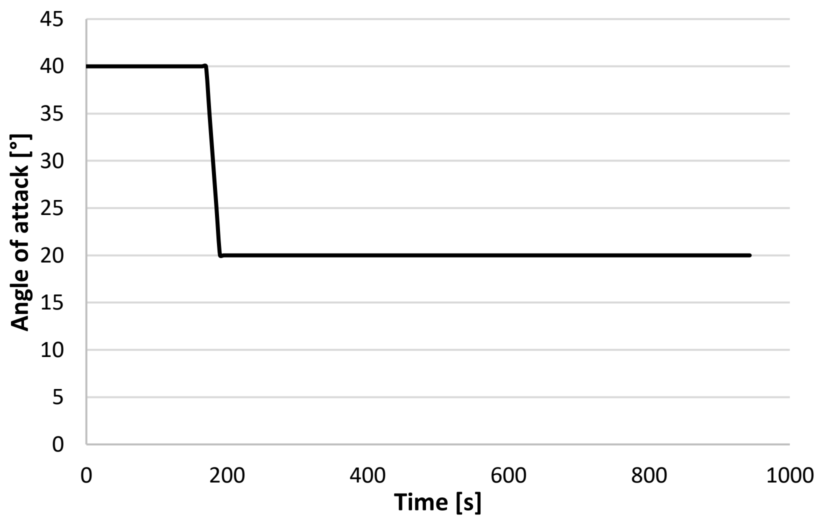

Figure 5.5 - Angle of attack during descent ($\alpha_{initial}$=40°)

The results are reported in Figure 5.6, Figure 5.7 and Figure 5.8.

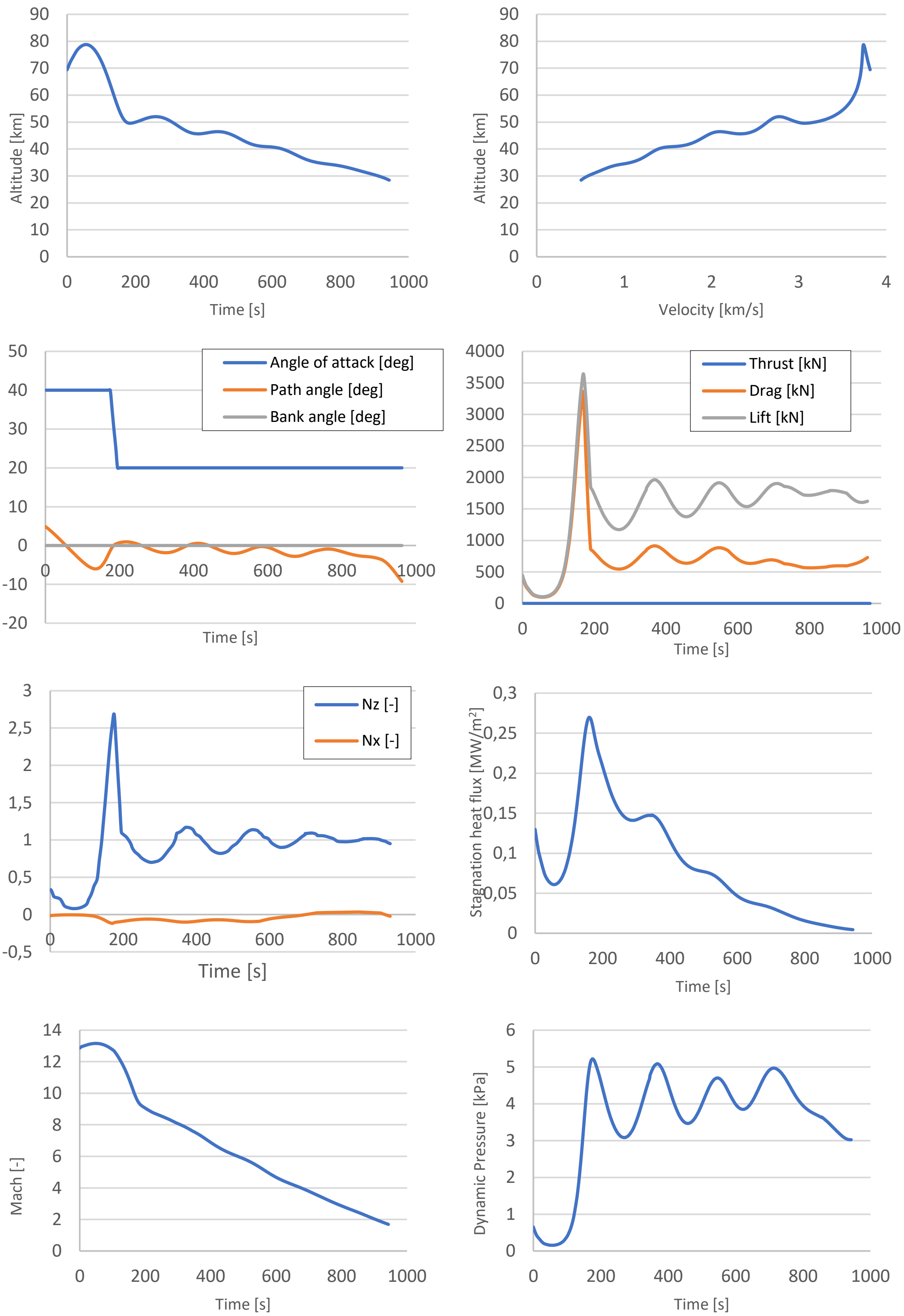

Figure 5.6 - Output data for $\alpha_{initial}$=40°

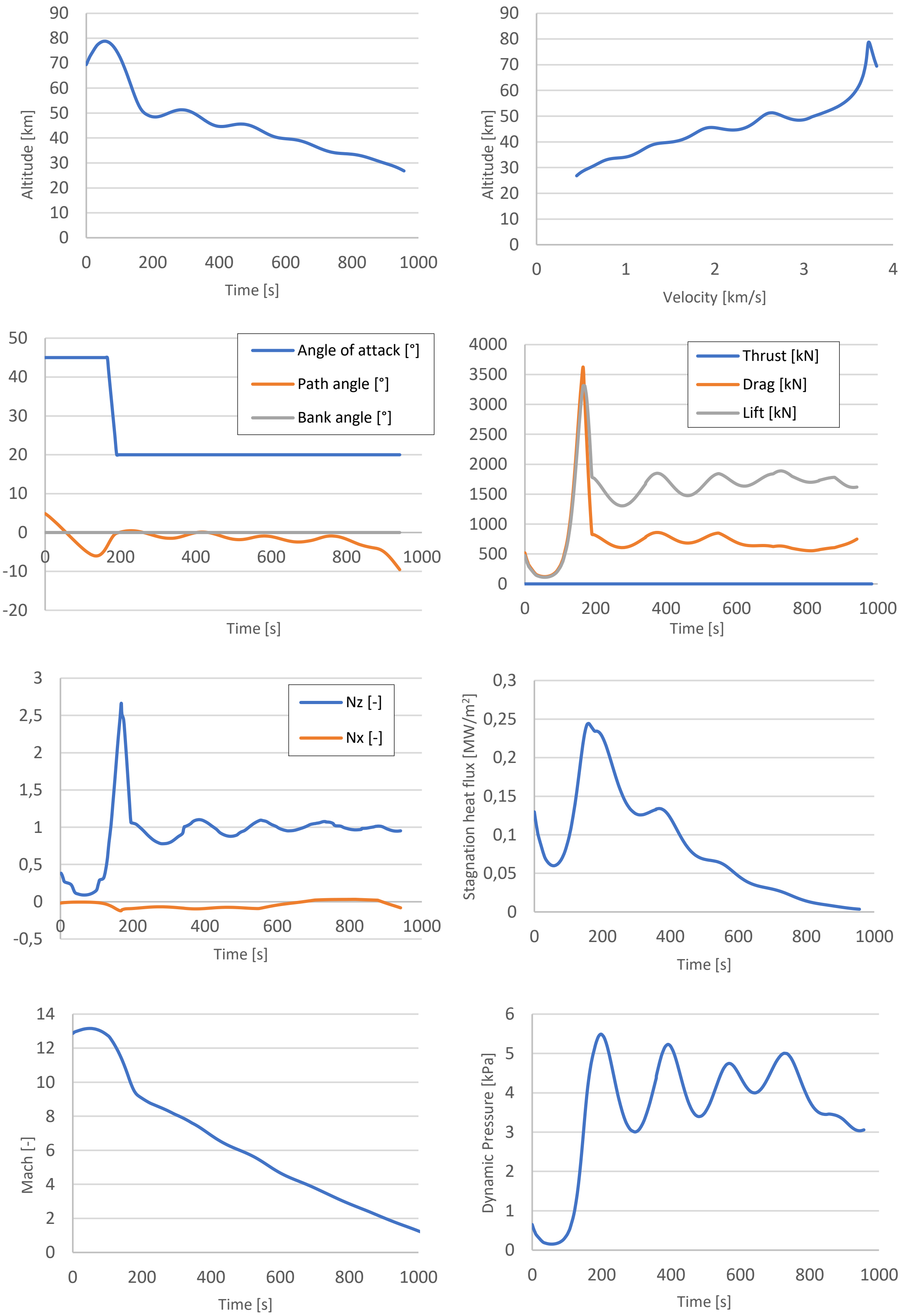

Figure 5.7 - Output data for $\alpha_{initial}$=45°

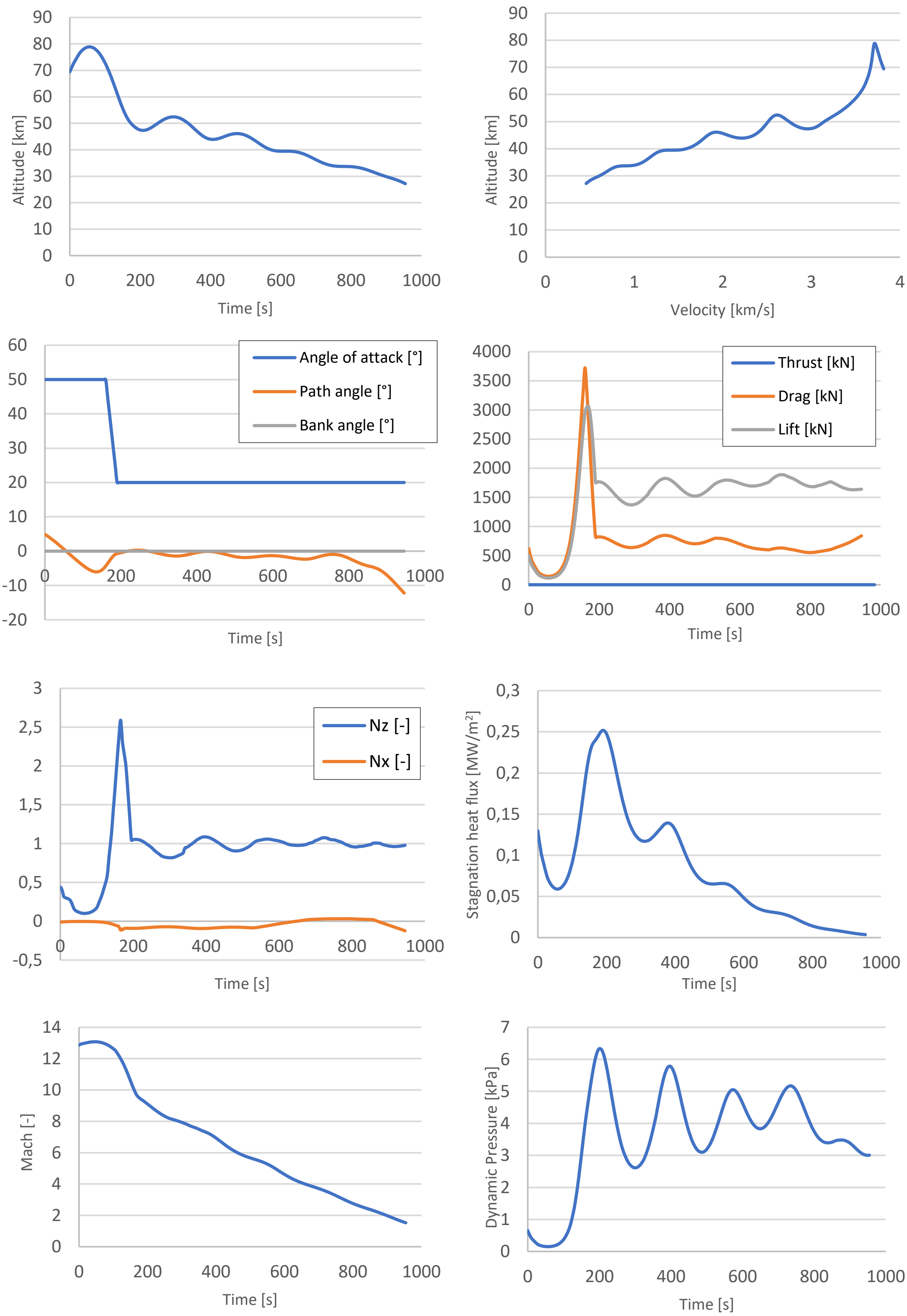

Figure 5.8 - Output data for $\alpha_{initial}$=50°

From this analysis it is possible to notice that, with the increase of the initial angle of attack, both the acceleration n_z and the stagnation point heat flux decrease. Instead, the dynamic pressure increases, but still maintains values that are quite below the operational limits. The results are presented in Table 5.3.

	α=40°	α=45°	α=50°
Dynamic pressure [kPa]	5.2	5.43	6.3
Acceleration n_z	2.63	2.47	2.10
Stagn. Pt. heat flux [MW/m^2]	0.27	0.25	0.24

Table 5.3 - Output data for α=40°, 45°, 50°

The best combination of angle of attack during the descent is the one with the maximum angle of 50°, which is shown in Figure 5.9.

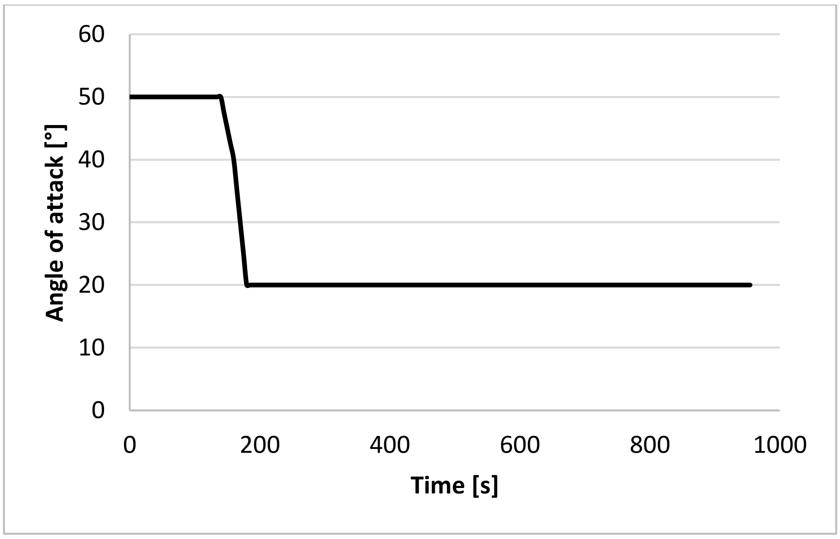

Figure 5.9 - Angle of attack during descent

Once a first simulation of the descent trajectory has been completed, the TPS that is needed for the descent is estimated using TOP. Then, it is possible to calculate the new SpaceLiner booster mass. The ascent trajectory can be evaluated considering the mass estimation upgrade.

In a first step, the ascent has been computed with TOSCA in simulation mode. The pitching rate has been manually modified in order to minimize dV_1. This velocity should be under 50 m/s, to avoid any convergence issue while computing the ascent with TOSCA in optimization mode.

5.1 Ascent trajectory

The ascent trajectory, resulting from the iterative process described previously, is presented here. The designated launch site is Kourou, French Guyana and the initial parameters are reported in Table 5.4.

Altitude [km]	Longitude [°]	Latitude [°]	Flight path angle [°]	Azimuth [°]
0	-52.77	5.24	90	0

Table 5.4 - Initial parameters for the ascent

The optimized final parameters, resulted from TOSCA, are presented in Figure 5.10. Looking at the plot of mass over time, it is possible to see that the total system mass is continuously decreasing during the ascent, as the booster fuel is consumed to produce thrust. However, 223 s after lift-off, the mass presents a sudden reduction, from approximately 545 000 kg to 337 000 kg. This variation in mass coincides with the separation of the orbiter from the booster: it takes place at an altitude of 65.3 Km with a velocity of about 3790 m/s. From this point on, the booster starts the descent with all its engines turned off. The orbiter instead, continues its flight to reach the final orbit using its own propellant.

An important parameter that has to be considered here is the dynamic pressure. Its maximum value is of around 34.3 KPa, which is an acceptable value since it is below the structural limits of the SpaceLiner.

After the ascent is optimized, the mass of the payload that is possible to bring to orbit is evaluated with RTS. The results are shown in Table 5.5.

Orbit perigee height [Km]	*Orbit apogee height [Km]*	*Payload mass [Kg]*
28.9	*248.9*	*27383*

Table 5.5 - Final orbit and payload data

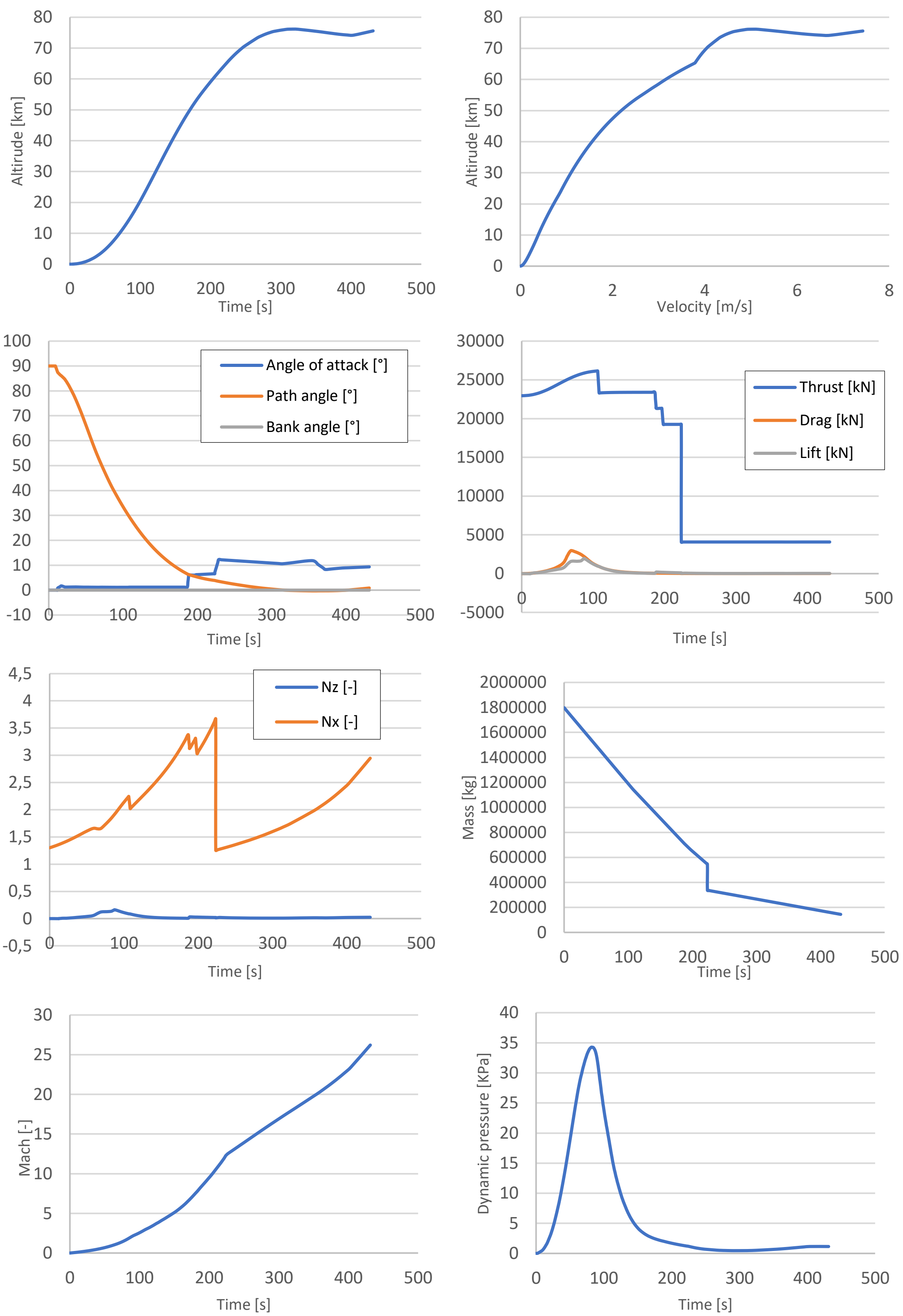

Figure 5.10 - Optimized parameters of the ascent trajectory

5.2 Descent trajectory

As previously stated, the booster starts its descent trajectory when the separation from the orbiter stage occurs. The initial parameters for the booster descent are shown in Table 5.6.

Altitude [km]	Longitude [°]	Latitude [°]	Velocity [m/s]	Flight path angle [°]	Azimuth [°]	Inclination [°]
65.3	-50.39	5.17	3789.80	3.88	-1.91	5.44

Table 5.6 - Initial parameters for the booster descent

The results of the descent simulation are reported in Figure 5.12, while the ground track is shown in Figure 5.11.

Figure 5.11 - Ground track of the descent trajectory

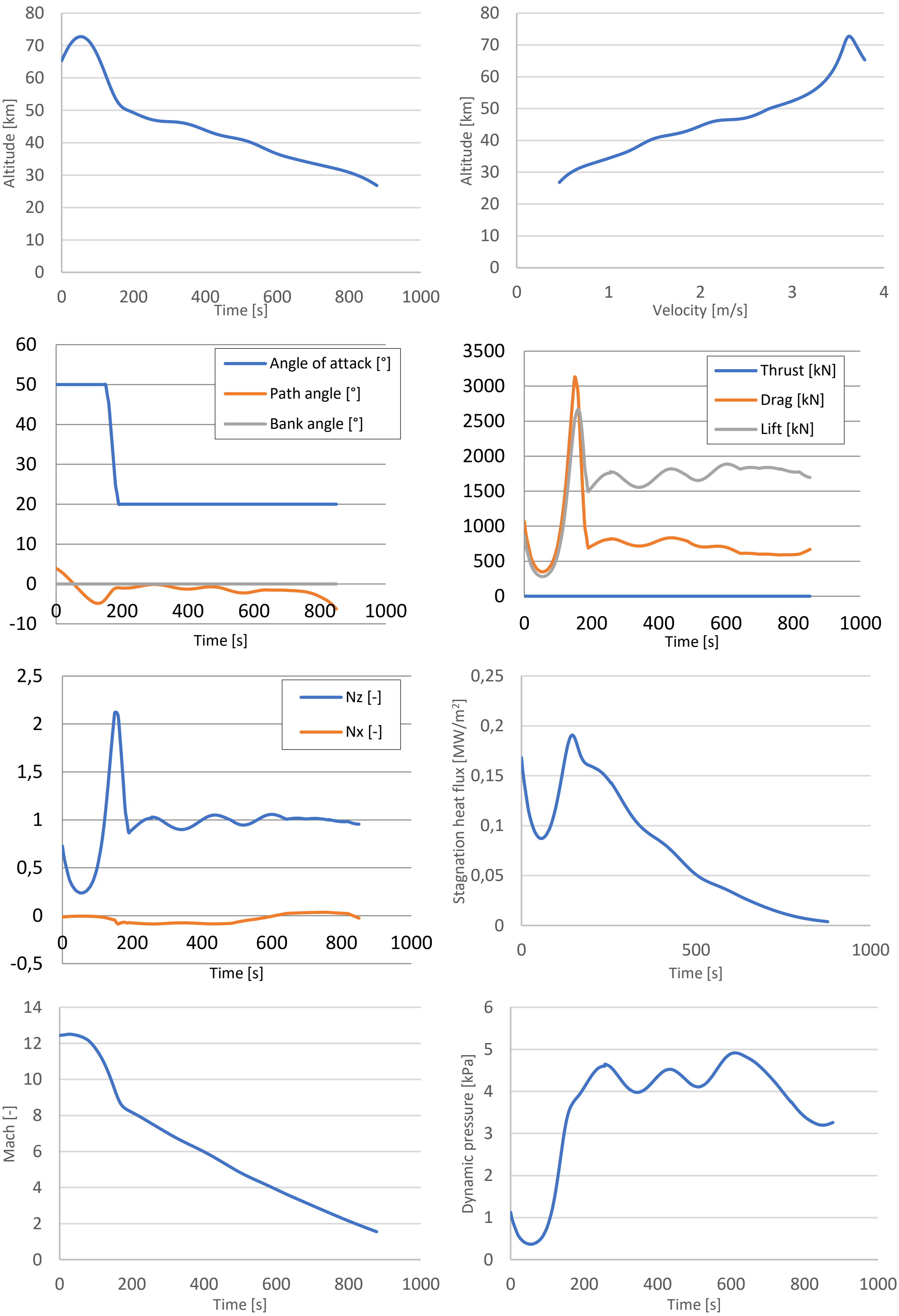

Figure 5.12 - Parameters for the booster descent

The values of both dynamic pressure and acceleration n_z are similar to those evaluated at the beginning of the iteration process. The maximum value of the dynamic pressure is equal to 4.9 kPa. The maximum value of the acceleration n_z is of about 2.1. The third parameter that has to be considered is the stagnation point heat flux: its maximum value is 0.19 MW/m^2 and Its trend is reported in Figure 5.13.

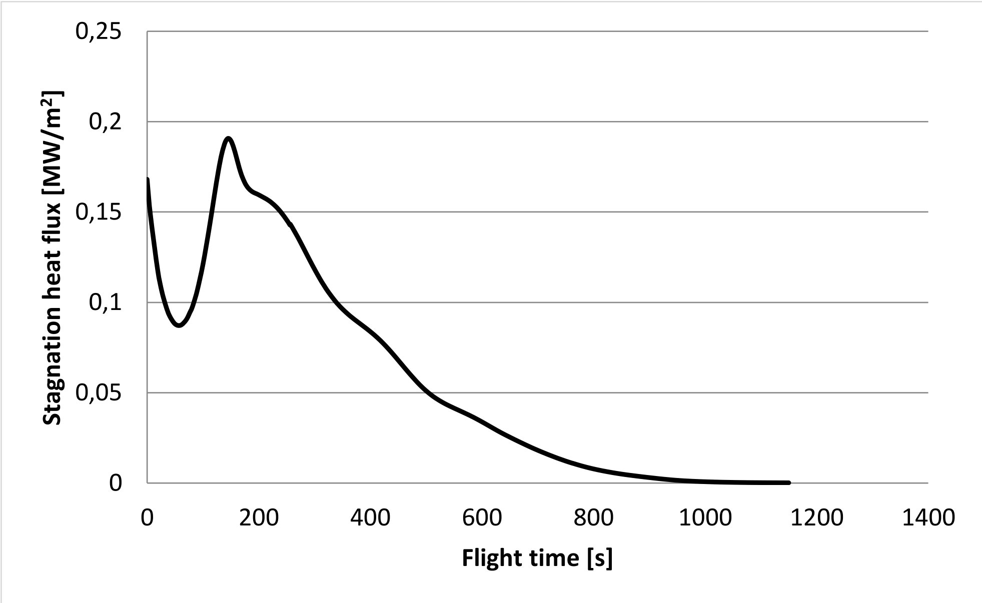

Figure 5.13 - Stagnation point heat flux during descent

5.3 Thermal Protection System

Once the descent trajectory is known, the thermal protection system configuration and mass can be evaluated. Here a passive TPS is considered. A total of 20 evenly distributed flight points are considered in the simulation with TOP. These points are selected only from the hypersonic part of the descent trajectory, which presents the most demanding conditions in terms of heat flux. For each flight point, the resulting heat flux and temperatures are evaluated on the whole surface of the booster. The surface is divided into 13 temperatures areas, according to the heat load that is present in each zone. Once the temperature distribution is known, the proper material is assigned to the different areas. The output of this computation shows the position of the centre of gravity, the mass for each surface area and the overall mass of the thermal protection system. Two cases are studied: for the first one a set of non-metallic materials is used, while for the second one both metallic and non-metallic materials are considered.

5.3.1 TPS with non-metallic materials

The set of materials that are used and the corresponding temperature range are presented in Table 5.7. The materials used are: Felt Reusable Surface Insulation (FRSI), Advanced Flexible Reusable Surface Insulation (AFRSI), Tailorable Advanced Blanket Insulation (TABI), Alumina Enhanced Thermal Barrier (AETB TUFI) and Ceramic Matrix Composite (CMC).

Material	Temperature range [K]
FRSI	400 < T < 500
AFRSI	500 < T < 600
AFRSI	600 < T < 700
AFRSI	700 < T < 800
TABI	800 < T < 900
TABI	900 < T < 1000
TABI	1000 < T < 1100
TABI	1100 < T < 1200
TABI	1200 < T < 1300
AETB TUFI	1300 < T < 1400
AETB TUFI	1400 < T <1500
CMC	1500 < T <1600
CMC	1600 < T <1700

Table 5.7 - Materials used for TPS

One of the inputs required for TOP simulation is the simulation time: here it has been selected as the time needed to reach M=1 plus a 30 min margin. The first one of these times is obtained from the TOSCA output file of the descent trajectory.
The thermal protection system mass has been calculated based on the latest booster ascent and descent trajectories and the results are shown in Table 5.8.

TPS mass [kg]	Empty Booster mass [kg]
12 990	196 320

Table 5.8 - TPS and Booster mass

The temperature distribution on the booster surface during descent is shown in Figure 5.14 and Figure 5.15, while a breakdown of TPS mass is shown in Figure 5.16.

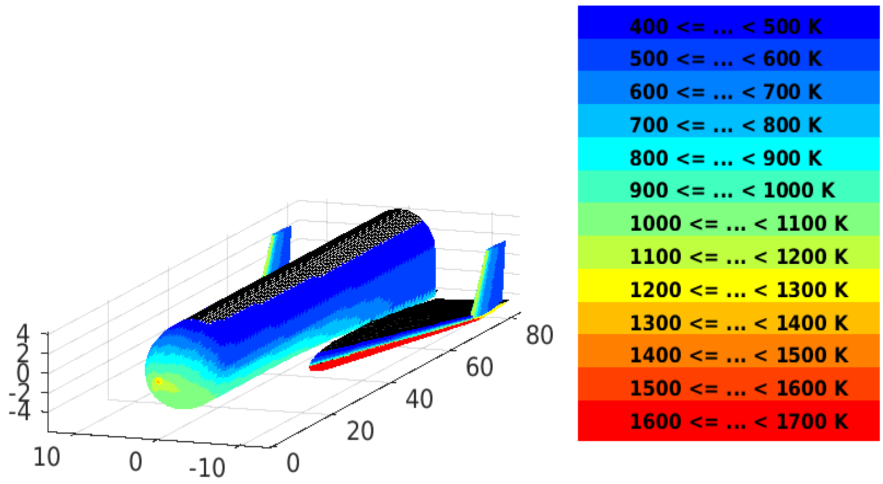

Figure 5.14 - Maximum temperature distribution during descent (front view)

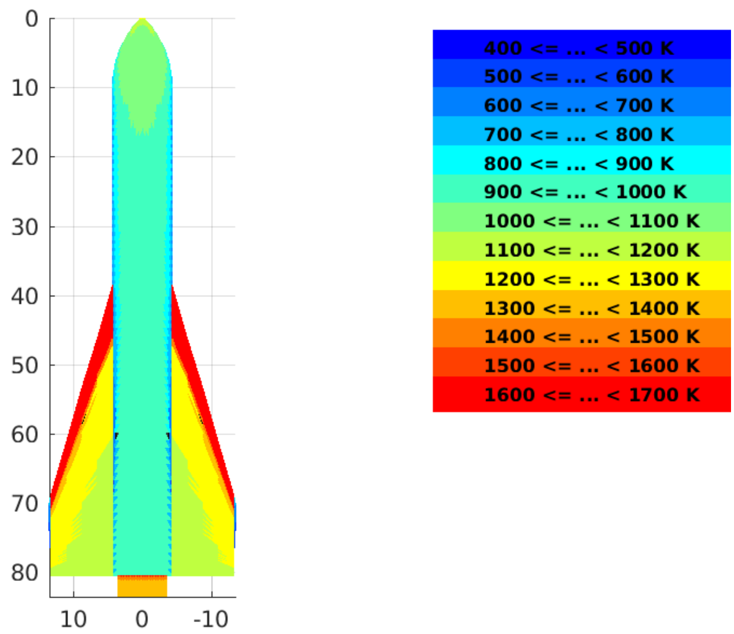

Figure 5.15 - Maximum temperature distribution during descent (bottom view)

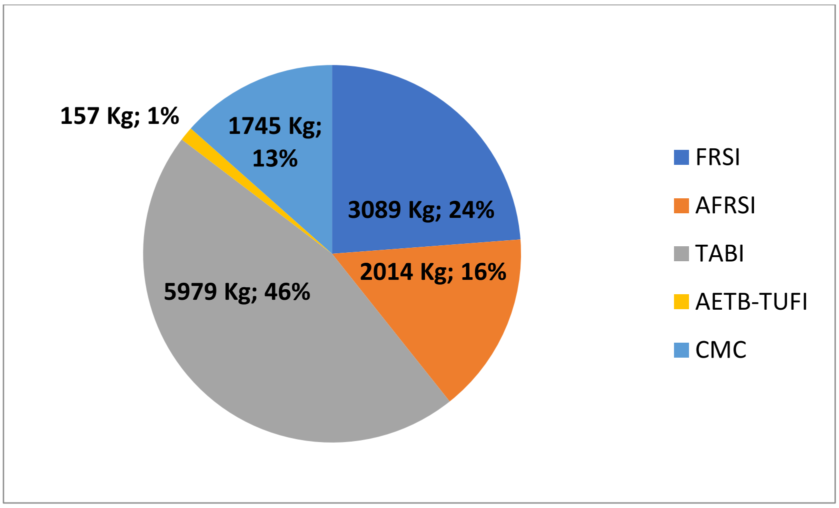

Figure 5.16 - TPS mass breakdown

5.3.2 TPS with metallic materials

In all the simulations that have been done until now, the TPS was composed by a set of non-metallic materials. However, in this study, an alternative configuration involving metallic materials has been also considered. This solution aims to reduce the costs for Reusable Launching Vehicles, offering some advantages from an operational point of view. The TPS has been computed again with the materials presented in Table 5.9. The metallic material has a maximum temperature of 1300 K, so there is still the need to use other kind of materials for higher temperatures, especially in the nose region and on the lower part of wings and fuselage. There is also a main disadvantage linked to the use of metallic materials: they are usually heavier than the others and they contribute to an increase of the overall mass of the stage.

Material	Temperature range [K]
Inconel	400 < T < 1300
TABI	1300 < T < 1400
AETB	1400 < T < 1600
CMC	1600 < T < 1700

Table 5.9 - Materials used for the TPS

A comparison of the TPS resulting mass in the two cases is presented in Table 5.10. If metallic materials are used, the mass increases from approximately 13 tons to 23 tons.

Non-metallic TPS [kg]	Metallic TPS [kg]	Empty booster mass [kg]
12 990	22 943	209 514

Table 5.10 - Comparison between the two TPS

The TPS mass breakdown is shown in Figure 5.17. It can be seen here that the majority of the TPS mass is represented by the metallic part.

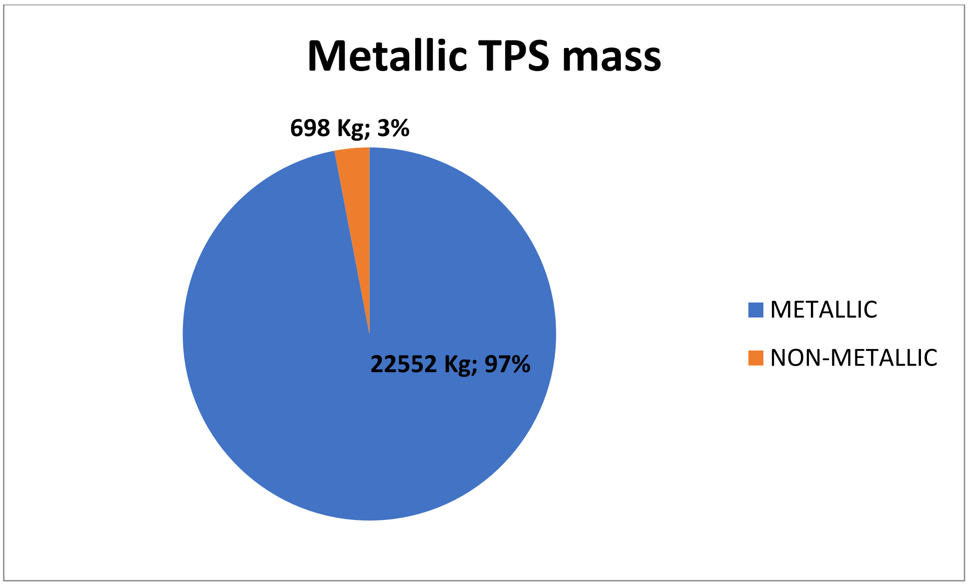

Figure 5.17 - Metallic TPS mass breakdown

Since the TPS mass is increasing, it is necessary to compute again the ascent and descent trajectories with the new TPS. The results of this iterative process are presented here.
The parameters for the ascent trajectories are the same used in the previous case and the results obtained are shown in Figure 5.19. From these data, it is possible to obtain the initial parameters for the descent, presented in Table 5.11.

Altitude [Km]	Longitude [°]	Latitude [°]	Velocity [m/s]	Flight path angle [°]	Azimuth [°]	Inclination [°]
65.73	-50.4414	5.1548	3725.47	4.02143	-2.25976	5.530785

Table 5.11 - Initial parameter for the descent

The parameters are quite similar to the previous case, since the launch configuration is almost the same: it presents only a small increment in mass, due to the TPS of the booster stage. The velocity is lower and the performances in general are slightly worse than before. The payload is also evaluated and the resulting masses are shown in Table 5.12, where a comparison with the previous case is presented. The use of a metallic TPS has a great effect on the final payload mass: the loss is of almost 4000 kg, since it is reduced from 28 382 kg to 23 394 kg. This value is still acceptable, but it represents a considerable disadvantage with respect to the non-metallic case.

Payload with non-metallic TPS [kg]	Payload with metallic TPS [kg]
27 382	23 394

Table 5.12 - Payload comparison

The next step consists in the simulation of the descent trajectory. The parameters that results from the simulation with TOSCA are shown in Figure 5.20, while the ground track of the descent is reported in Figure 5.18**Errore. L'origine riferimento non è stata trovata.**.

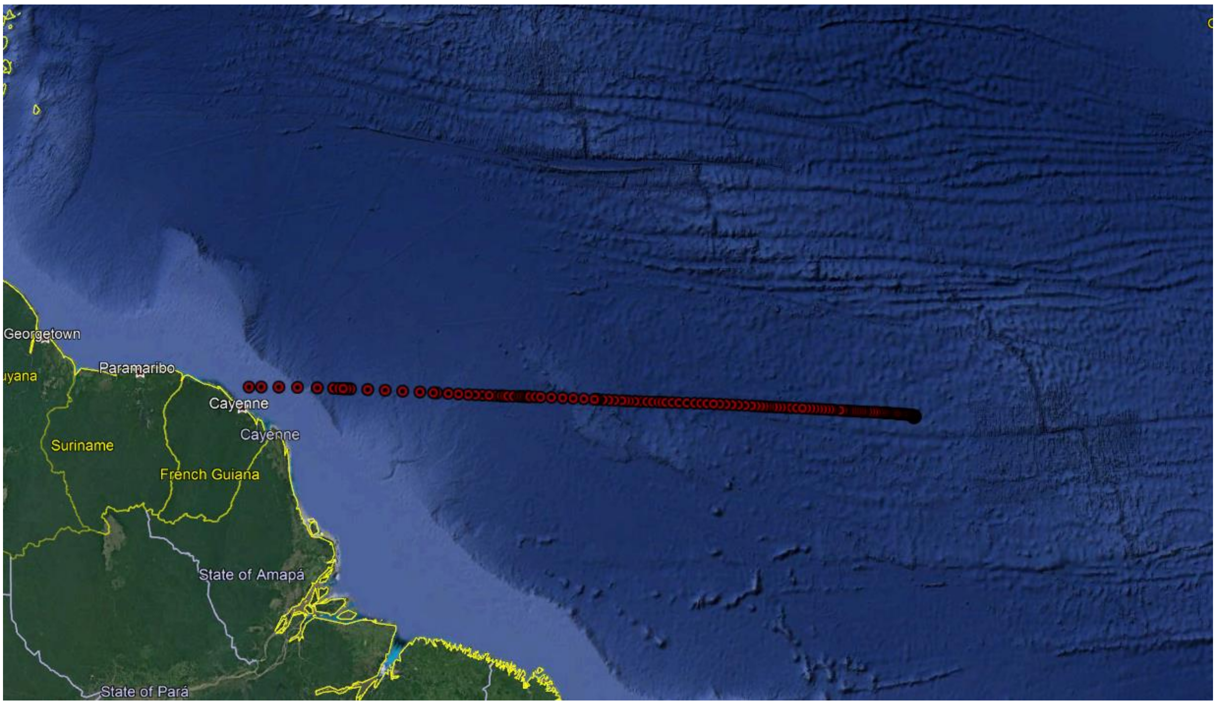

Figure 5.18 - Ground track for the descent trajectory (Metallic TPS)

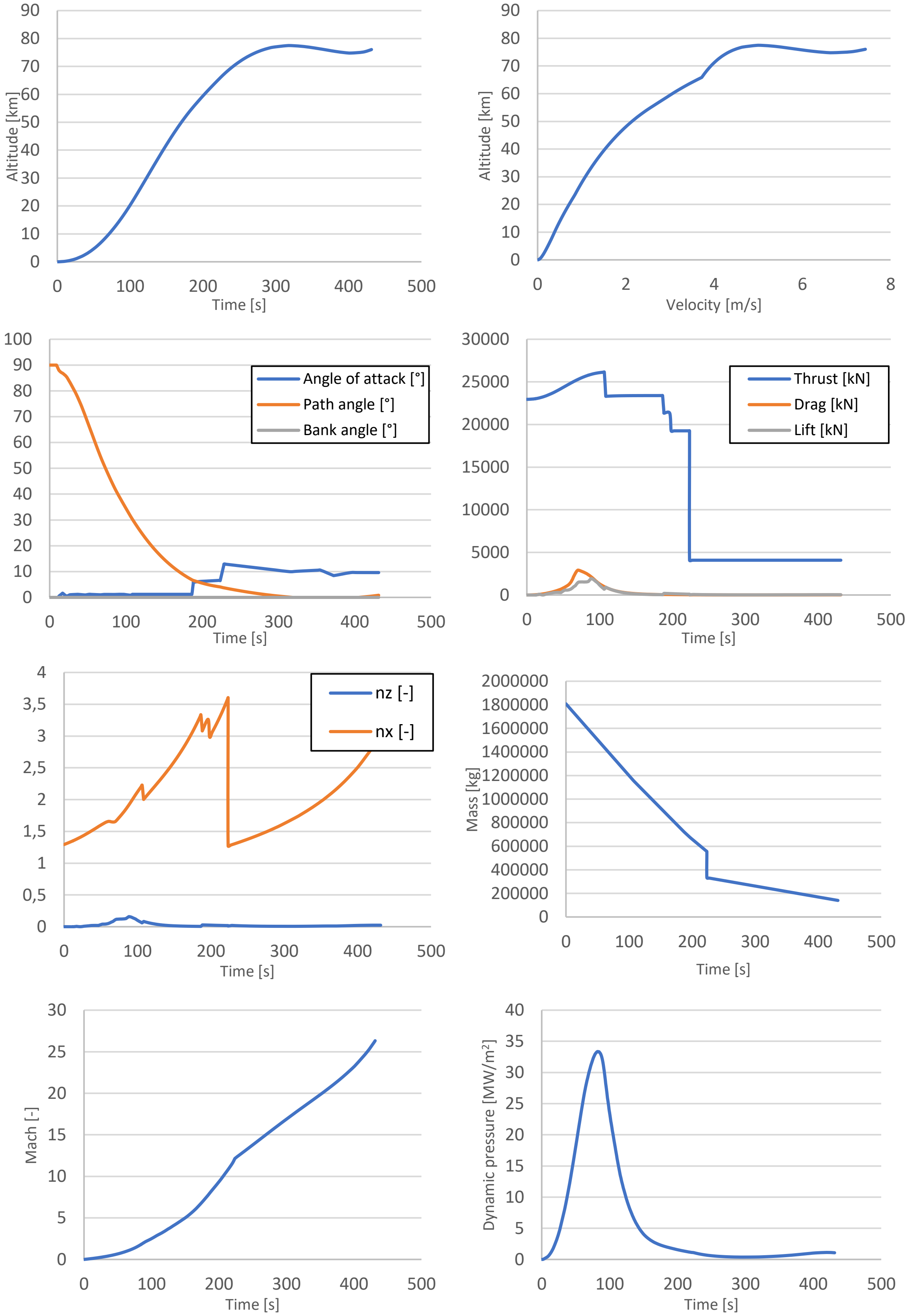

Figure 5.19 - Parameters for ascent trajectory (Metallic TPS)

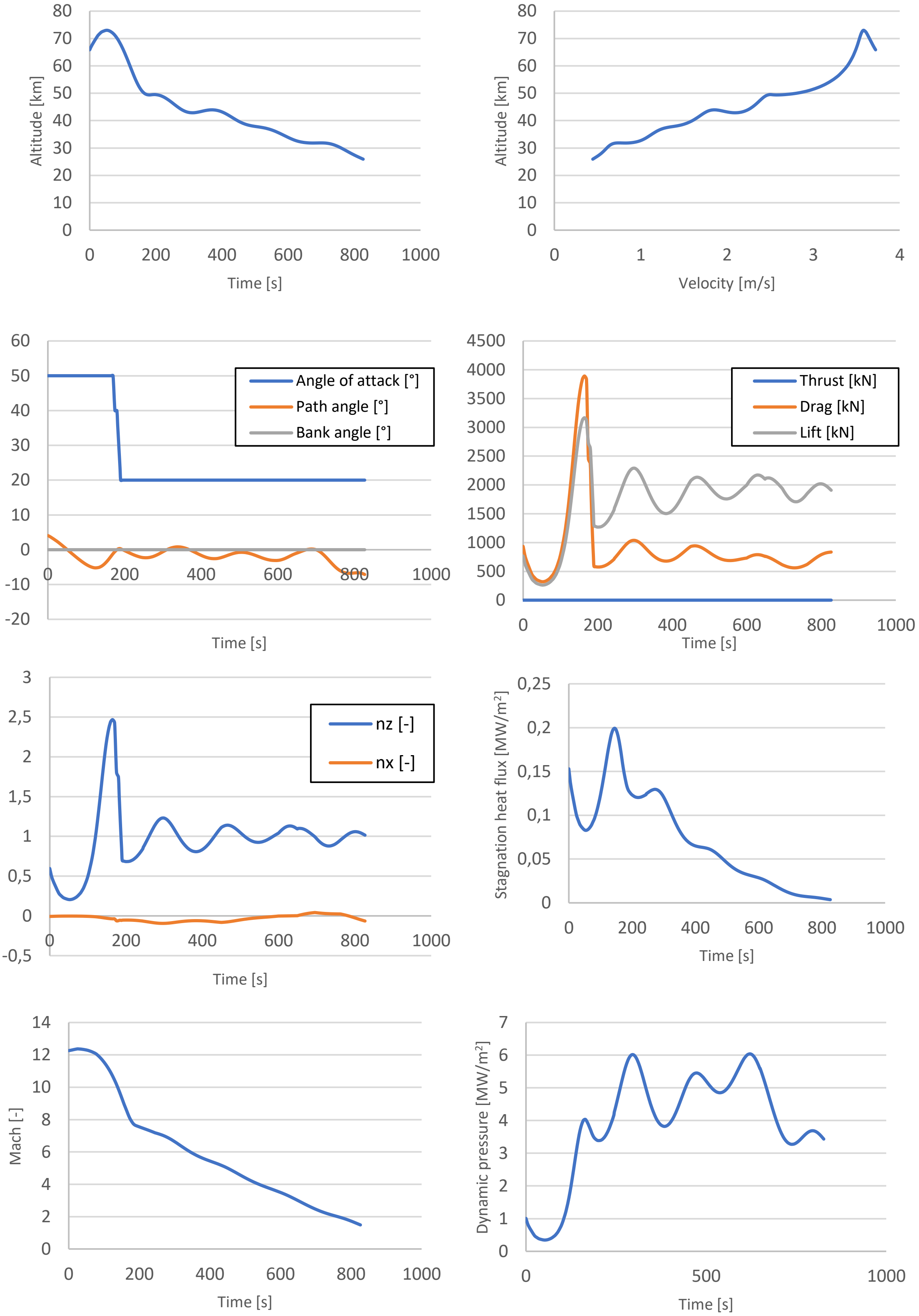

Figure 5.20 - Parameters for the descent trajectories (Metallic TPS)

The resulting values are compared with the ones found previously. First, one can notice that the peak of the acceleration n_z is slightly higher than before. The same can be said for the dynamic pressure, which has a peak of about 6.3 KPa. The stagnation point heat flux reaches a maximum of about 0.21 MW/m^2. However, it is possible to affirm that the comparison between these values and the ones found with a non-metallic TPS shows small differences, as one can expect. This happens because the configuration is the same in the two cases, with only the only difference being in the TPS mass.

5.4 Comparison with SL7

Once both the ascent and the descent trajectories have been computed for the new SpaceLiner Booster configuration, it is possible to compare the results with the previous SL7 configuration. For what concerns the ascent phase dynamic pressure, acceleration and drag coefficient are compared.

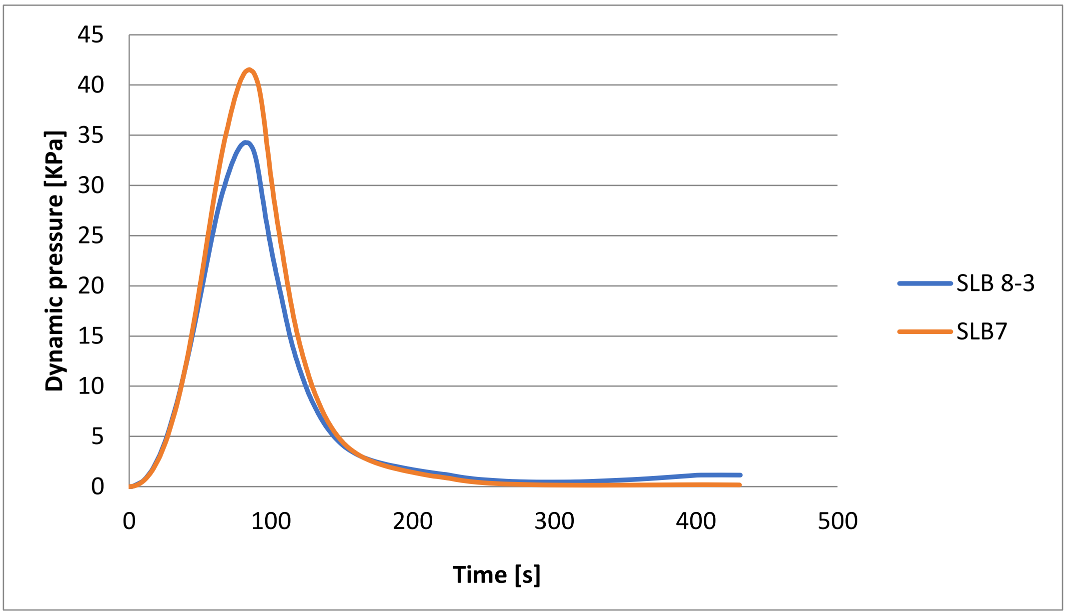

Figure 5.21 - Comparison of dynamic pressure during ascent

From these graphs it is clear that the dynamic pressure is lower with respect to the SL7. This difference however is not so big between the two cases.

Moreover, the mass of the booster, the payload and the velocity at separation have been compared. The results are reported in Table 5.13.

	SLB 8-3	SLB 7
Total mass at lift-off [kg]	1 797 979	1 811 906
Ascent propellant [kg]	1 025 057	1 039 057
Empty booster mass [kg]	196 320	193 240
Payload [kg]	27 382	28 776
Velocity (at separation) [m/s]	3 791	3 841

Table 5.13 - Mass and velocity comparison

From the comparison of these data, it is clear that the achieved performances in terms of payload are slightly decreasing. However, the new value is still acceptable and does not place any limits to the successful result of the mission.

Once the ascent trajectories have been compared, it is possible to analyse the parameters of the descent trajectory. In Figure 5.22 and Figure 5.23, the dynamic pressure and the acceleration along the z-axis (n_z) are shown.

The maximum value for the dynamic pressure is higher with the SLB 7 and this difference is equal to approximately 1 kPa. However, values of dynamic pressure in both cases are not so high and they do not represent a serious issue for the descent flight.

The maximum value of the acceleration along the z-axis has a similar value in both cases and it is equal to 2.1 g_0. The overall trend, instead, presents some differences. With the new configuration, after its first peak, it maintains a value around 1 and it presents some small oscillations. With the SLB 7, instead, its oscillations have a greater amplitude.

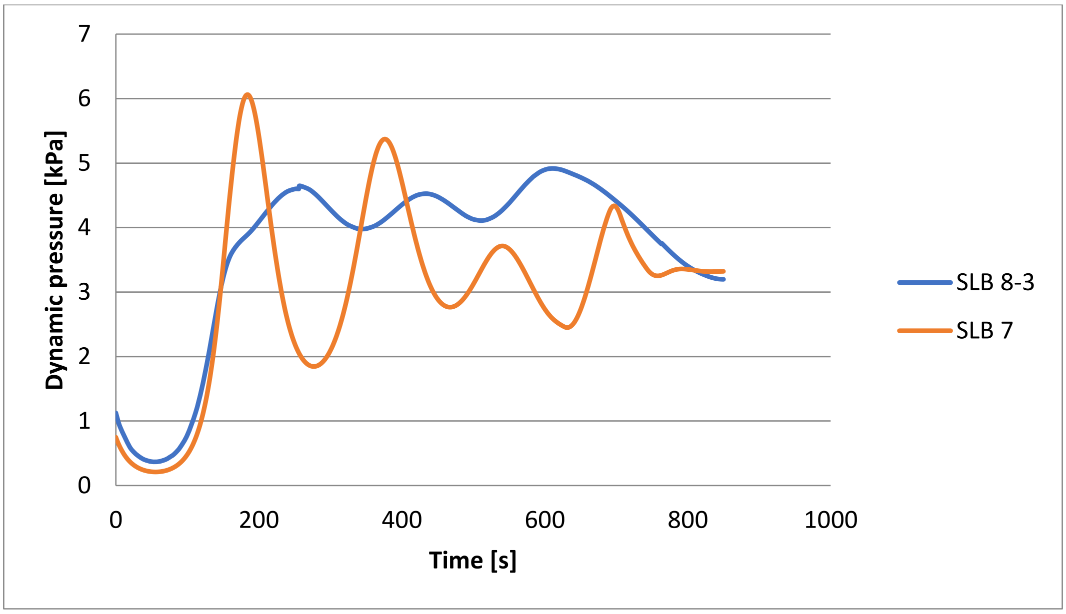

Figure 5.22 - Comparison of dynamic pressure during descent

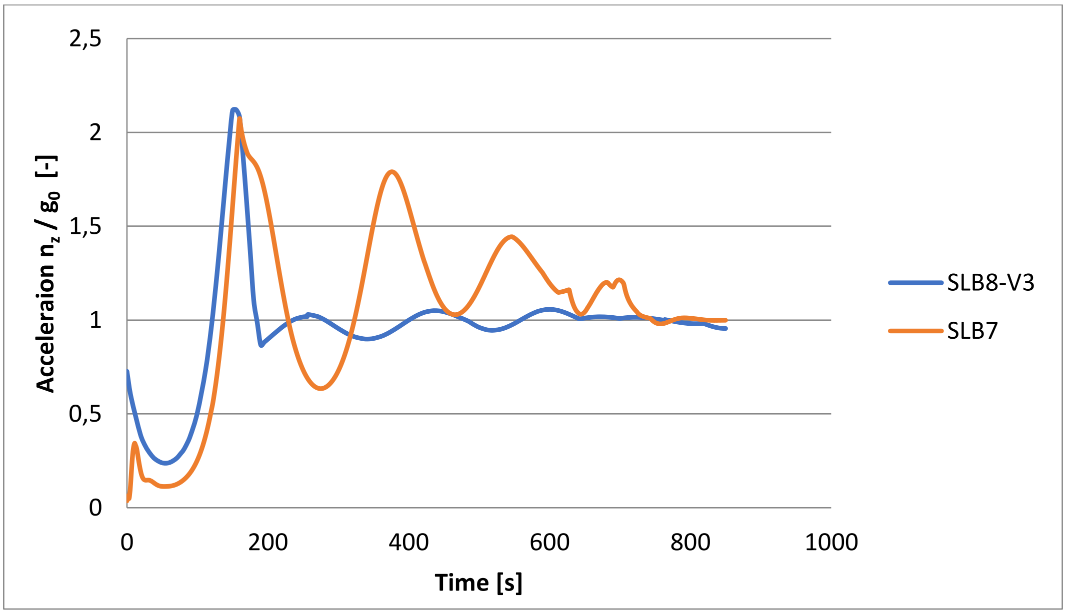

Figure 5.23 - Comparison of acceleration n_z during descent

5.5 Payload estimation with different mechanism mass

During previous trajectory computations, the mass of the sweeping mechanism that was considered was the same as estimated with STSM. Now a different mass is used, taking as a reference a study on variable wings that was carried on at DLR in the past. The mass used for the sweeping mechanism is equal to 1250 kg on each side of the wing [15].
However, since the configuration considered in this study is different from the SL booster, this mass is still a very preliminary estimation. For that reason, two computation are done. The first one considers a mechanism mass that is equal to the one of the reference study, while the second one is a conservative estimation: the mass is now doubled.

The ascent is computed for the two cases and the results are shown in Figure 5.24 and Figure 5.25. A metallic TPS is considered here. The results obtained for the ascent trajectory are quite similar in these two cases. The main difference lies on the payload that is possible to bring to orbit: with the increase of the mechanism mass, the payload decreases to values below 23 000 kg. In particular with the first mechanism mass of 2500 kg, the payload is reduced to 22 656 kg, while with the conservative approach it decrease to 21 860 kg. The results are shown in Table 5.14.

Mechanism mass [kg]	Payload [kg]
1990	23 594
2500	22 656
5000	21 860

Table 5.14 - Payload with different mechanism mass

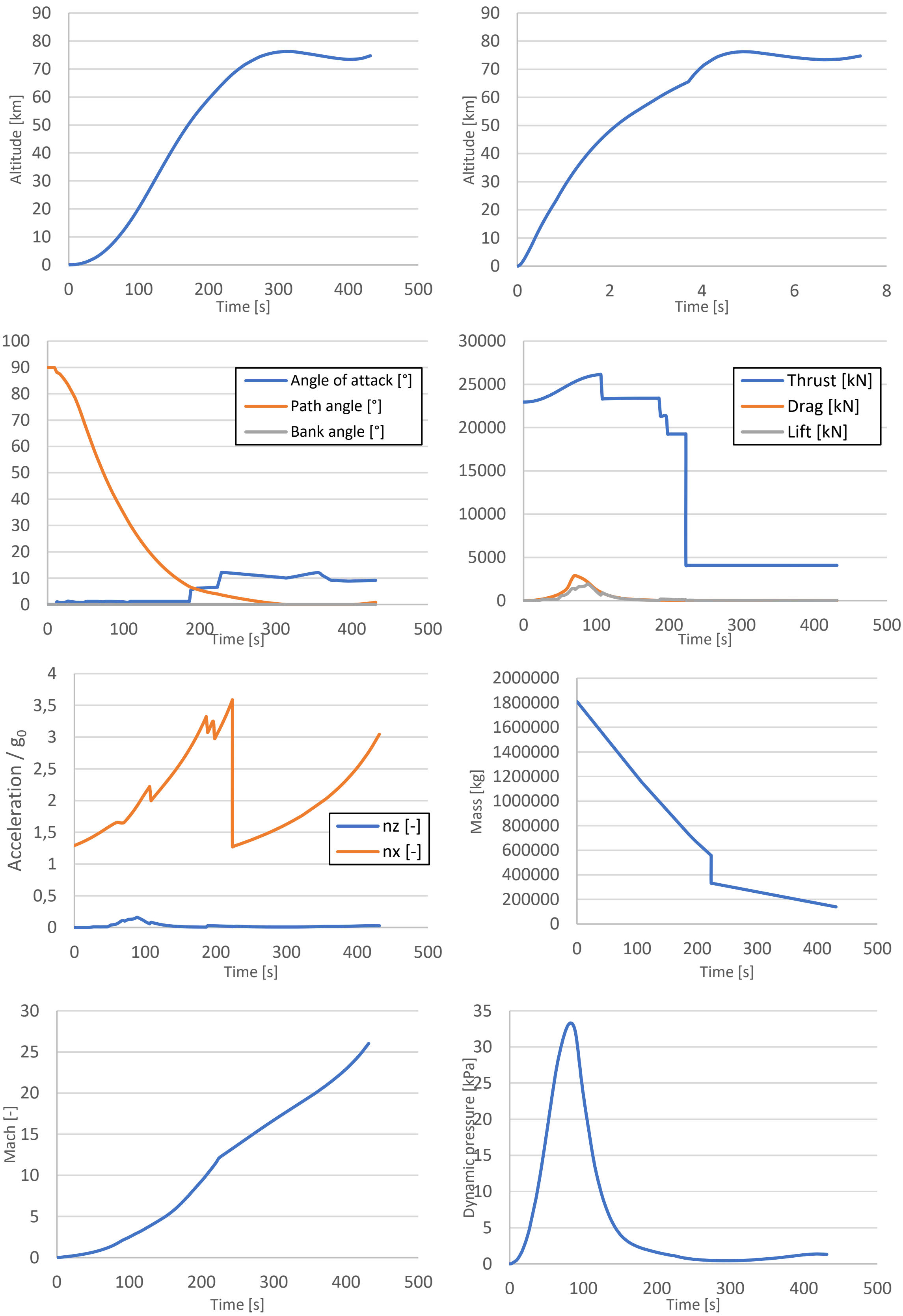

Figure 5.24 - Ascent trajectory with mechanism mass from previous study

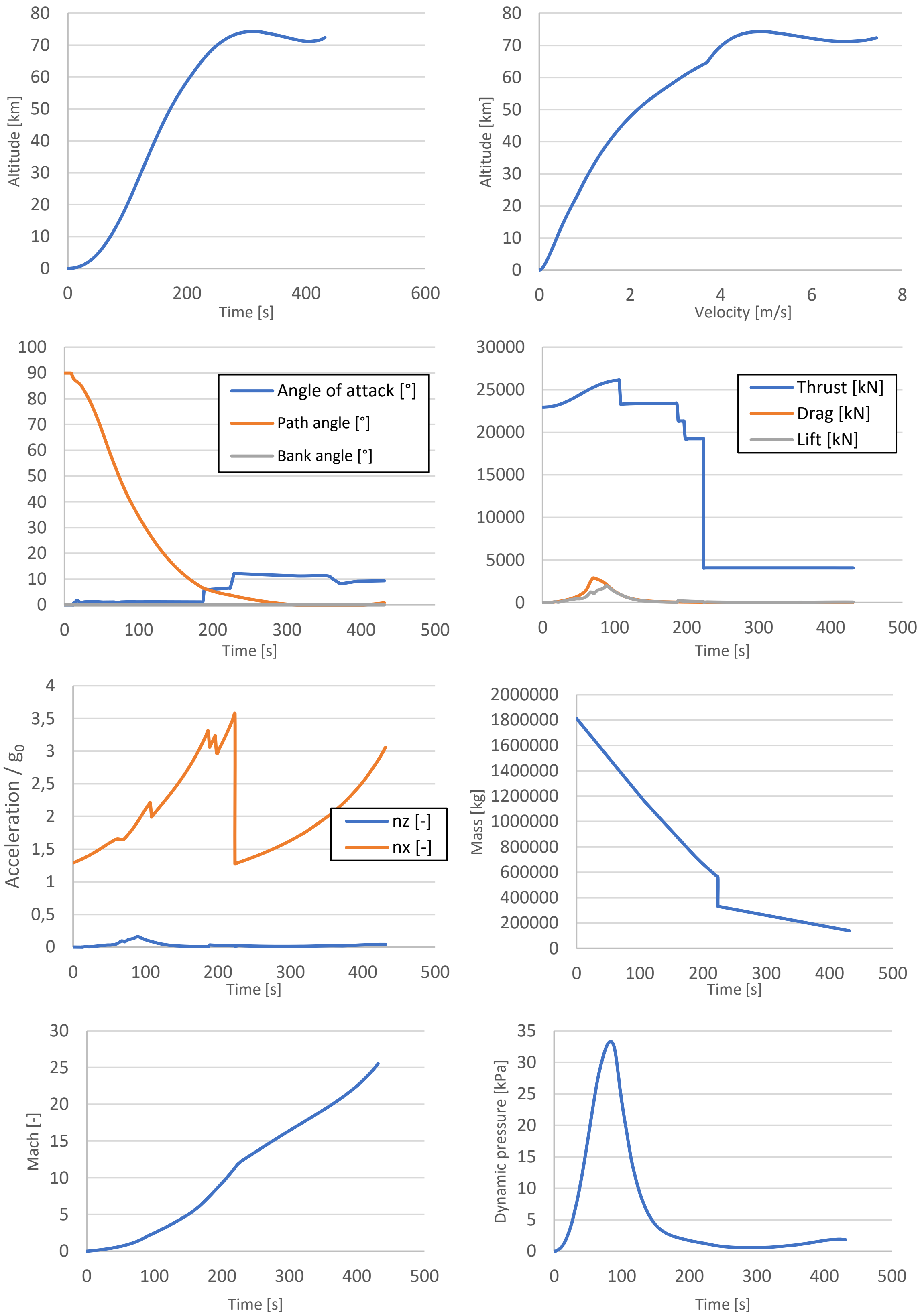

Figure 5.25 - Ascent trajectory with mechanism mass from previous study (conservative case)

Chapter 6 Aerodynamic data comparison with Missile Datcom

A different tool can be used to evaluate the aerodynamic coefficients of the SLB 8-3 configuration. The tool selected is Missile Datcom, since it is able to provide aerodynamic results with a satisfactory accuracy for a preliminary analysis. Those data, in particular the lift and the drag coefficients, are compared with the same data resulting from the computation with CAC and HOTSOSE, in order to validate the analysis that has been done up to this point. However, it must be highlighted that each of these tool provides only a preliminary estimation.
The subsonic computation has been carried on for three different Mach numbers: M=0,2, M=0.4 and M=0.6. The comparison between CAC and Missile Datcom for the subsonic regime is presented in Figure 6.1, Figure 6.2 and Figure 6.3. The red line corresponds to the CAC data, while the blue line is equivalent to the Missile Datcom data. For a first analysis, the deflection of flap is not considered (δ_{flap}=0°).

A good correlation is found between the C_L evaluated with CAC and the same coefficient computed with Missile Datcom. The slope of the resulting C_L curve is almost the same and the values of lift coefficients are quite similar for a wide range of angles of attack. This can be considered as a first validation of the data obtained with CAC. Something similar can be asserted for what concerns C_D. In this case the drag coefficient values present a good correlation for low angles of attack (α<10°). However, for higher angles of attack, this is no longer true: C_D resulting from Missile Datcom is greater than C_D resulting from CAC. This discrepancy could be caused by the different methods used in CAC and Missile Datcom.

The same computation is carried on for the supersonic regime, with two different Mach numbers (M=3 and M=4). The results obtained are shown in Figure 6.4 and Figure 6.5. The good correlation between CAC and Missile Datcom is also valid for supersonic velocities. For what concerns the lift coefficient, indeed, a great similarity is found for the entire range of angles of attack (-5°<α<20°). The same cannot be said for the drag coefficient: while the general trend of the C_D curve is identical, the values computed with Missile Datcom are higher than the values evaluated with CAC. However, this behaviour is not something completely unexpected. Missile Datcom, indeed, can be more precise in the evaluation of the C_{D0} than CAC, since it takes into account some non-linear effects for the computation of the drag coefficient.

The last comparison is done between HOTSOSE (red line) and Missile Datcom (blue line), for the hypersonic Mach range. The results are shown in Figure 6.6, Figure 6.7 and Figure 6.8, respectively for M=5, M=9 and M=13. Lift and drag coefficients follow a similar trend. In particular, for low angles of attack (α<10°) the two lines present the same values, while some differences arise for higher α. This is exactly what one could expect from this comparison: since the two tools are different, a complete similarity of the results is not possible. However, since the differences in this case are limited, these comparison can be considered as a further validation of the HOTSOSE computation.

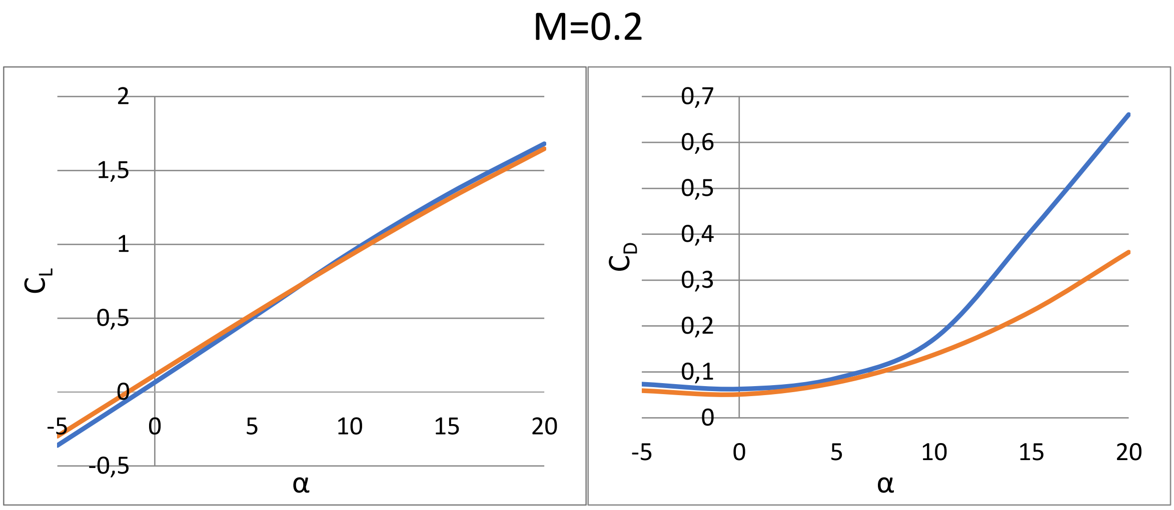

Figure 6.1 - C_L and C_D comparison for M=0.2

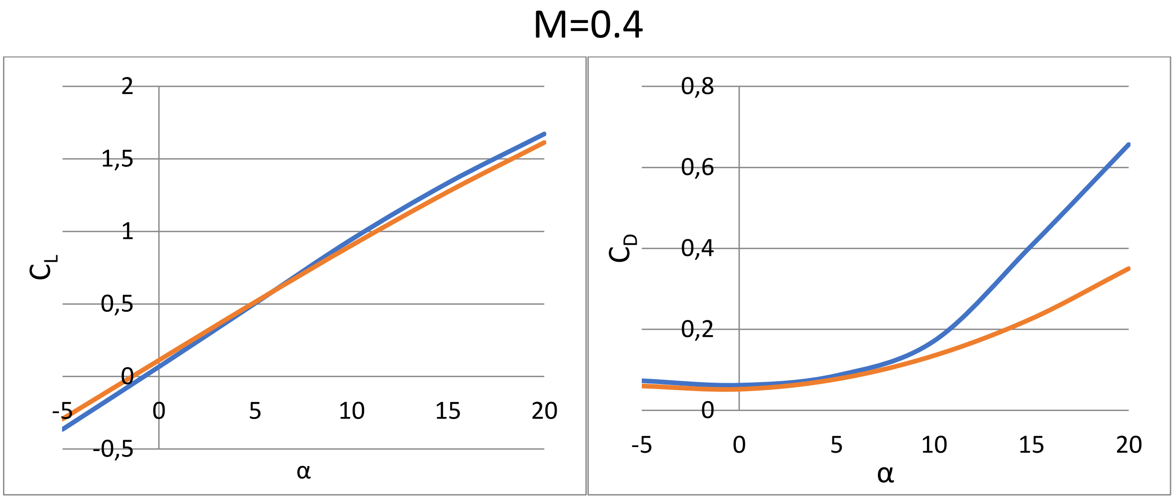

Figure 6.2 - C_L and C_D comparison for M=0.4

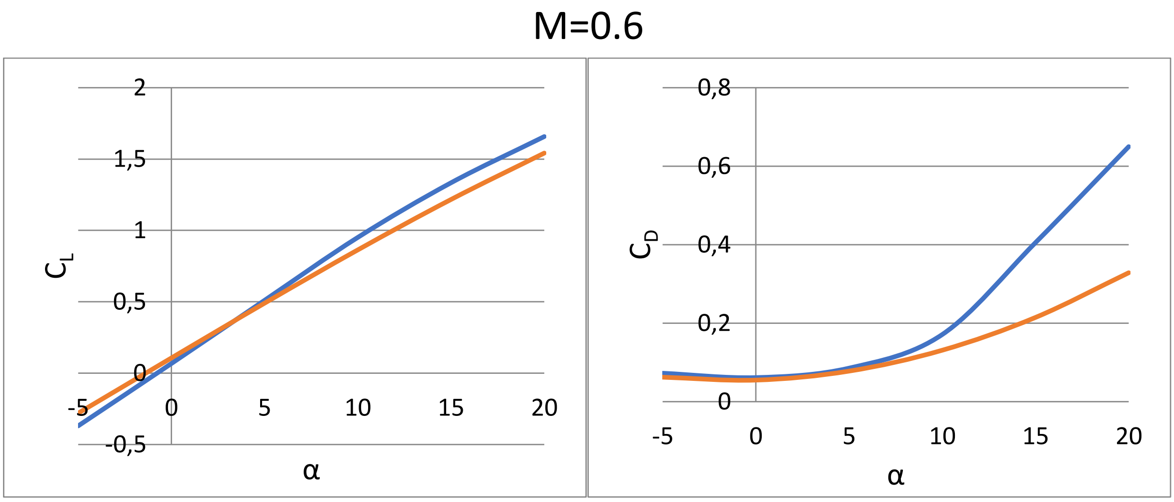

Figure 6.3 - C_L and C_D comparison for M=0.6

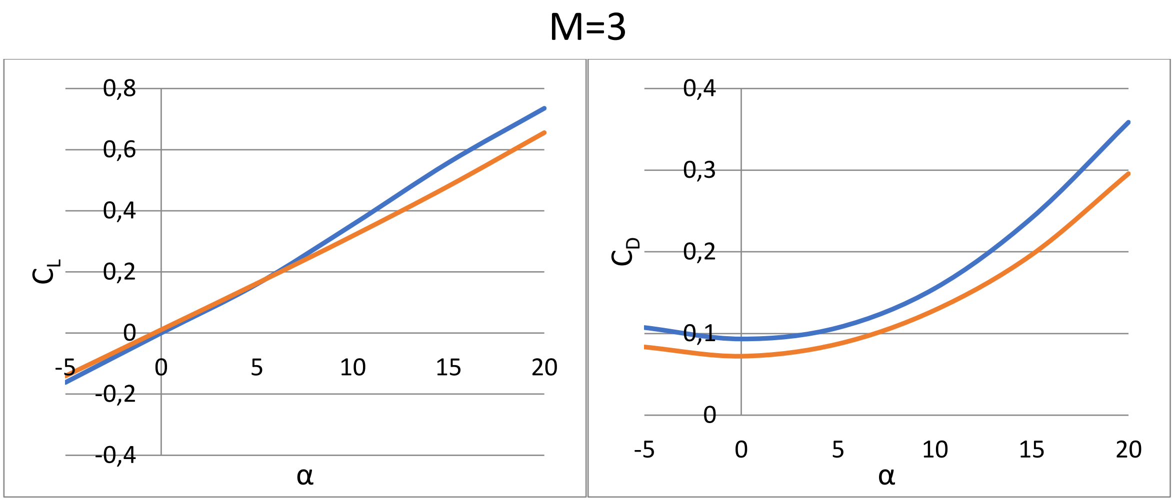

Figure 6.4 - C_L and C_D comparison for M=3

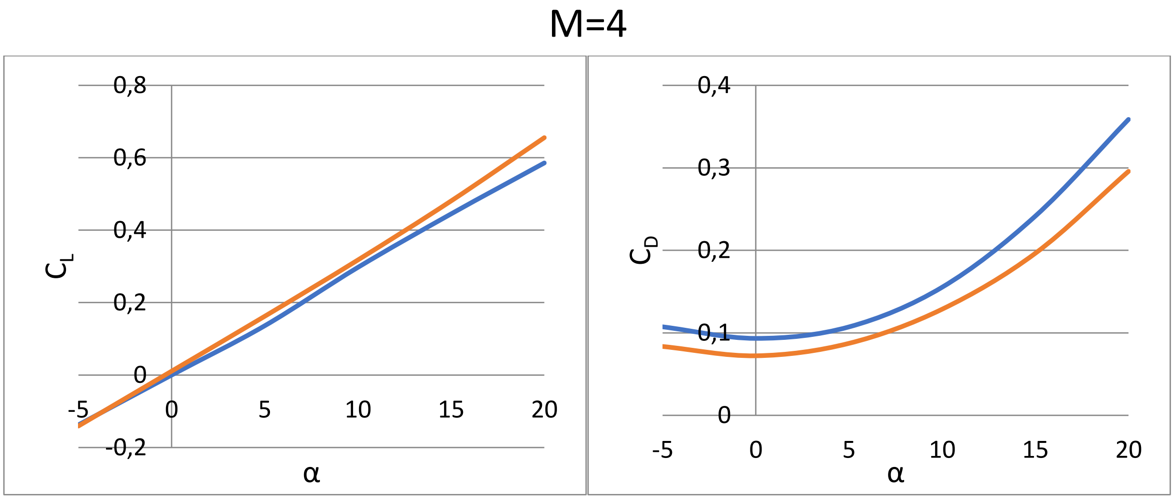

Figure 6.5 - C_L and C_D comparison for M=4

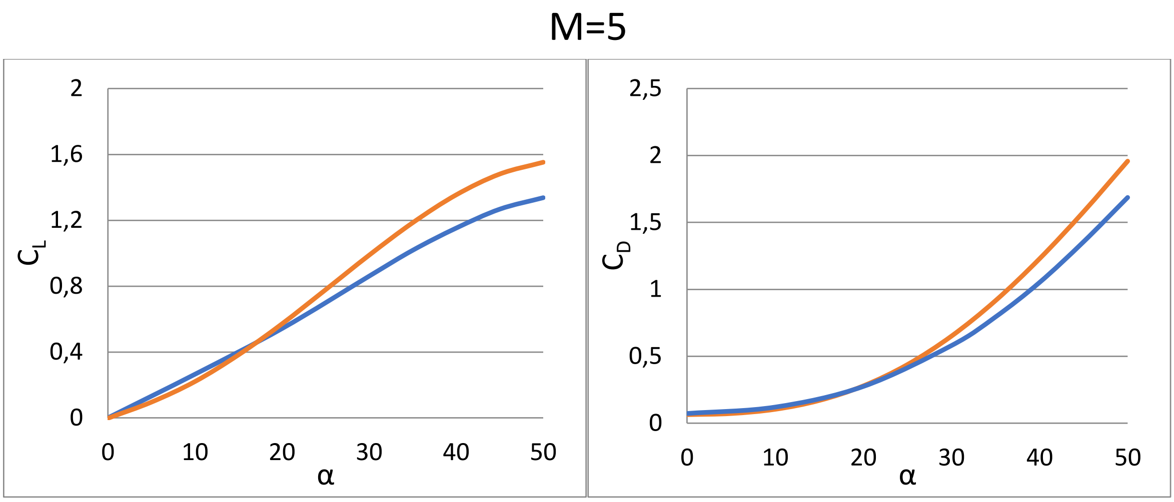

Figure 6.6 - C_L and C_D comparison for M=5

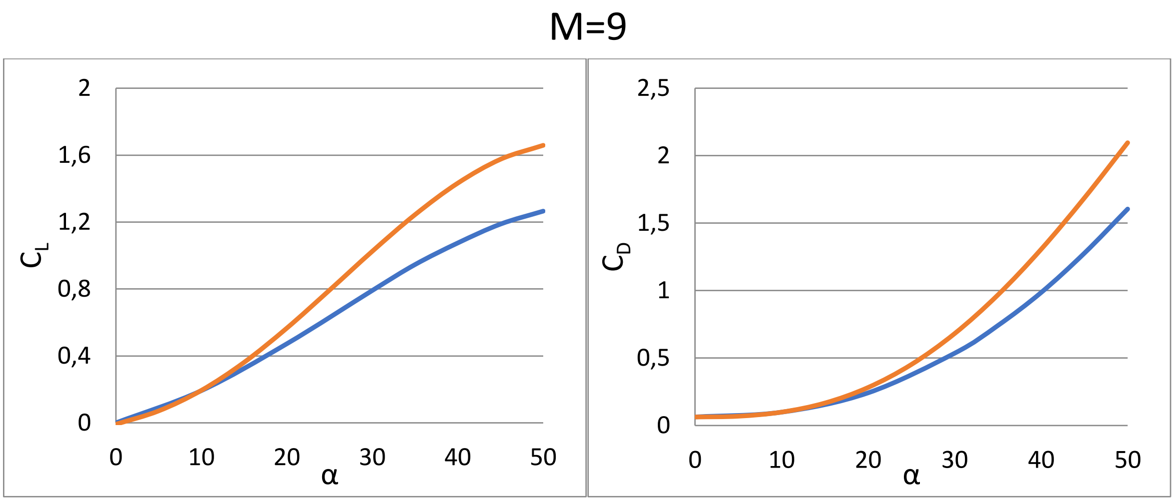

Figure 6.7 - C_L and C_D comparison for M=9

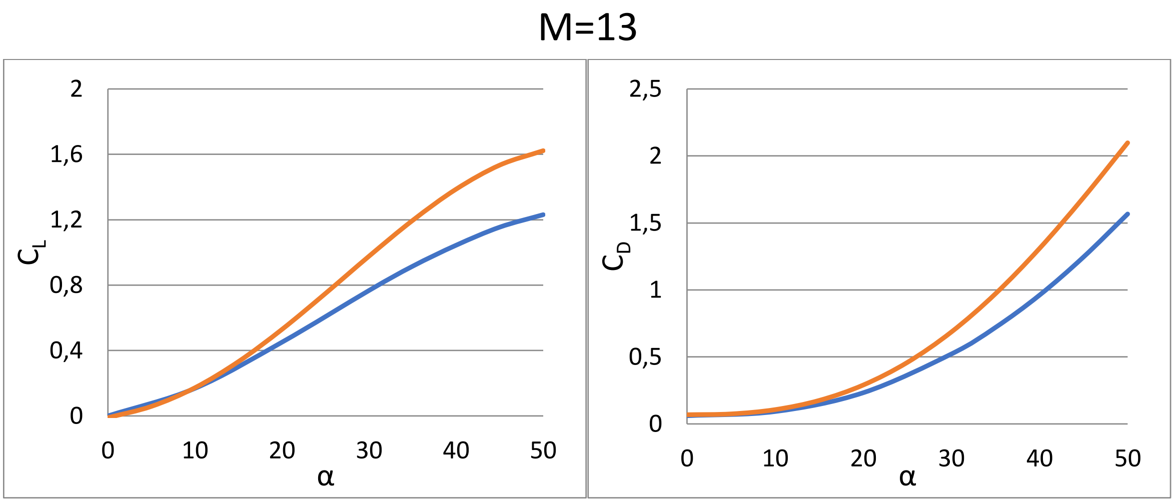

Figure 6.8 - C_L and C_D comparison for M=13

In the next step of this comparison, the effect of flaps mounted on the SLB 8-3 configuration is considered. Since the flaps are placed both on the upper and on the lower side of the wing, some preliminary observations about the flap definition in Missile Datcom input file are required. if flaps are defined as trailing edge control surfaces, as it is usually done for typical configurations, some differences between the real booster configuration and the one defined with Missile Datcom could arise. However, another method can be used: flaps can be defined as an additional pair of fins that is placed on the upper and lower part of the wing. Both these cases are considered in this comparison. The blue line corresponds to the data obtained with the first case, while the red line corresponds to the second one.
The results for the subsonic regime are presented in Figure 6.9, Figure 6.10 and Figure 6.11. In this case, a flap deflection of -5° is considered. The comparison shows that the best match between Missile Datcom and CAC is obtained if flaps are defined as a trailing edge control surface. The lift coefficient is almost the same if computed with Missile Datcom and CAC. The drag coefficient, instead, presents similar values only for low angles of attack. This is the same trend that has been found in the previous evaluation without flaps.

For the next comparisons, only the case with the trailing edge flaps is considered, as it is the one that better describes the flap behaviour. The results for the supersonic regime are reported in Figure 6.12 and Figure 6.13. The flap deflection is now set to 5°. There is a clear similarity between CAC and Missile Datcom for what concerns the lift coefficients, while a small difference is present if the drag coefficient is compared. This is, again, exactly the same trend that has been found in the previous case without flaps.

The results for the hypersonic speed range are reported in Figure 6.14, Figure 6.15 and Figure 6.16. Here, the aerodynamic data resulting from HOTSOSE are compared with the ones from Missile Datcom. The general trend is similar to the previous comparison. A good match exists at low angles of attack, while the difference between the two lines increases with higher α.

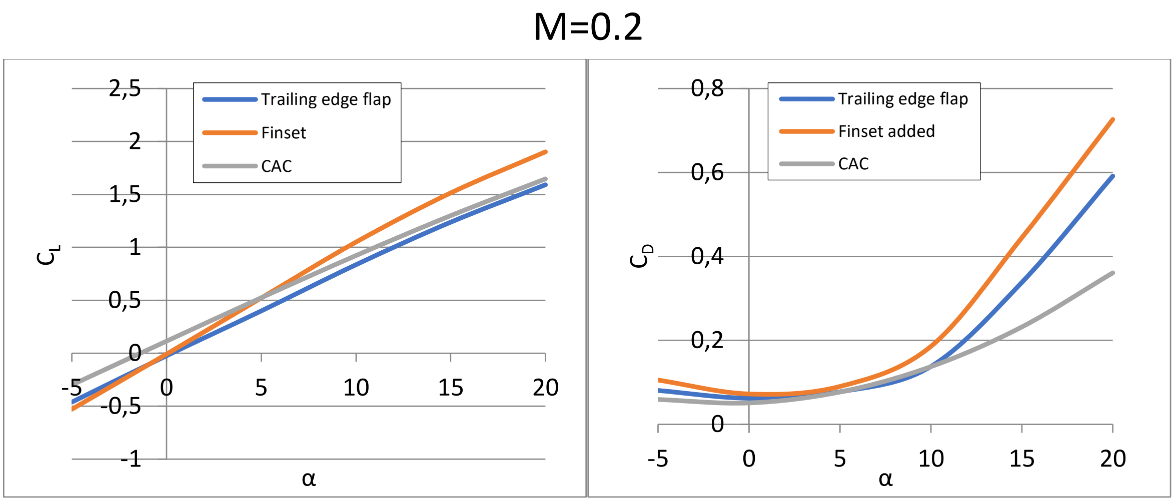

Figure 6.9 - C_L and C_D comparison for M=0.2 (δ_{flap}=-5°)

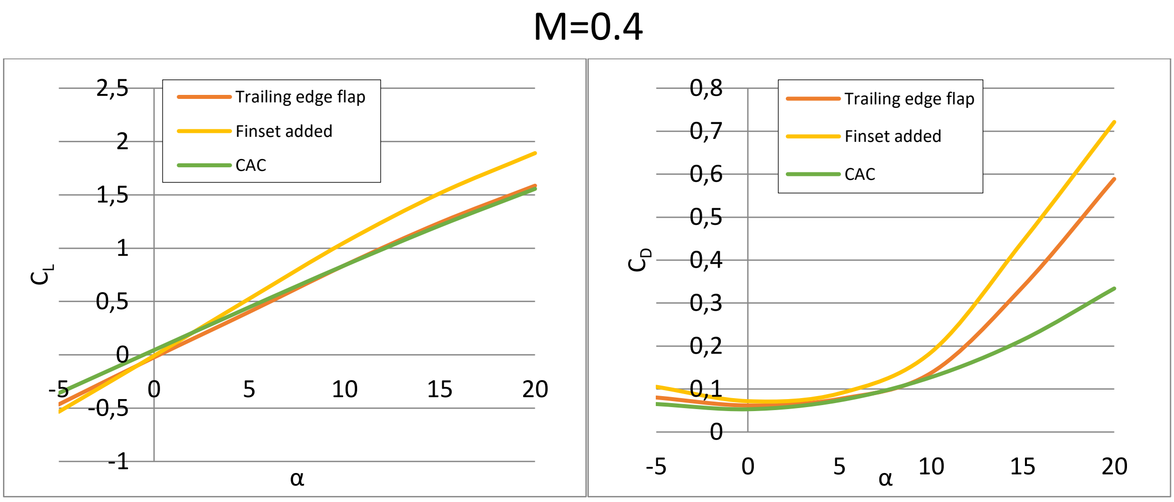

Figure 6.10 - C_L and C_D comparison for M=0.4 (δ_{flap}=-5°)

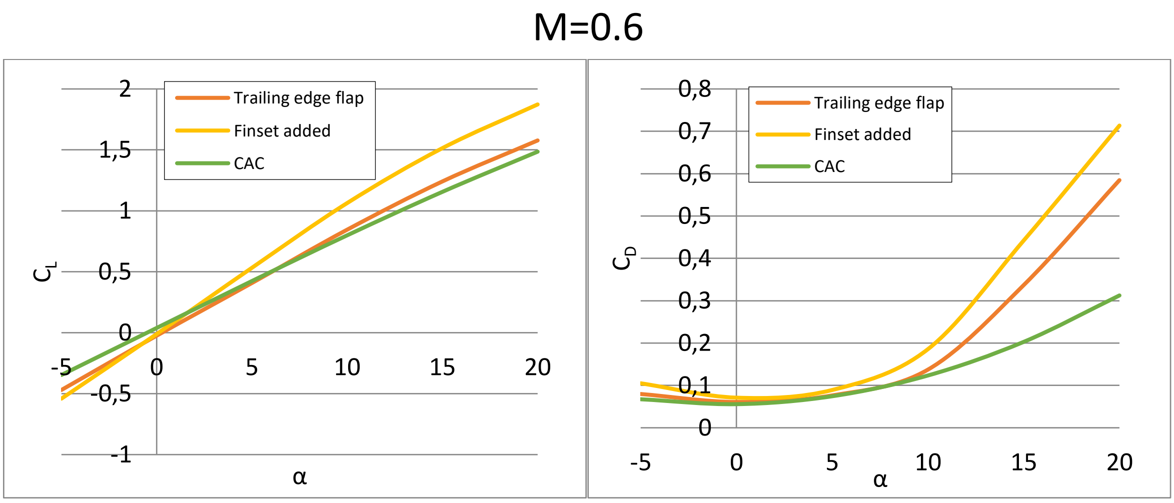

Figure 6.11 - C_L and C_D comparison for M=0.6 (δ_{flap}=-5°)

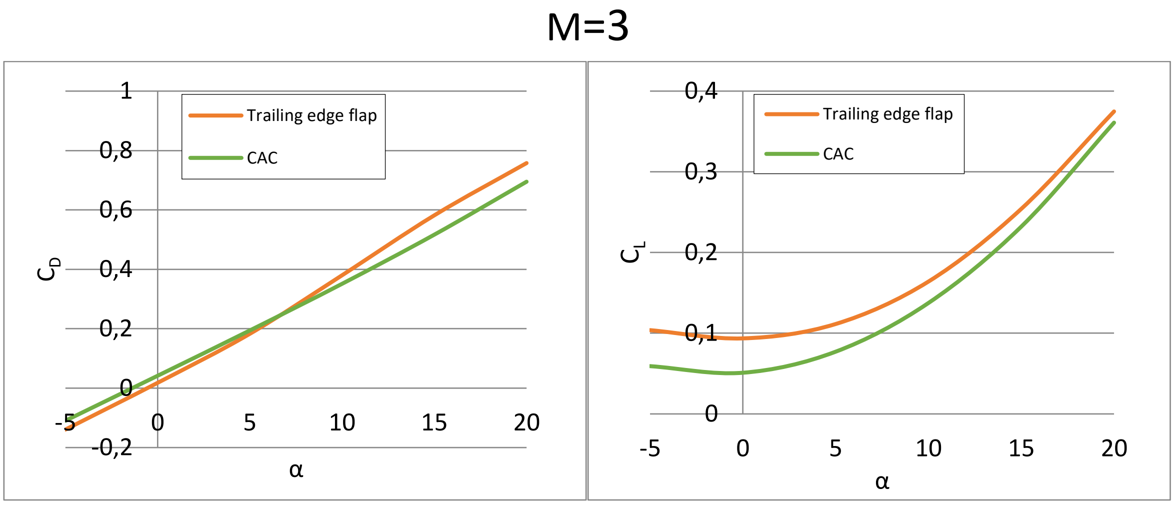

Figure 6.12 - C_L and C_D comparison for M=3 (δ_{flap}=5°)

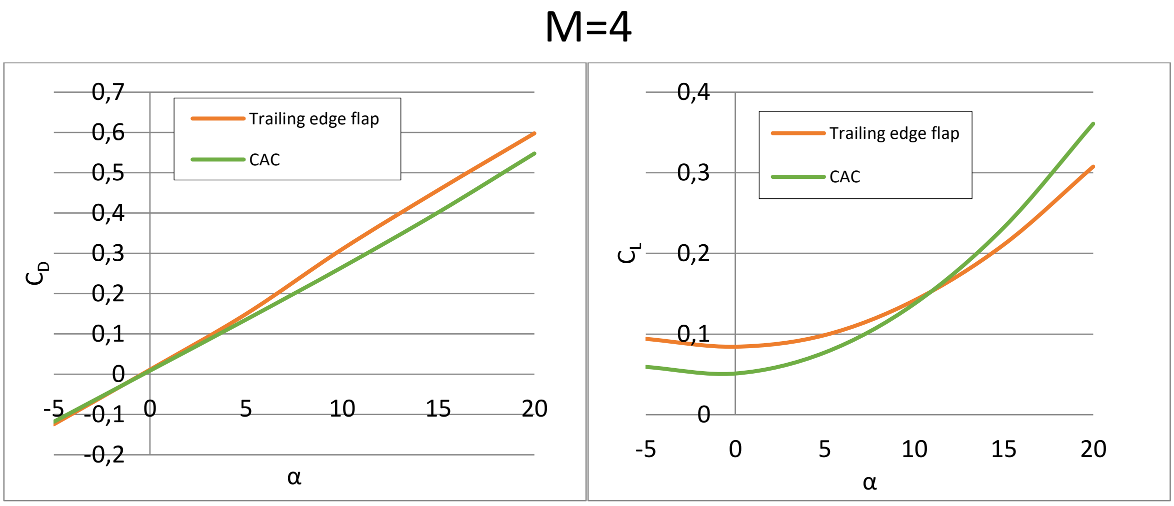

Figure 6.13 - C_L and C_D comparison for M=4 (δ_{flap}=5°)

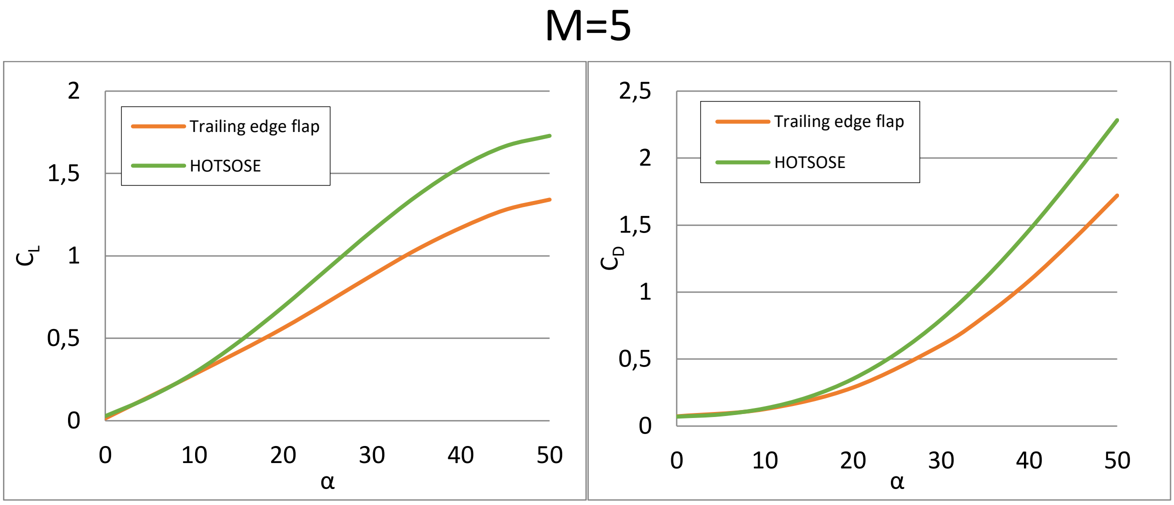

Figure 6.14 - C_L and C_D comparison for M=5 (δ_{flap}=15°)

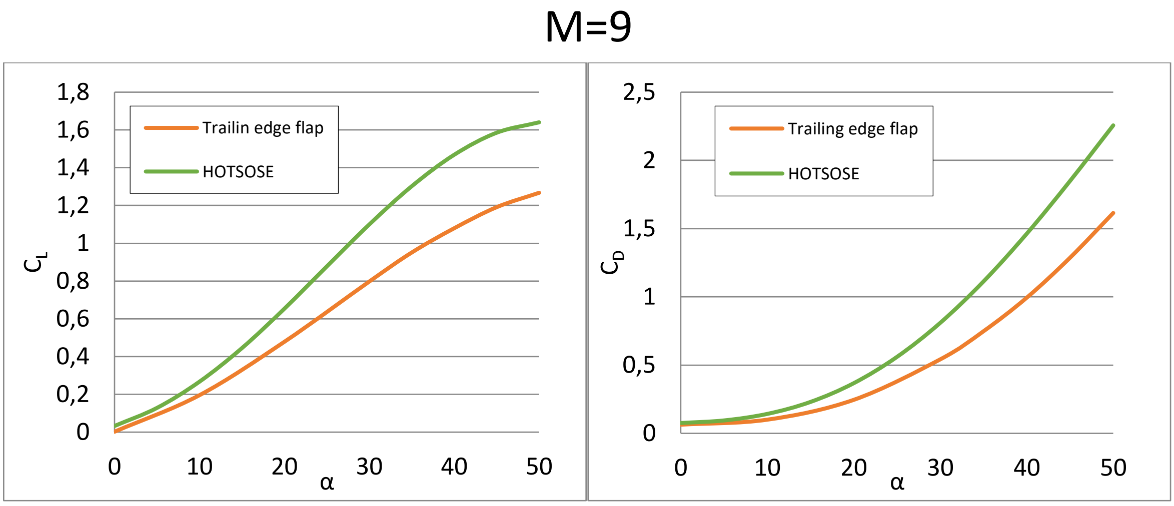

Figure 6.15 - C_L and C_D comparison for M=9 (δ_{flap}=15°)

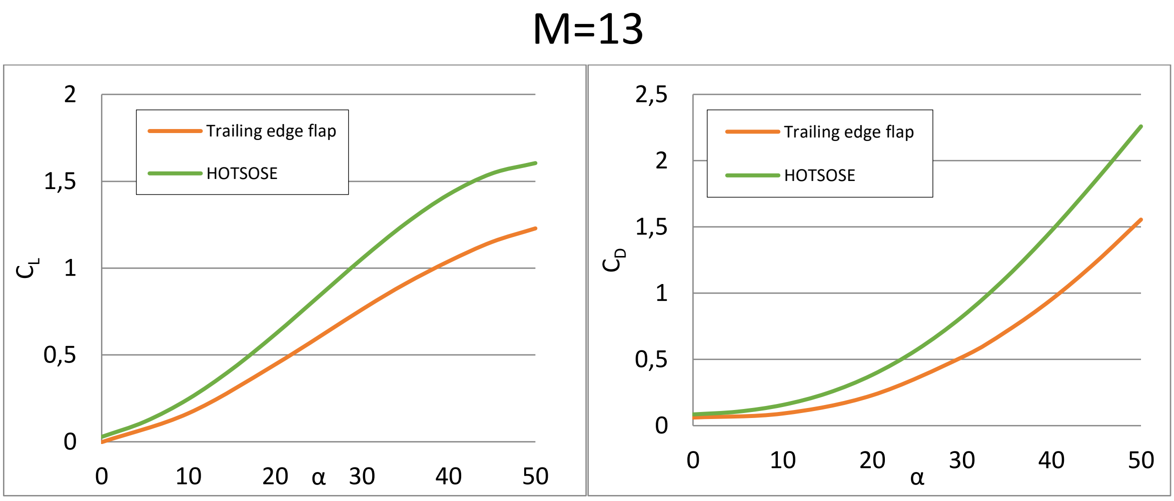

Figure 6.16 - C_L and C_D comparison for M=13 (δ_{flap}=15°)

Chapter 7 Vertical fins design

The final step of this investigation concerns the preliminary design of the vertical fins of the SL booster. During previous computations, the vertical fins are derived from the ones of the SL7 configuration. The overall surface, in particular, is the same and the geometry is adapted to fit for the new wing. Since the outer part is movable, they are placed at the tip of the inner part of the wing so that any interference is avoided during the rotation. This choice is taken at the beginning of this study because no data on the yaw moment coefficient C_Y are available with CAC and HOTSOSE. Now, instead, these C_Y data can be provided by Missile Datcom. At this point, it is possible to estimate the vertical fins area and the geometry that is needed for directional stability and control. Moreover, some empirical relations, valid for general aircraft, are taken into account for a preliminary sizing. The first relation is the *vertical tail volume coefficient* V_v [16]:

$$V_V = \frac{S_v\, l_v}{S\, b}$$

Where S_v is the vertical tail area, l_v is the distance between the aerodynamic centre of the vertical tail and the COG, S is the wing area and b is the wing span.
Aspect ratio and *taper ratio* are also considered for the vertical fins sizing [17].

$$AR = \frac{b^2}{S} \text{ and } TR = \frac{c_t}{c_r}$$

Where c_t is the tip chord and c_r is the root chord of the fin.
The suggested range of values, valid for typical aircraft, are shown in Table 7.1.

Coefficient	Range
Vv	0.02 - 0.05
AR	0.9 - 2.0
TR	0.2 - 1.0

Table 7.1 - Ranges for the vertical tail coefficients

The geometry of the vertical fins is defined taking into account for these three relations. The final vertical fins data are reported in Table 7.2 and they are compared to the geometry that was used previously.

	Now	Previous
Root chord	8 m	10 m
Tip chord	4 m	6 m
Span	10.5 m	6.5 m
Area	52 m^2	63 m^2
Sweep angle	30°	40°

Table 7.2 - Vertical fins geometry

Once these data are known, it is possible to evaluate V_V, AR and TR and to check if they are included in the ranges described before. The results are reported in Table 7.3.

V_V	AR	TR
0.036	1.75	0.50

Table 7.3 - Vertical fins coefficients

The yaw moment coefficient is then evaluated with different sideslip angle β and for different angle of attack α. For a first estimation, the control surface on the vertical tails is not considered.

In Missile Datcom, the sideslip angle β is measured as shown in Figure 7.1. If this definition is used, the sign convention for the yaw moment coefficient can be also defined. When the curve of the C_Y over β has a positive trend, the directional stability is confirmed. While, if the slope is negative, the vehicle presents an unstable behaviour [Figure 7.2].

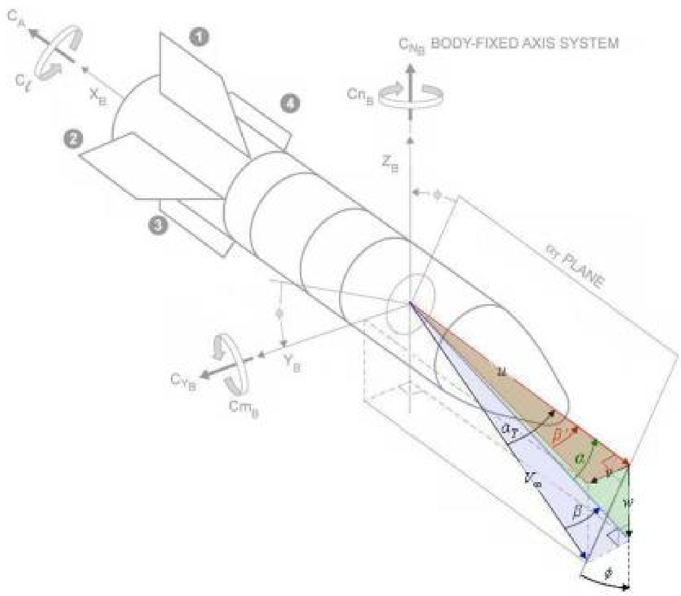

Figure 7.1 - Missile Datcom axis system [10]

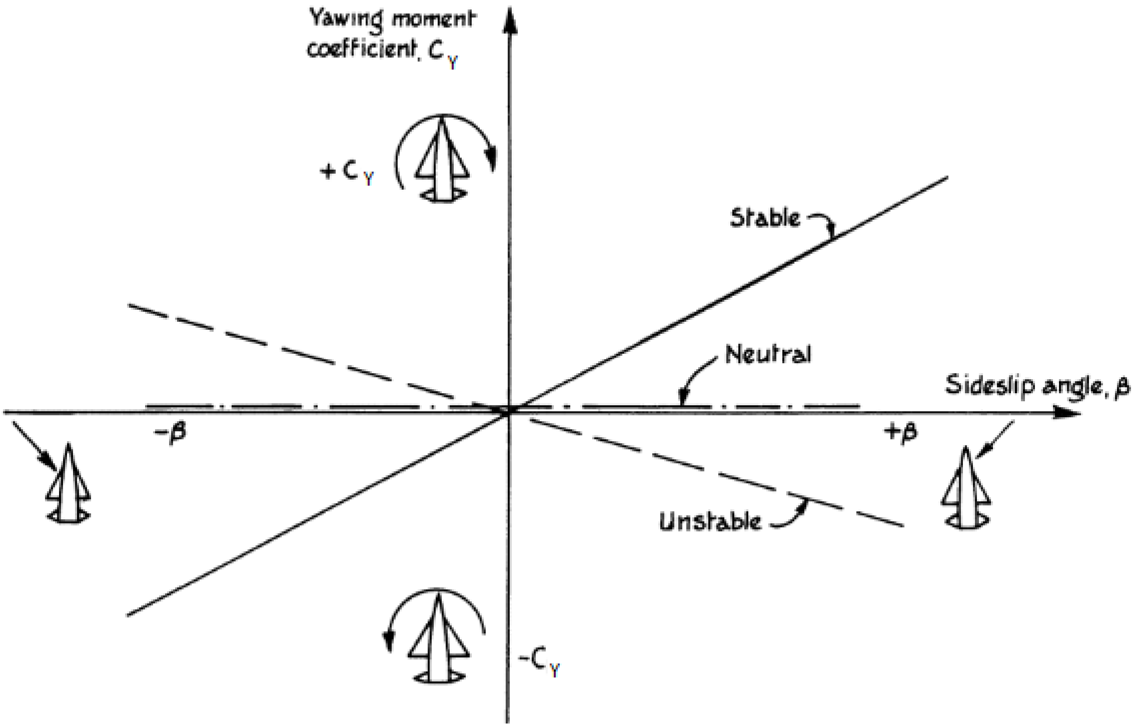

Figure 7.2 - Directional stability [18]

First, the directional stability has been investigated for the subsonic regime. The results for M=0.2, M=0.4 and M=0.6 are presented in Figure 7.3, for different angles of attack. The β range that has been considered here is included between -5° to 5°. The sideslip angle, indeed, should never exceed this value during subsonic flight. Since the yaw moment trend is characterized by a positive slope, the SL configuration presents a stable behaviour in this Mach range. However, for supersonic and hypersonic flight this is not true anymore. C_Y trend for M=3 and M=4 is reported in Figure 7.4, while the trend for the hypersonic regime is shown in Figure 7.5. The curve slopes becomes negative, suggesting the existence of an unstable behaviour for M>1.

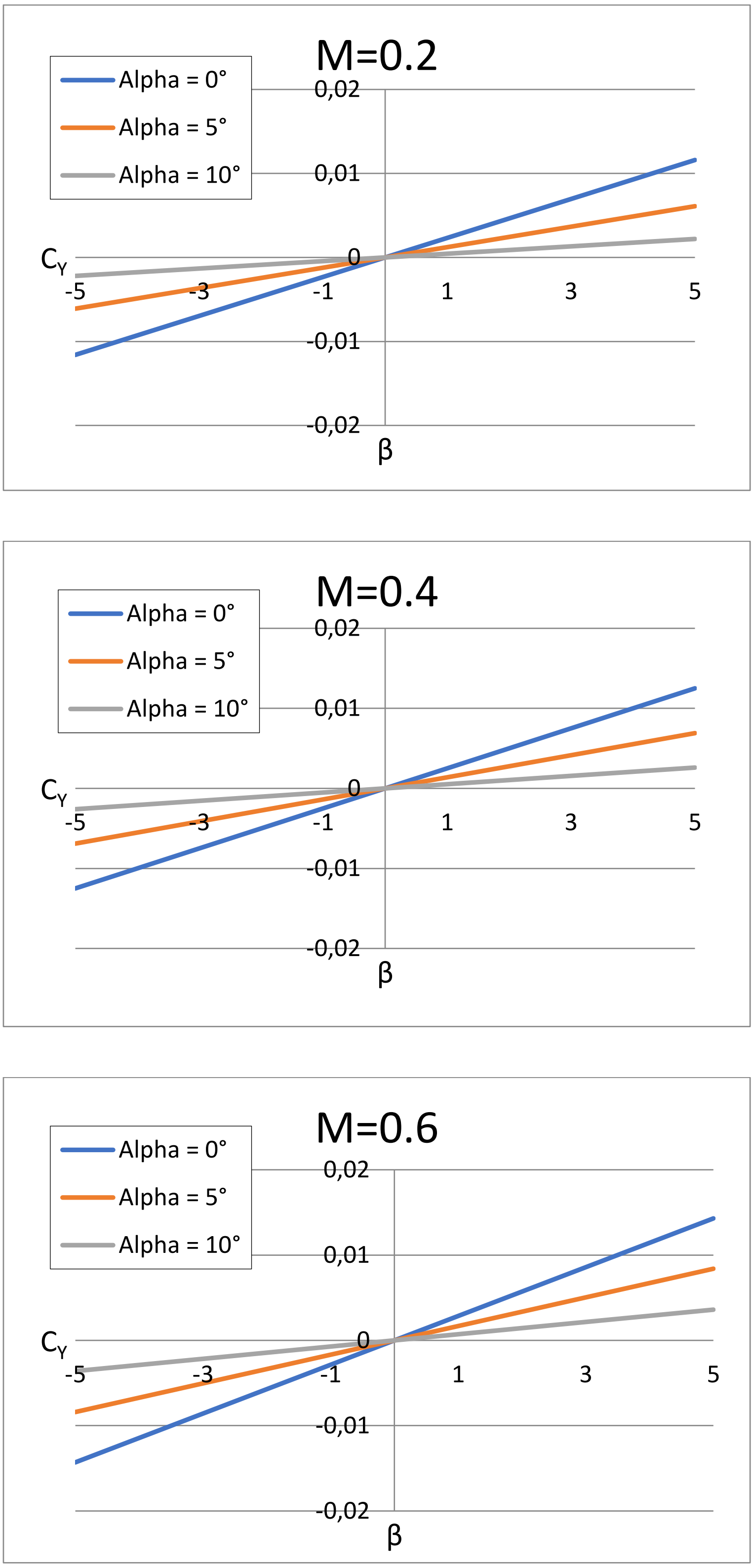

Figure 7.3 - Yaw moment coefficient (subsonic)

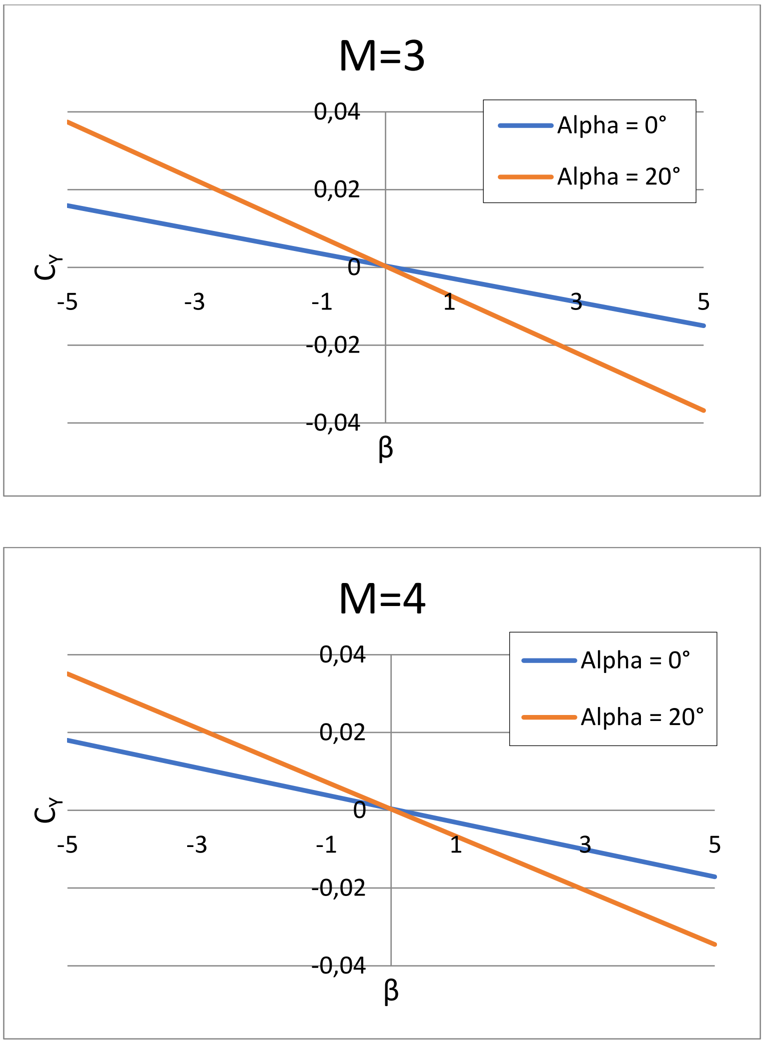

Figure 7.4 - Yaw moment coefficient (supersonic)

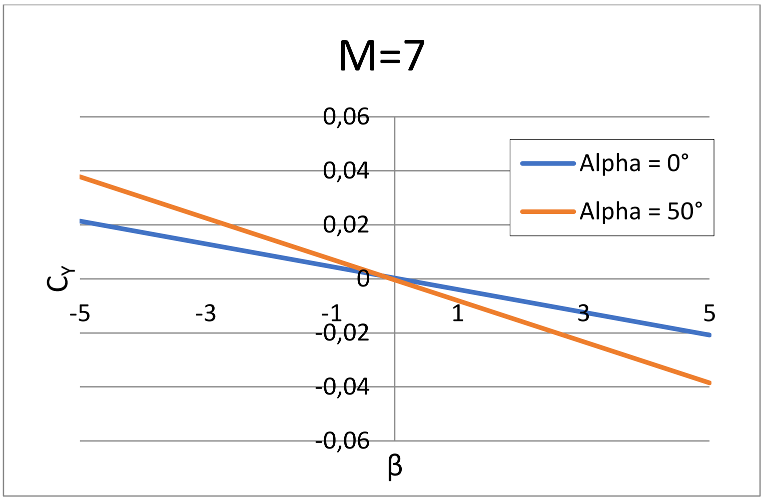

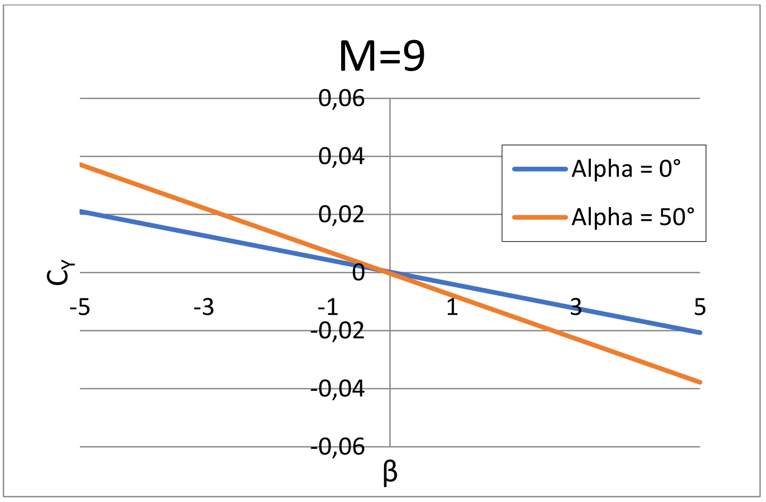

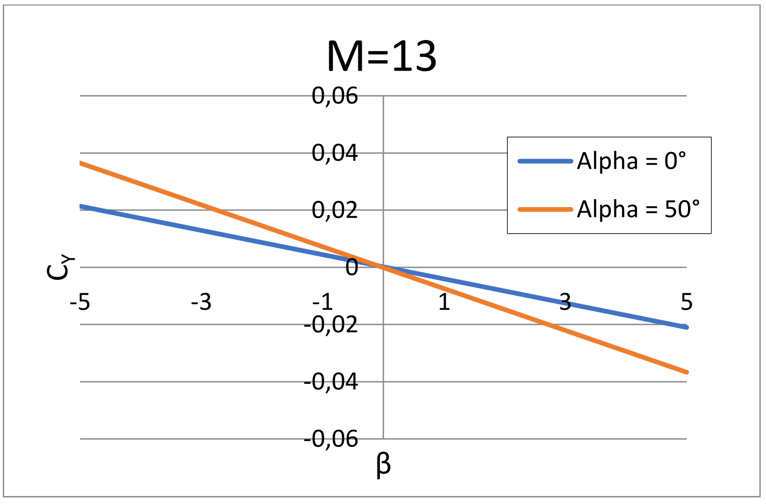

Figure 7.5 - Yaw moment coefficient (hypersonic)

A control surface is then added on vertical fins, in order to investigate the existence of a trimmed conditions with varying sideslip angles. The portion of vertical fin that is occupied by the control surface is equal to the 50% of the fin chord.
The resulting yaw moment coefficient for the subsonic regime is presented in Figure 7.6. An angle of attack equal to 5° has been chosen for this analysis. The β range that has been

selected is the same as before and it is included between -5° and 5°. The results show that a trimmed condition can be found with a deflection of the vertical fin flaps that is lower than ±5°.

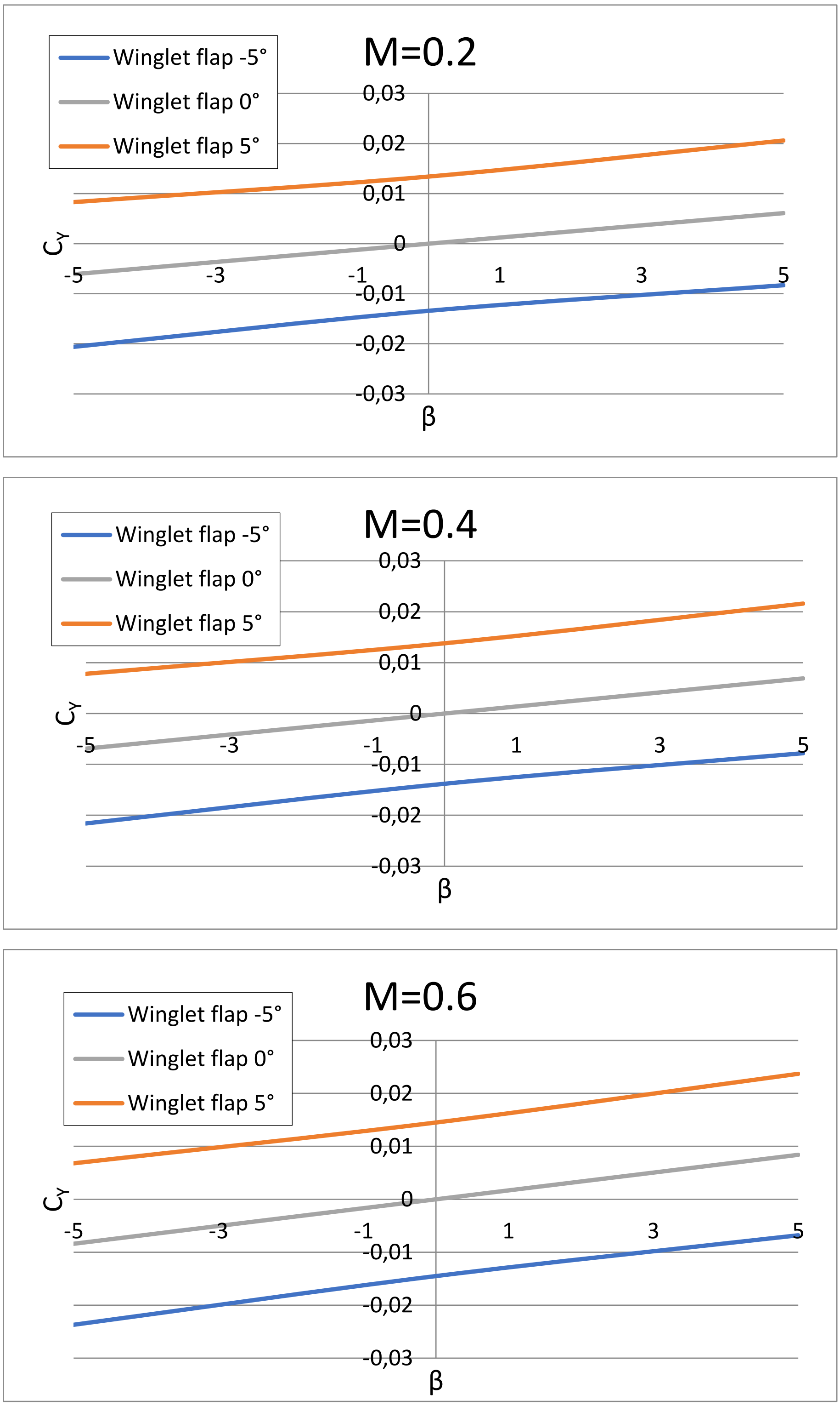

Figure 7.6 - Yaw moment coefficient with control surface (subsonic)

The resulting yaw moment coefficient for supersonic Mach numbers is presented in Figure 7.7. The selected angle of attack is now equal to 20°. The analysis is now restricted

to β included between -2° and 2°, since the booster could become uncontrollable for higher sideslip angles. From these data, it is possible to notice that the trimmed condition is guaranteed only for a very limited range of sideslip angles, that approximately goes from -0.5° to 0.5°. This reduction in the effectiveness of the vertical control surface is due to the position of the vertical fins: since they are placed in a rearward position, they are in shadow with respect to the airflow if a high angle of attack is used.
Something similar can be said if the hypersonic Mach range is considered. The results for that case are reported in Figure 7.8.

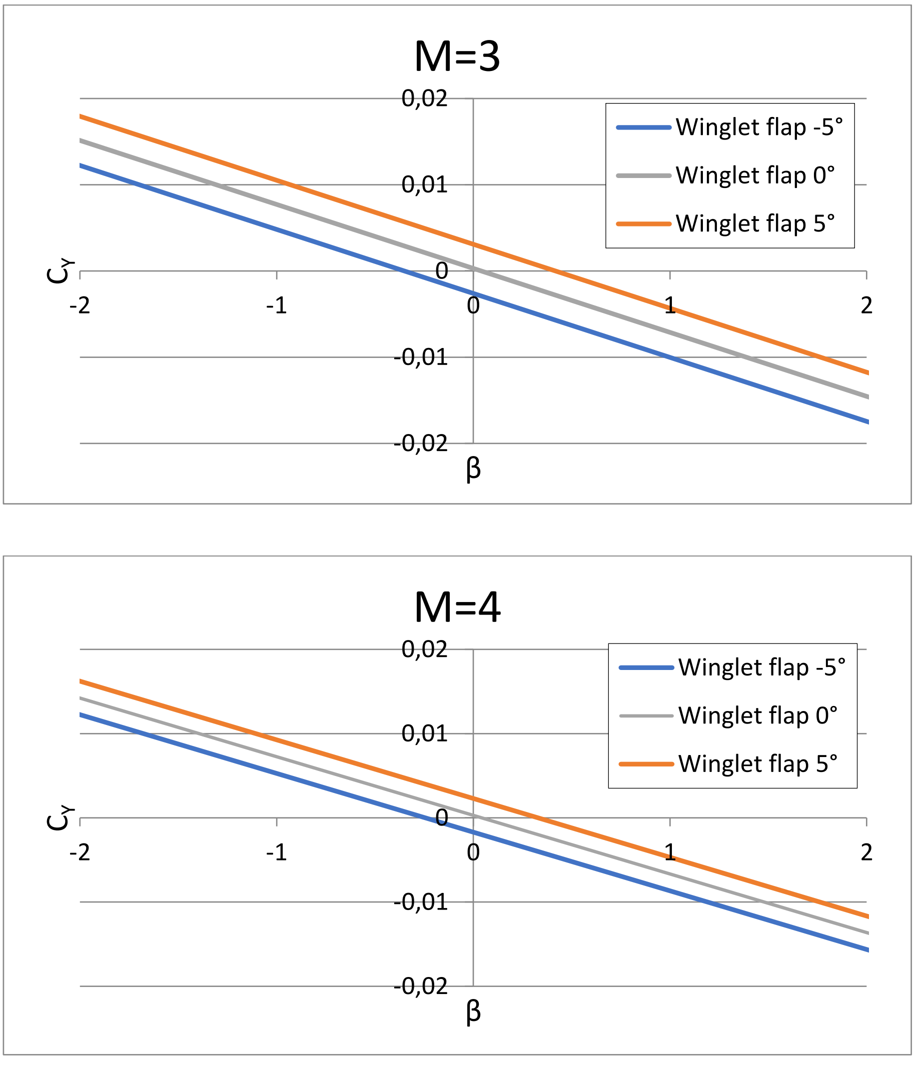

Figure 7.7 - Yaw moment coefficient with control surface (supersonic)

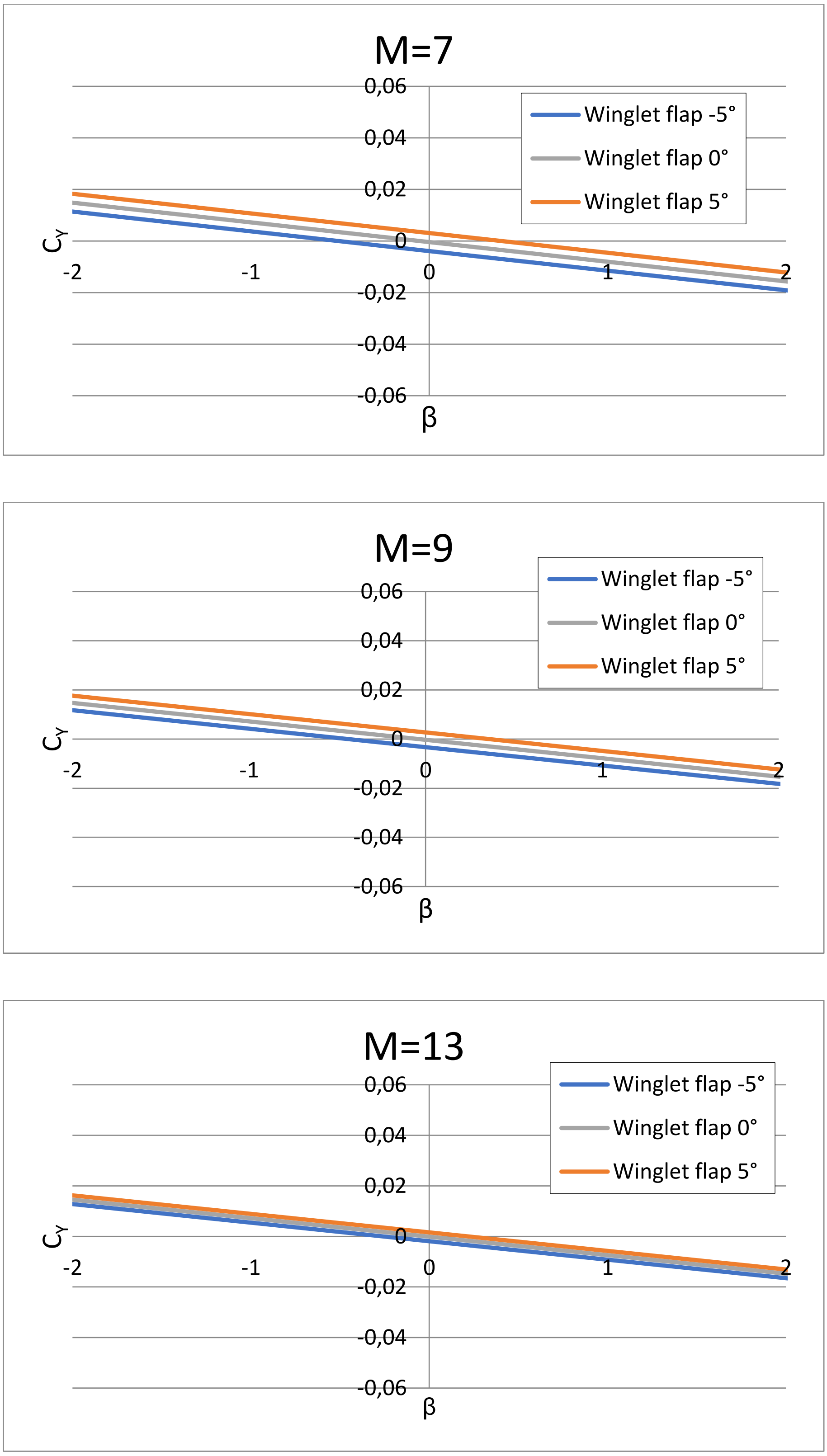

Figure 7.8 - Yaw moment coefficient with control surface (hypersonic)

Chapter 8 Conclusion

During the hypersonic re-entry a high span wing is not needed. In addition to this, a shock interaction with the leading edge of the booster wing has been detected. Even if no detailed analysis has been conducted to understand how severe this interaction is, this problem has to be avoided. For those reasons, the reduction of the wing span is one of the main requirements of this study. On the other hand, a large wing is helpful in subsonic regime. This is the best way to maximise the performance during the descent and the tow-back flight. Different solutions have been taken into account during this analysis, involving both fixed and variable wings. The latter solution is the most interesting one, since it could be useful to satisfy the requirements during both hypersonic and subsonic flight. Mass and aerodynamic data sets have been computed for each configuration and the wing geometry has been adapted to reach the maximum aerodynamic performances, while keeping the mass as low as possible.

The variable sweep wing configuration has been selected as the most promising among those studied. It is composed by two parts: the inner part is fixed, while the outer part is able to rotate. Two positions exists for the outer wing: deployed or stored inside the inner part. The wing remains in the stored position during the whole duration of the ascent and during the hypersonic and supersonic part of the descent. Then, it is deployed for $M<1$ and it contributes to increase lift at subsonic velocities.

Preliminary calculation on the tow-back flight performances, with a particular focus on the L/D, L/W and T/D ratios, has shown that this kind of flight is possible. However, only a very simplified evaluation has been done here, so a more detailed analysis is required to further verify these results.
Then, the existence of stable and trimmed conditions has been investigated for the whole descent flight. The results show that the stability is confirmed both for subsonic and hypersonic flight, while an approximately neutral behaviour is found during supersonic flight. On the other hand, it has been demonstrated that a trimmed condition can be guaranteed for the entire Mach range.

Simulations of the ascent and the descent trajectory have been performed. For what concerns the descent, acceptable values of dynamic pressure, acceleration and heat flux have been detected. In particular, a further reduction of these parameters has been achieved with a manual optimization of the angles of attack during the diverse phases of the descent. Once the heat flux has been evaluated, the thermal protection system has been computed. A comparison between two types of passive TPS, one composed by non-metallic materials and another one composed by both metallic and non-metallic materials, has been done. This choice has been made because some advantages from an operational point of view can be achieved, if metallic materials are used. A moderate TPS mass has been found with the set of non-metallic materials, while a remarkable increase in mass has been discovered in the latter case. This increase in the overall mass of the booster has an effect on the mission performances. The ascent trajectory for the TSTO mission and the payload have been evaluated: while with the non-metallic TPS, the payload presents a promising value, in the other case the payload is subject to a considerable decrease. However, even if the payload is reduced, it is still acceptable and interesting from a practical point of view. The mission can be still performed, but the number of spacecraft that can be transported to the target orbit could be lower in this case.

Finally, a first validation of the aerodynamic data resulting from the DLR tools has been performed. The aerodynamic data have been evaluated with Missile Datcom and they have been compared with the data resulting from CAC and HOTSOSE. This comparison has highlighted a very good accordance between them.

As this study solely gives a preliminary estimation of the booster aerodynamic performances, many aspects can be further improved. First of all, it must be said again that the sweeping mechanism has not been designed and a real estimation of its mass is not known. However, this is a fundamental aspect that must be investigated if one wants to perform a more detailed analysis. The actual increase in the overall complexity of the booster is also not considered. Another important point is the exact positioning of the pivot for the rotation of the wing, that would also help to understand which is the real amount of space that is needed for the wing storage. Once the overall configuration will be more precisely defined, a more detailed analysis on the aerodynamic performances of the booster will be required.

Literature

[1] M. Sippel, "SpaceLiner - a Visionary Concept of an Ultra Fast Passenger Transport under Investigation in FAST20XX," in *16th AIAA/DLR/DGLR International Space Planes and Hypersonic Systems and Technologies Conference*, Bremen, 2009.

[2] M. Sippel, L. Bussler and A. Kopp, "Advanced Simulations of Reusable Hypersonic Rocket-Powered Stages," in *21st AIAA International Space Planes and Hypersonics Technologies Conference*, Xiamen, China, 2017.

[3] M. Sippel, T. Schwanekamp, O. Trivailo, A. Kopp, C. Bauer and N. Garbers, "SpaceLiner Technical Progress and Mission Definition," in *20th AIAA International Space Planes and Hypersonic Systems and Technologies Conference*, Glasgow, UK, 2015.

[4] M. Sippel, S. Stappert and A. Koch, "Assessment of Multiple Mission Reusable Launch Vehicles," in *69th International Astronautical Congress (IAC)*, Bremen, 2018.

[5] M. Sippel and J. Klevanski, "Progresses in Simulating the Advanced In-Air-Capturing Method," in *5th International Conference on Launcher Technology*, Madrid, Spain, 2003.

[6] R. Kress, "Variable sweep wing design," in *Aircraft Prototype and Technology Demonstrator Symposium*, Dayton, 1983.

[7] T. A. Weisshaar, "Morphing Aircraft Systems: Historical Perspectives and Future Challenges," *Journal of Aircraft,* vol. 50, no. 2, pp. 337-353, 2013.

[8] R. L. Perry, "Variable-Sweep Aircraft: A Case History of Multiple Re-Innovation," in *3rd Annual Meeting of the American Institute of Aeronautics and Astronautics*, Boston, US, 1966.

[9] J. Pappalardo, "Swing Wings," [Online]. Available: https://www.airspacemag.com/flight-today/swing-wings-9189621/. [Accessed February 2019].

[10] C. Rosema, J. Doyle, L. Auman and M. Underwood, "MISSILE DATCOM User's Manual - 2011 Revision," Army Aviation &Missile Research, Development and Engineering Center, US Air Force, 2011.

[11] E. Casali, M. Sippel and L. Bussler, "Investigation of feasible flight trajectories and re-entry atmospheric guidance for SpaceLiner 7-3," Bremen, 2015.

[12] "Stability Characteristics of the Boeing 747," [Online]. Available: https://courses.cit.cornell.edu/mae5070/B747_Data.pdf. [Accessed November 2018].

[13] K. Min, R. Plumley and A. Brooks. [Online]. Available: http://www.dept.aoe.vt.edu/~mason/Mason_f/B747PresS07.pdf. [Accessed November 2018].

[14] J. Roskam and C.-T. E. Lan, Airplane aerodynamics and performance, DARcorporation, 1997.

[15] J. Weickmann , "Designanalyse für Flügel, Rumpfstrukturen einer rückführbaren Boosterstufe," 2005.

[16] "Basic Aircraft Design Rules," [Online]. Available: https://ocw.mit.edu/courses/aeronautics-and-astronautics/16-01-unified-engineering-i-ii-iii-iv-fall-2005-spring-2006/systems-labs-06/spl8.pdf. [Accessed January 2018].

[17] P. Barua, T. Sousa and D. Scholz, "Empennage Statistics and Sizing Methods for Dorsal Fins," 2013.

[18] R. Whitford, Design for Air Combat, London: Jane's Publishing Company, 1987.

[19] M. L. Blosser, "Development of Metallic Thermal Protection Systems for the Reusable Launch Vehicle," in *Space Technology and Applications International Forum*, Albuquerque, US, 1996.

[20] M. Sippel, J. Klevanski and U. Atanassov, "Search for technically viable options to improve RLV by variable wings," in *55th International Astronautical Congress*, Vancouver, Canada, 2004.

[21] R. K. Heffley and W. F. Jewell, "Aircraft Handling Qualities Data," NASA, Washington D.C., US, 1972.